

A new strategy for fatigue analysis in presence of general multiaxial time varying loadings

Ma Zepeng^{a,*}, Patrick Le Tallec^b, Habibou Maitournam^c

^a*Laboratory of Solid Mechanics, Ecole Polytechnique, 91128 Palaiseau Cedex, France*

^b*Laboratory of Solid Mechanics, Ecole Polytechnique, 91128 Palaiseau Cedex, France*

^c*IMSLA, ENSTA ParisTech, CNRS, CEA, EDF, Université Paris-Saclay, 828 bd des Maréchaux, 91762 Palaiseau cedex France*

Abstract

The purpose of this paper is to propose an energy based multiscale fatigue approach which handles multidimensional time varying loading histories.

Our fundamental thought is to assume that the energy dissipated at small scales governs fatigue at failure. We follow the Dang Van paradigm at macro scale. The structure is elastic at the macroscopic scale. At each material points, there is a stochastic distribution of weak points which will undergo strong plastic yielding, which contribute to energy dissipation without affecting the overall macroscopic stress. The basis of our model is to consider a plastic behavior at the mesoscopic scales with a dependence of the yield function not only on the deviatoric part of the stress but also on the hydrostatic part. A kinematic hardening under the assumption of associative plasticity is also considered.

Instead of using the number of cycles, we use the concept of damage accumulation during the considered load history. Non-linear damage accumulation law based on plastic dissipation is also considered in our model. Fatigue will then be determined from the plastic shakedown cycle and from a phenomenological fatigue law linking lifetime and accumulated mesoscopic plastic dissipation.

Keywords: Fatigue; Energy; High cycle; Plasticity; Mean stress

^{*}Corresponding author. Email address: zepeng.ma@polytechnique.edu

Nomenclature

S_a	maximum deviatoric stress during the loading cycles, the second principal invariant of the stress deviatoric tensor
s_{-1}	tensile fatigue limit for $R = -1$
b	back stress
\dot{w}	energy dissipation rate at a certain scale
\dot{W}	energy dissipation rate at all scales
W	dissipated energy at all scales per unit time
W_{cyc}	dissipated energy at all scales per cycle
N	current number of cycles
N_F	number of cycles to failure
$\dot{\varepsilon}_p$	rate of effective plastic strain
W_0	reference density of damage energy
E	Young's modulus
$k = 500 \sim 800 \text{ MPa}$	hardening parameter
$\beta = 1 \sim 50$	weakening scales distribution exponent
$\gamma = 0 \sim 50$	material parameter from Chaboche law
$\alpha = 1 - a \left\langle \frac{\frac{1}{2}J_2(t) - \sigma_{-1}(1 - 3c\sigma_{H,max}(t))}{\sigma_u - J_2(t)} \right\rangle$	characterizes non-linearity of damage accumulation(c is constant)
J_2	The second principal invariant of the stress deviatoric tensor
a	material parameter from Chaboche law
σ_y	macroscopic yield stress(normal or shear)
$\lambda = 0 \sim 5$	hydrostatic pressure sensitivity
$\underline{\underline{S}} = \text{dev} \dot{\underline{\underline{\Sigma}}}$	deviatoric part of the stress tensor
Σ_H	macroscopic hydrostatic pressure
$A_{II} = \tau_{oct,a} = \sqrt{\frac{1}{6}J_2}$	the amplitude of octahedral shear stress
$\sigma_{VM} = \sqrt{3J_2}$	Von Mises stress
$\langle \rangle$	Macaulay bracket symbol. $\langle \rangle$ is defined as $\langle m \rangle = 0$ if $m \leq 0$

1 Introduction

Fatigue failure is a damage accumulation process in which material property deteriorates continuously under fatigue loading and the damage depends on the size of stress and strain. With the accumulation of fatigue damage, some accidents occur for these components. Thus, it is important to formulate an accurate method to evaluate the fatigue damage accumulation and effectively predict the fatigue life of these components.

The basis of the Stress-Life method is the Wohler S-N diagram, which plots nominal stress amplitude S versus cycles to failure N . Certain materials have a fatigue limit or endurance limit which represents a stress level below which the material does not fail and can be cycled infinitely. If the applied stress level is below the endurance limit of the material, the structure is said to have an infinite life. This is the characteristic of steel and titanium in benign environmental conditions. Many non-ferrous metals and alloys, such as aluminum, magnesium and copper alloys, do not exhibit well-defined endurance limits. These materials instead displays a continuously decreasing S-N response. An effective endurance limit for these materials is sometimes defined as the stress that causes failure at 1×10^8 or 5×10^8 loading cycles.

The problem is then to define criteria able to predict this endurance limit. The micro-macro approach applied to the field of endurance was born with the work of [1], and since it has been used many times, including by [2] to take better account of loading path effects. For simplicity and to avoid too costly identification procedures of fatigue data, criteria are often expressed using two parameters. The first relates generally to a shear stress τ (on a plane or on average over an elementary volume) while the second σ reflects the normal stress effects (mean and amplitude) often through the hydrostatic stress are the most numerous ([3], [4], [5], [6]). The normal stress acting on the material plane is sometimes defined from a critical plane ([7]), or through integration at every plane of an elementary volume ([8]). In particular, a probabilistic approach based on this type of integration is proposed in [6].

Other authors use energy based approaches. [9] is one of the first to propose a fatigue criterion based on cyclic shear deformation energy. This approach was taken up and complemented by [10] and [11] for the case of multiaxial loadings. In France, this approach is reflected in the work of [12] and then in [13] and [14]. In recent years, a new class of criteria coupling mesoplasticity and damage has also emerged. In [15], for example, the author use the approach introduced by [16] based on the thermodynamics of irreversible processes and the mechanics of continuous media. Models based on plasticity-damage coupling were also proposed in [17], [18]. In the case of fatigue, we usually employ in this damage framework the concept of the loading cycle instead of time to evaluate the evolution of damage and to measure the fatigue lifetime. The equations then depend on the load through globally defined quantities over a cycle, such as amplitude, maximum value, mean value. The growth equation of fatigue damage is therefore taken in the form:

$$\delta D = f(D)\delta N$$

3

$$\delta N = f_n \delta t$$

where δt is a time sampling of the history in a given number of time intervals $\delta t_1, \delta t_2, \dots, \delta t_i, \dots$ and f_n is the mean frequency of those cycles during the considered time step.

The problem in these approaches is then to take into account the presence of complex variations of the stress tensor. Heuristic formulations with different multiaxial fatigue criteria have been proposed, but most of them still requires the notion of load cycles. The objective of this work is to contribute to the development of life models that take into account such complex variations while avoiding the notion of load cycle. Our fundamental thought is to assume within a micro-macro approach that the local dissipated energy at small scale contributes to the damage which governs fatigue at failure. We follow the Dang Van paradigm. The structure is elastic at the macroscopic scale. At each material point, there is a stochastic distribution of weak points which will undergo strong plastic yielding, which contributes to energy dissipation and cause damage, without affecting the overall macroscopic stress.

Our model considers a plastic behavior at the mesoscopic scales with a dependence of the yield function not only on the deviatoric part of the stress but also on the hydrostatic part. A kinematic hardening under the assumption of associative plasticity is also introduced.

Instead of using the number of cycles, we will use in addition as in [15] the concept of nonlinear damage accumulation during the loading history. To approach real life loading history more accurately, non-linear damage accumulation laws are also considered in our model to take into account the sequencing effect. Fatigue will then be determined from the energy plastically dissipated at all scales during plastic shakedown cycles and from a phenomenological fatigue law linking damage evolution and accumulated mesoscopic plastic dissipation.

The paper is organized as follows. In section 2, we introduce the notion of weakening scales and multiscale yield function and describe the plastic dissipation resulting from this notion. Section 3 introduces the proposed nonlinear damage accumulation law and summarizes the full model that we propose. Its numerical implementation is presented in section 4, while section 5 is devoted to various validations on typical load histories classically treated in the literature. Identification strategy is presented in section 6 while various experimental applications are then treated in section 7.

2 Weakening scales and yield function

2.1. The concept of weakening scales

We follow the Dang Van paradigm. The structure is elastic at the macroscopic scale. At each material points, there is a stochastic distribution of weak points which will undergo strong plastic yielding, without contributing to the overall macroscopic stress. From a microscopic point of view, there is a distribution of weakening scales, namely $s \in [1, \infty)$. In order to introduce our concept, let us imagine that we can

measure the macroscopic stress intensity at present time by a given value S_a . Let σ_y be the yield limit before weakening. Then we imagine that for a given scale s :

- either $1 \leq s \leq \sigma_y/S_a$, then $S_a \leq \sigma_y/s$, the material stays in the elastic regime and there is no energy dissipation at this scale.
- or $\sigma_y/S_a \leq s \leq \infty$, then $S_a \geq \sigma_y/s$, the material is in plastic regime at this scale, which evolves through kinematic hardening, say from zero initial plastic strain $\underline{\underline{\varepsilon}}_p(s)$ and zero initial backstress $\underline{b}(s)$ at initial time t_0 . This is then dissipated energy at scale s contributing to the fatigue limit.

2.2. Distribution of weakening scales

We assume the weakening scales have a probability distribution function of power law:

$$P(s) = Hs^{-\beta} = (\beta - 1)s^{-\beta}, \quad (1)$$

where β is a material constant. The choice of a power law has two reasons: on one hand, this type of distribution corresponds to a scale invariant process, on the other hand it leads in cyclic loading to a prediction of a number of cycles to life limit as a power law function of the stress intensity. More general laws can also be proposed, without changing the spirit of the model.

The probability of weakening scales is shown in Figure 1 and Figure 2. We can see that smaller β leads to larger probability of weakening for large s .

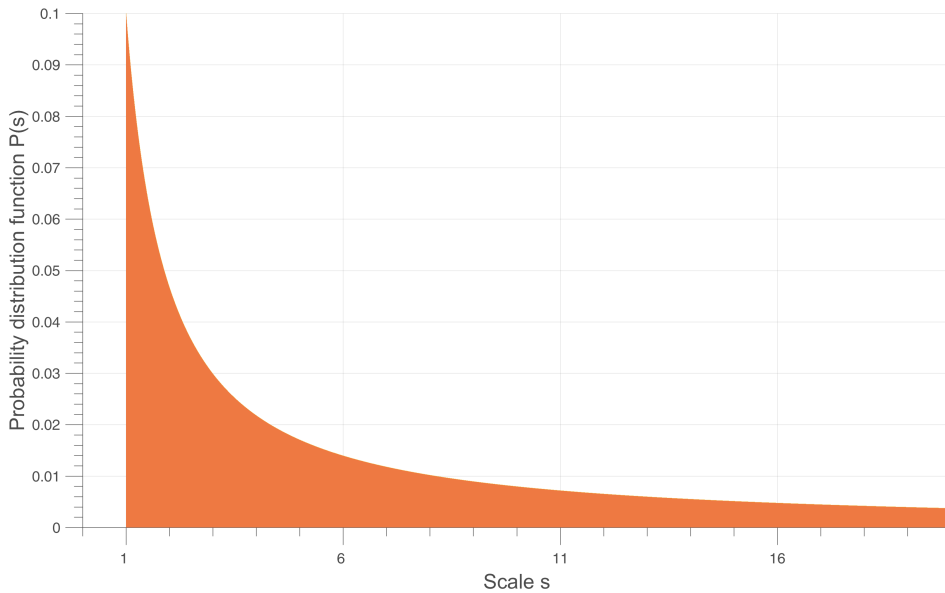


Figure 1: Weakening scales s probability distribution curve when $\beta = 1.5$

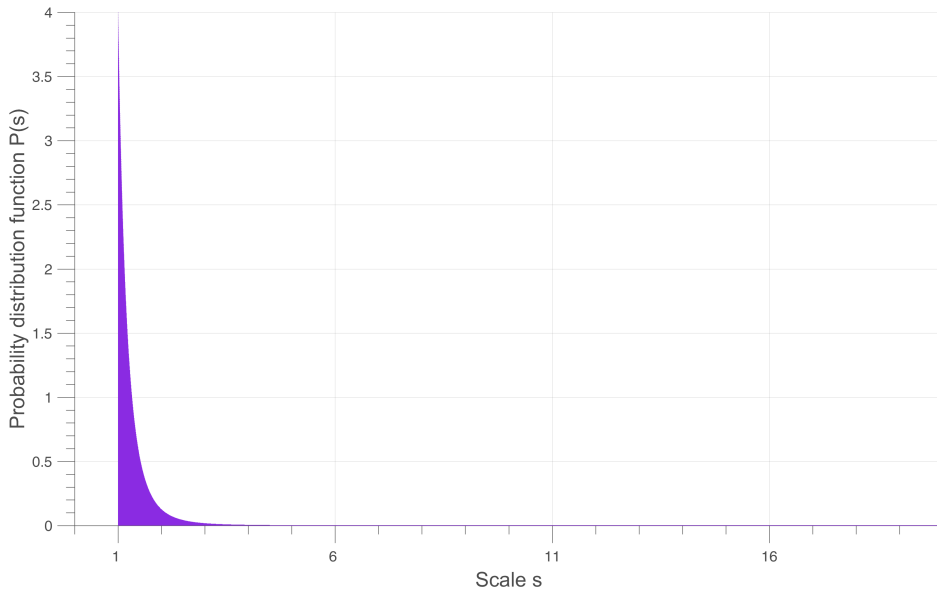


Figure 2: Weakening scales s probability distribution curve when $\beta = 5$

2.3. Yield function with mean stress effect

Positive mean stress clearly reduces the fatigue life of the material. In design evaluation of multiaxial fatigue with mean stress, a simplified, conservative relation between mean stress and equivalent alternating stress is necessary. We can improve the model to come by modifying the yield function σ_y and the localization tensor.

The idea is to consider as in Maitournam and Krebs[19] that the yield limit σ_y can be reduced in presence of positive mean stress. The mesoscopic yield function at scale s can therefore be written as:

$$f(s) = \|\underline{\underline{S}}(s) - \underline{\underline{b}}(s)\| + (\lambda \Sigma_H - \sigma_y) / s \leq 0 \quad (2)$$

with $\underline{\underline{S}}$ denoting the deviatoric part of the stress tensor at microscale, and $\underline{\underline{b}}(s)$ the corresponding backstress at the same scale. The material remain in elastic regime when $f < 0$ and in plastic regime when $f = 0$.

2.4. Local plastic model

We can now describe the mesoscopic stress state. The model considers a plastic behavior at the mesoscopic scale. The mesoscopic stress evolution equations are thus:

$$\dot{\underline{\underline{S}}}(s, M, t) = dev \dot{\underline{\underline{\Sigma}}}(M, t) - \frac{E}{1 + \nu} \dot{\underline{\underline{\varepsilon}}}^p(s, M, t), \quad (3)$$

which defines a Taylor-Lin scale transition model with unit localization tensor[20]. It is complemented by

$$\dot{\underline{\underline{b}}}(s, M, t) = \frac{kE}{E_6 - k} \dot{\underline{\underline{\varepsilon}}}^p(s, M, t), \quad (4)$$

which is our kinematic hardening model, and by

$$\underline{\dot{\epsilon}}^p(s, M, t) = C \frac{\partial f(s, M, t)}{\partial \underline{S}}, \quad (5)$$

which is the associated plastic flow rule assuming $C = 0$ when $f < 0$ and $C \geq 0$ when $f = 0$.

Here E denotes the Young's modulus and k the hardening parameter. The local dissipated energy rate per unit volume at weakening scales s is given by the local entropy dissipation:

$$\dot{W}(s, M, t) = (\underline{S} - \underline{b})(s, M, t) : \underline{\dot{\epsilon}}^p(s, M, t). \quad (6)$$

3 Construction of an energy based fatigue approach

In a preliminary step, we will consider a simple macroscopic loading history $\underline{\Sigma}(M, t)$ which is uniaxial and time periodic of deviatoric amplitude S_a and constant mean stress Σ_H , and a Von Mises flow rule to see if we get a prediction of local failure for a number of cycles N_F varying as $S_a^{-\gamma}$.

In uniaxial cyclic loading, there will be 3 kinds of loading patterns, as is shown in Figure 3:

1. Elastic regime, in phase 2 and 4, where we have no plastic flow $\underline{\dot{\epsilon}}^p(s, M, t) = 0$, and where the stress is below the yield limit $|\underline{S} - \underline{b}| < (\sigma_y - \lambda \Sigma_H) / s$.
2. Plastic regime according to plastic flow rule, with increasing plastic deformation, in phase 5 and 1, where $\underline{\dot{\epsilon}}^p(s, M, t) = \xi \frac{\underline{S}(s) - \underline{b}(s)}{\|\underline{S}(s) - \underline{b}(s)\|} > 0$ with $\xi = \text{dev} \underline{\dot{\epsilon}} \left(\frac{kE}{E-k} + \frac{E}{1+\nu} \right)^{-1}$ (detailed in annex), $\underline{S} - \underline{b} = (\sigma_y - \lambda \Sigma_H) / s$ and $\dot{\underline{S}} - \dot{\underline{b}} = 0$.
3. Plastic regime in the other direction, in phase 3, where we now have $\underline{\dot{\epsilon}}^p(s, M, t) < 0$, then $\underline{S} - \underline{b} = -(\sigma_y - \lambda \Sigma_H) / s$ and $\dot{\underline{S}} - \dot{\underline{b}} = 0$.

In phase 1, a direct analysis yields the energy dissipation at scale s :

$$dW = (S - b) d\epsilon^p = \frac{(E - k)(1 + \nu)}{E(E + k\nu)} \frac{(\sigma_y - \lambda \Sigma_H)}{s} \left(S_a - \frac{(\sigma_y - \lambda \Sigma_H)}{s} \right). \quad (7)$$

A similar analysis yields

$$dW(\text{phase1}) = dW(\text{phase5}) = \frac{1}{2} dW(\text{phase3}).$$

We can then calculate the local dissipated energy W at point M during one cycle by cumulating the input of all sub-scales plastic regime with their probabilities [21].

$$\begin{aligned} W_{\text{cyc}} &= 4 \int_{(\sigma_y - \lambda \Sigma_H)/S_a}^{\infty} dW(s, M, t) P(s) ds \\ &= 4 \int_{(\sigma_y - \lambda \Sigma_H)/S_a}^{\infty} \frac{(E - k)(1 + \nu)}{E(E + k\nu)} \frac{(\sigma_y - \lambda \Sigma_H)}{s} \left(S_a - \frac{(\sigma_y - \lambda \Sigma_H)}{s} \right) (\beta - 1) s^{-\beta} ds \\ &= \frac{4(E - k)(1 + \nu)(\beta - 1)}{E(E + k\nu)\beta(\beta + 1)} \frac{S_a^{\beta+1}}{(\sigma_y - \lambda \Sigma_H)^{\beta-1}}. \end{aligned} \quad (8)$$

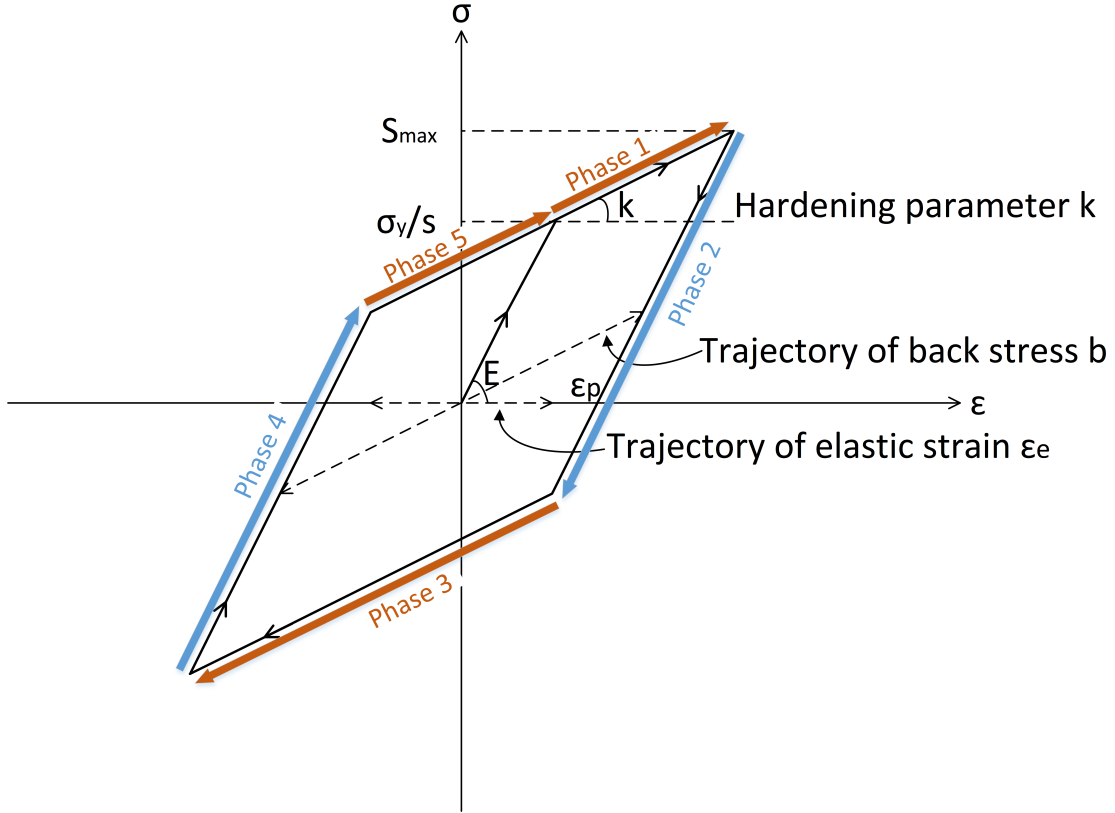


Figure 3: Uniaxial load with plastic dissipation

So we have a power law relationship between stress intensity and the dissipated energy per cycle.

$$W_{cyc} = C_1 S_a^{\beta+1}, \quad (9)$$

with

$$C_1 = f(\lambda, \beta) = \frac{4(E - k)(1 + \nu)(\beta - 1)}{E(E + kv)\beta(\beta + 1)(\sigma_y - \lambda\Sigma_H)^{\beta-1}}.$$

If the dissipated energy accumulates until a failure value W_0 , we can get directly the number of cycles to failure from Eq.(9) as:

$$N_F = \frac{W_0}{W_{cyc}} = \frac{W_0}{C_1} S_a^{-\beta-1}. \quad (10)$$

As for the time to failure in cyclic loading, it will be:

$$T_F = N_F t_{cyc}.$$

From Eq.(8), we then obtain that in uniaxial cyclic loading the model predicts as expected a power law dependence of the number of cycles to failure in function of S_a . However, experiments shows that the damage or the energy accumulation of a material evolves non-linearly in time. We should introduce below a method to handle such a nonlinearity.

4 Nonlinearity of damage accumulation

4.1. Energy approach with Chaboche law

The Chaboche law[22] is essentially a damage incremental law for cyclic loads with a deviatoric stress intensity A_{II} and hydrostatic mean part Σ_H , defining the damage increase by:

$$\delta D = \left(1 - (1 - D)^{\gamma+1}\right)^\alpha \left(\frac{A_{II}}{M(\sigma_H)(1 - D)}\right)^\gamma \delta N, \quad (11)$$

using an effective intensity $A_{II}^* = A_{II}/(1 - D)$ evolving with damage D . And the mean stress effect is present both in exponential factor α and in denominator $M(\sigma_H)$.

$$\alpha = 1 - a \left(\frac{\frac{1}{2}A_{II} - \sigma_{-1}M(\sigma_H)}{\sigma_u - A_{II}} \right),$$

$$M(\sigma_H) = M_0 (1 - 3c\sigma_{H,max}).$$

Eq.(11) writes equivalently:

$$\delta[1 - (1 - D)^{\gamma+1}]^{1-\alpha} = (1 - \alpha)(\gamma + 1) \left(\frac{A_{II}}{M(\Sigma_H)}\right)^\gamma \delta N = \frac{1}{N_F(\sigma)} \delta N. \quad (12)$$

Here $N_F(\sigma)$ denotes the number of cycles at intensity σ to failure as obtained by integration of Eq.(12) from $D = 0$ to $D = 1$.

Similar to Eq.(12), we define here the “equivalent damage” \tilde{D} (Figure 13) :

$$\tilde{D} = 1 - (1 - D)^{\gamma+1}, \quad (13)$$

with D the damage variable introduced by Chaboche in its model to scale the stress intensity:

$$A_{II} \longrightarrow \frac{A_{II}}{1 - D}.$$

We have

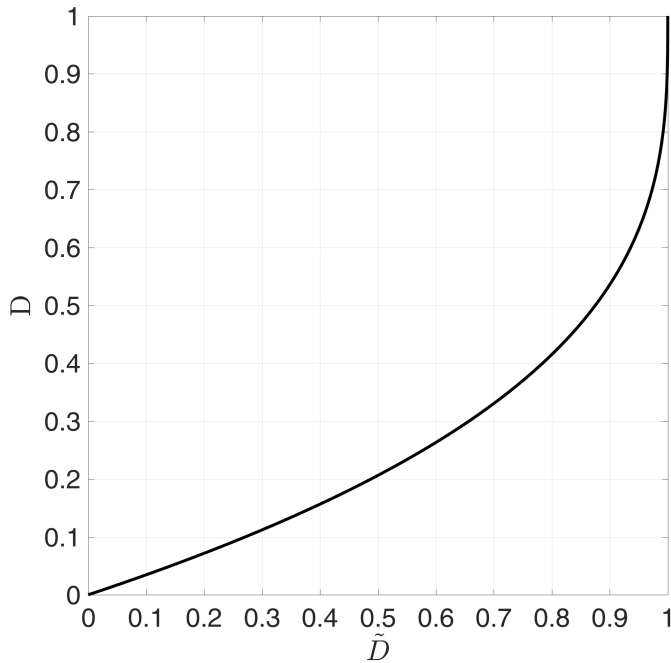
- $\tilde{D} = 0$ when $D = 0$ (undamaged material),
- $\tilde{D} = 1$ when $D = 1$ (failure of material),

and a nonlinear relation in between as in Figure 4:

$$\delta\tilde{D} = (\gamma + 1)(1 - D)^\gamma \delta D.$$

Change of damage measure $\tilde{D} = 1 - (1 - D)^{\gamma+1}$ makes the evolution (11) explicit. It writes

$$\frac{d\tilde{D}}{dN} = c_D \tilde{D}^\alpha \left(\frac{A_{II}}{M(\Sigma_H)}\right)^\gamma, \quad (14)$$

Figure 4: The relation between \tilde{D} and D when $\gamma = 2$

yielding after integration from $\tilde{D} = 0$ to $\tilde{D} = 1$ a number of cycles to fatigue at constant load given by

$$N_F = \frac{1}{(1-\alpha)} \left(\frac{A_H}{M(\Sigma_H)} \right)^{-\gamma}.$$

This method as written requires cycle counting which is difficult and technical for complex load histories. In addition, it allows only a limited influence of multiaxiality.

Now in our model we use the same growth rule as in Chaboche in cyclic load regime, but replace stress intensity by multiscale dissipated energy in Eq.(14), which removes cycle counting.

The evolution (14) then writes

$$\frac{d\tilde{D}}{dt} = \tilde{D}^\alpha \dot{W}/W_0,$$

or in a differential form

$$d\tilde{D} = \tilde{D}^\alpha \frac{dW}{W_0} = \tilde{D}^\alpha \frac{W_{cyc} dN}{W_0}. \quad (15)$$

The number of cycles to failure in constant loading case, obtained by integrating \tilde{D} from \tilde{D}_0 to 1 is then:

$$N_F = \frac{W_0}{(1-\alpha) W_{cyc}} \left(1 - \tilde{D}_0^{1-\alpha} \right),$$

with initial damage $D_0 = 0$, we finally get:

$$N_F = \frac{W_0}{(1-\alpha) W_{cyc}} = \frac{W_0}{(1-\alpha) C_1} S_a^{-\beta-1}. \quad (16)$$

From Eq.(16), we see $(-\beta - 1) = -\gamma$ is related to the slopes in S-N curve and that $\frac{W_0}{(1 - \alpha)C_1}$ defines the number of cycles to failure.

4.2. Sequence effect

Experiments show fatigue tests started with high stress then change to low stress has less fatigue life than the combination of high stress life proportion plus the low one. This phenomenon of sequence effect is load history dependent, so we need a stress induced parameter to describe it.

This is done in Chaboche with three ingredients:

1. a damage sensitive effective stress:

$$\sigma_D^{eff} = J_2(\underline{\Sigma})/(1 - D) = A_{II}/(1 - D);$$

2. a $(\sigma_D^{eff})^\gamma$ controlled law for damage growth

$$\frac{dD}{dN} = c_\gamma \tilde{D}^\alpha (\sigma_D^{eff})^\gamma;$$

3. a load dependence of exponent α (from 1 at zero load to 0 at large loads). In Chaboche model, the proposition of α is

$$\alpha = 1 - a \left\langle \frac{\sigma_{eq} - \sigma_{fatigue}}{\sigma_u - \sigma_{eq}} \right\rangle \quad (17)$$

in order to recover the proper high-low sequencing effect.

Many fatigue damage accumulation models are based on the two level loading experiments which is one of the basic random loading analysis. To facilitate the validation and interpretation of an α dependence on stress we use two-stress level loading, the specimen is firstly loaded at stress Σ_1 for T_1 cycles and then at stress Σ_2 for T_2 cycles until failure. We can then observe if the experimental results are satisfactory.

After a loading time T_1 , we cycle from $\tilde{D} = 0$ to $\tilde{D} = \tilde{D}_1$. By integrating Eq.(15), we get:

$$(1 - \tilde{D}_1)^{1-\alpha_1} = \frac{T_1}{T_{F1}}, \quad (18)$$

with T_{F1} the time to failure with this loading.

Then we cycle from $\tilde{D} = \tilde{D}_1$ to failure $\tilde{D} = 1$, which yields

$$1 - (1 - \tilde{D}_1)^{1-\alpha_2} = \frac{T_2}{T_{F2}}. \quad (19)$$

From Eq.(18) and Eq.(19), after elimination of $(1 - D_1)$ we get:

$$\frac{T_2}{T_{F2}} = 1 - \left(\frac{T_1}{T_{F1}} \right)^\eta, \quad (20)$$

with

$$\eta = \frac{1 - \alpha_2}{1 - \alpha_1}. \quad (21)$$

In the case of high-low loading sequence we have $\Sigma_1 > \Sigma_2$, which gives $\alpha_1 < \alpha_2$, so it comes to:

$$\eta = \frac{1 - \alpha_2}{1 - \alpha_1} < 1 \implies \frac{T_2}{T_{F2}} = 1 - \left(\frac{T_1}{T_{F1}} \right)^\eta < 1 - \frac{T_1}{T_{F1}} \implies \frac{T_1}{T_{F1}} + \frac{T_2}{T_{F2}} < 1.$$

The α dependence on stress intensity does therefore predict a sequencing effect where a low loading sequence following a high one will reduce the life of the structure.

To get the same effect in our construction, we propose here to introduce s_{min} , which is the minimum scale that experiences plastic dissipation thus causes energy loss:

$$s_{min} = \frac{(\sigma_y - \lambda \Sigma_H)}{S_a}. \quad (22)$$

We propose a load dependent α through s_{min} . Possible choice of α is expressed as Eq.(23):

$$\alpha = 1 - a \left(\frac{\frac{1}{s_{min}}}{1 - \frac{1}{s_{min}}} \right). \quad (23)$$

There is no notion of fatigue limit in our model, $\sigma_{fatigue} = 0$. The intensity of loading

$$\frac{\sigma_{eq} - \sigma_{fatigue}}{\sigma_u - \sigma_{eq}} = \frac{1}{\frac{\sigma_u}{\sigma_{eq}} - 1}$$

is measured by

$$\left(\frac{\frac{1}{s_{min}}}{1 - \frac{1}{s_{min}}} \right) = (s_{min} - 1)^{-1}.$$

This means that we measure the distance of load to ultimate failure by local variable s_{min} through

$$\frac{\sigma_u}{\sigma_{eq}} - 1 \longrightarrow (s_{min} - 1)$$

We can see from Figure 5 that cycling 1 for fifty percent of its failure time leaves a reserve before failure to cycle 2 much less than fifty percent. To conclude, the cumulative damage under high-low loading sequence, as we deduced, has the addition of partial lives less than unit. Similarly, the cumulative damage under low-high loading sequence has addition of partial lives more than 1

$$\frac{T_1}{T_{F1}} + \frac{T_2}{T_{F2}} > 1.$$

The curve is depicted in Figure 5. For constant two-level stress loading, $\alpha_1 = \alpha_2$, the Chaboche law returns to the Miner rule where:

$$\frac{T_1}{T_{F1}} + \frac{T_2}{T_{F2}} = 1.$$

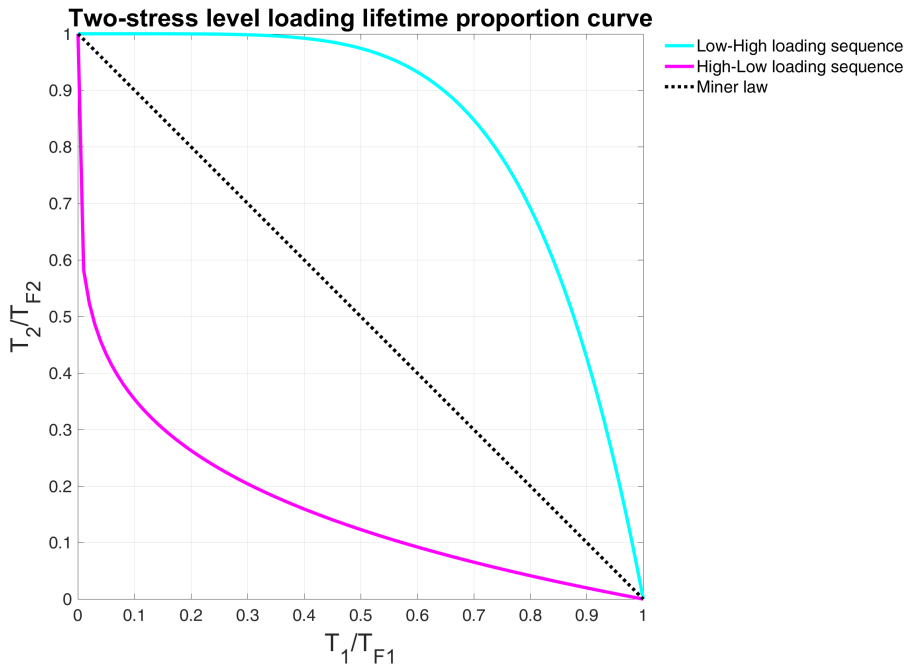


Figure 5: High to low and low to high loading sequence comparison (with the proposed model)

4.3. The final model

In summary, our damage based fatigue life criterion using a damage evolution governed by a multiscale plastic energy dissipation, has four ingredients.

- a scale dependent yield limit

$$\frac{1}{s}(\sigma_y - \lambda \Sigma_H^{macro})$$

associated to a microscopic plastic evolution governed by the standard plastic evolution laws Eq.(3) - Eq.(5);

- a multiscale plastic energy dissipation

$$\dot{W}(M, t) = \int_{s=1}^{\infty} \left(\underline{S} - \underline{\underline{b}} \right) (s, M, t) : \underline{\underline{\dot{\varepsilon}}}^p (s, M, t) s^{-\beta} ds; \quad (24)$$

- a load intensity sequencing effect that we have represented by the formula :

$$1 - \alpha = a(s_{min} - 1)^{-\beta}; \quad (25)$$

- a exponential damage evolution law :

$$\frac{d\tilde{D}}{dt} = \tilde{D}^\alpha \dot{W}/W_0. \quad (26)$$

In this model we have four independent coefficients in addition to the construction of the local plastic model Eq.(3) - Eq.(5) :

1. reference density of damage energy : W_0 (in MPa)
2. mean stress effect coefficient : λ
3. slope of SN curve : $\beta + 1$
4. sensitivity to load intensity a .

5 Numerical strategy

5.1. Scale discretization

Our first approach takes one cycle as unit time. We compute analytically the energy dissipation at each scale during this cycle. The method is valid for simple loading history and which includes the integration on all weakening scales. The damage \tilde{D} is then accumulated after each cycle by numerical integration of Eq.(26).

However, there are certain limitations of this method. Firstly we need a load history decomposition in cycles. Secondly in real life the perfect close loop cycle is hardly applicable. Finally, we need to compute the average α per cycle.

Thus we propose in a more general method which can be integrated by a step by step strategy. We compute numerically the dissipation at different scales using an implicit Euler time integration of the constitutive laws of section 2.4. After which we make a numerical integration on different scales. Then we can update the damage and go to next time step.

Instead of doing the scale integration directly which can be difficult for complex loading, the Gaussian Quadrature rule with Legendre points is used to give the value of local dissipated energy rate.

To use the Gaussian quadrature rule the limit range of integral must be from -1 to 1 , while the total dissipated energy is expressed by integrating all the weakening scale s ranging from 1 to infinity with their occurrence probabilities:

$$\dot{W} = \int_1^\infty \dot{w}(s)(\beta - 1)(s)^{-\beta} ds.$$

To change the limit range of integral from $[1, \infty]$ to $[1, 0]$ we take as new integration variable $u(s) = s^{1-\beta}$. Therefore the dissipated energy summed on all scales is:

$$\begin{aligned} \dot{W} &= \int_1^\infty \dot{w}(s)(\beta - 1)(s)^{-\beta} ds \\ &= \int_0^1 \dot{w}(u^{\frac{1}{1-\beta}}) du \\ &= \frac{1}{2} \int_{-1}^1 \dot{w}\left[\left(\frac{x+1}{2}\right)^{\frac{1}{1-\beta}}\right] dx \end{aligned} \quad (27)$$

given $u = \frac{x+1}{2}$. So the dissipated energy rate integrated over all scales takes the form of Eq.(28):

$$\dot{W} = \frac{1}{2} \int_{-1}^1 \dot{w}\left[\left(\frac{x+1}{2}\right)^{\frac{1}{1-\beta}}, t\right] dx \approx \frac{1}{2} \sum_i \omega_i \dot{w}\left[\left(\frac{x_i+1}{2}\right)^{\frac{1}{1-\beta}}, t\right], \quad (28)$$

where ω_i and x_i are respectively the weights and nodes of the Gauss Legendre integration rule used for the numerical integration. In this work, we used 64 points[23] with $s_i = \left(\frac{x_i+1}{2}\right)^{\frac{1}{1-\beta}}$ being the associated scale.

5.2. Local plastic dissipation

The material could be both in elastic and plastic regime at different scales. To be more elaborate, we reuse the fundamental equations in different regimes. At scale s , we have a dissipation rate given by:

$$\dot{w}(s) = \left(\underline{\underline{S}} - \underline{\underline{b}} \right) : \dot{\underline{\underline{\epsilon}}}^p,$$

which differs between plastic and elastic regime.

Elastic regime:

There we have plastic strain rate $\dot{\underline{\underline{\epsilon}}}^p = 0$, back stress rate $\dot{\underline{\underline{b}}} = 0$ and deviatoric stress rate $\dot{\underline{\underline{S}}} = \text{dev} \dot{\underline{\underline{\Sigma}}}$, leading to

$$\dot{\underline{\underline{S}}} - \dot{\underline{\underline{b}}} = \text{dev} \dot{\underline{\underline{\Sigma}}},$$

meaning

$$\left(\underline{\underline{S}} - \underline{\underline{b}} \right) (t + dt) = \left(\underline{\underline{S}} - \underline{\underline{b}} \right) (t) + \text{dev} \dot{\underline{\underline{\Sigma}}} dt.$$

At each time step we define a trial stress:

$$\left(\underline{\underline{S}} - \underline{\underline{b}} \right)_{\text{trial}} := \left(\underline{\underline{S}} - \underline{\underline{b}} \right) (t + dt). \quad (29)$$

We are in elastic regime at scale s as long as we satisfy

$$\left(\underline{\underline{S}} - \underline{\underline{b}} \right)_{\text{trial}} \leq (\sigma_y - \lambda \Sigma_H) / s.$$

Plastic regime:

When we leave elastic regime at scale s , we have:

$$\left\{ \begin{array}{ll} \dot{\underline{\underline{\epsilon}}}^p = \xi \frac{\underline{\underline{S}} - \underline{\underline{b}}}{\| \underline{\underline{S}} - \underline{\underline{b}} \|}, \xi > 0, & \text{plastic flow,} \\ \| \underline{\underline{S}} - \underline{\underline{b}} \| = (\sigma_y - \lambda \Sigma_H) / s, & \text{yield limit,} \end{array} \right. \quad (30)$$

$$\left\{ \begin{array}{ll} \left(\underline{\underline{S}} - \underline{\underline{b}} \right) : \left(\dot{\underline{\underline{S}}} - \dot{\underline{\underline{b}}} \right) = 0, & \text{yield limit time invariance,} \end{array} \right. \quad (31)$$

$$\left\{ \begin{array}{ll} \dot{\underline{\underline{b}}} = \frac{kE}{E - k} \dot{\underline{\underline{\epsilon}}}^p, & \text{kinematic hardening rule,} \end{array} \right. \quad (32)$$

$$\left\{ \begin{array}{ll} \dot{\underline{\underline{S}}} = \text{dev} \dot{\underline{\underline{\Sigma}}} - \frac{E}{1 + \nu} \dot{\underline{\underline{\epsilon}}}^p, & \text{localisation rule.} \end{array} \right. \quad (33)$$

$$\left\{ \begin{array}{ll} \dot{\underline{\underline{S}}} = \text{dev} \dot{\underline{\underline{\Sigma}}} - \frac{E}{1 + \nu} \dot{\underline{\underline{\epsilon}}}^p, & \text{localisation rule.} \end{array} \right. \quad (34)$$

In all cases, we get

$$\left(\underline{\underline{S}} - \underline{\underline{b}} \right) (s, t + dt) = \frac{\left(\underline{\underline{S}} - \underline{\underline{b}} \right)_{\text{trial}} (s, t + dt)}{1 + \eta}, \quad (35)$$

with

$$\eta = \max \left\{ \underbrace{0}_{\text{elastic regime}}, \underbrace{\frac{\|\underline{S} - \underline{b}\|_{\text{trial}}}{(\sigma_y - \lambda \Sigma_H)/s} - 1}_{\text{plastic regime when this number is positive}} \right\},$$

$$(\underline{S} - \underline{b})_{\text{trial}}(s, t + dt) = (\underline{S} - \underline{b})(s, t) + \text{dev} \dot{\underline{\Sigma}}(t) dt.$$

That is to say, when the structure is in elastic regime at time t and scale s , we have $(\underline{S} - \underline{b})(s, t) = (\underline{S} - \underline{b})_{\text{trial}}(s, t)$. Otherwise, if the norm of $(\underline{S} - \underline{b})_{\text{trial}}(s, t)$ is greater than the local yield limit $(\sigma_y - \lambda \Sigma_H)(1 - \tilde{D})^\delta / s$, $(\underline{S} - \underline{b})(s, t)$ will be projected on the yield limit.

Knowing the distinction between elastic and plastic regime under multiple scales, we compute the general expression of the dissipated energy rate.

$$\dot{w}(s) = (\underline{S} - \underline{b}) : \dot{\underline{\epsilon}}^p = \gamma \frac{(\sigma_y - \lambda \Sigma_H)}{s}. \quad (36)$$

From Eq.(??) and Eq.(??) in annex, we get:

$$\begin{aligned} E\gamma dt &= \left\langle \|\underline{S} - \underline{b}\|_{\text{trial}} - \frac{(\sigma_y - \lambda \Sigma_H)}{s} \right\rangle / \left(\frac{1}{1+\nu} + \frac{k}{E-k} \right) \\ &= \left\langle \|\underline{S} - \underline{b}\|_{\text{trial}} - \frac{(\sigma_y - \lambda \Sigma_H)}{s} \right\rangle \frac{(E-k)(1+\nu)}{(E+k\nu)}, \end{aligned} \quad (37)$$

where $\langle \rangle$ is Macaulay bracket symbol defined as $\langle m \rangle = 0$ if $m \leq 0$, otherwise $\langle m \rangle = m$.

We replace γ deduced from Eq.(37) in Eq.(36) to give the expression of local energy dissipation rate at scale s :

$$\dot{w}(s) dt = \frac{(E-k)(1+\nu)}{E(E+k\nu)} \left\langle \|\underline{S} - \underline{b}\|_{\text{trial}} - \frac{(\sigma_y - \lambda \Sigma_H)}{s} \right\rangle \frac{(\sigma_y - \lambda \Sigma_H)}{s}. \quad (38)$$

With Eq.(28), the final expression of energy dissipation W during time step dt writes:

$$\begin{aligned} W &= \dot{W} dt \\ &= \frac{1}{2} \sum_i \omega_i \dot{w} \left[\left(\frac{x_i + 1}{2} \right)^{\frac{1}{1-\beta}} \right] dt \\ &= \frac{(E-k)(1+\nu)}{2E(E+k\nu)} \sum_i \omega_i \left\langle \|\underline{S} - \underline{b}\|_{\text{trial}} - \frac{(\sigma_y - \lambda \Sigma_H)}{\left(\frac{x_i + 1}{2} \right)^{\frac{1}{1-\beta}}} \right\rangle \frac{(\sigma_y - \lambda \Sigma_H)}{\left(\frac{x_i + 1}{2} \right)^{\frac{1}{1-\beta}}}. \end{aligned} \quad (39)$$

The mean stress effect term in Chaboche model is $s_{-1} \left(1 - 3 \frac{\sigma_H}{\sigma_u} \right)$, where the fatigue limit at zero mean stress s_{-1} is reduced in the presence of σ_H . In our model, the yield limit decreases with positive mean stress.

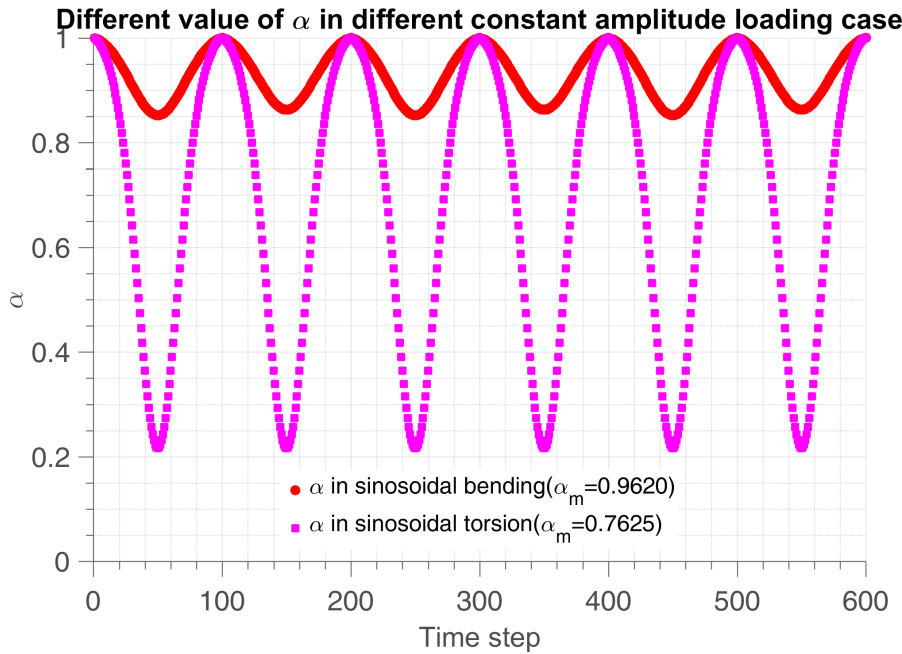


Figure 6: The evolution of α in bending and torsion with $\Sigma = \sigma_y/2$, $a = 0.3$ and 200 time steps in one cycle

5.3. Damage integration algorithm

Numerically if we divide one cycle into several number of steps, the change of α is extremely nonlinear with time. From Figure 6 we can see the mean value of α depends on loading pattern.

Because of the possible large variations in time of α , the evolution problem in damage is very nonlinear and thus, one needs to develop and validate an improved numerical time integration strategy at least for two specific cases: the constant amplitude case and the random load case.

We propose in constant amplitude load to numerically calculate W_{cyc} and the mean values of α through one cycle or several cycles(out-of-phase condition) and apply the result to life prediction by using Eq.(16):

$$N_F = \frac{W_0}{(1 - \alpha_m) W_{cyc}}, \quad (40)$$

which is obtained by direct integration of our damage law assuming time uniform dissipation in one cycle and frozen α . In this way the numerical cost is not as high as for the numerical implementation of all the loading points in random loading case.

Because of the symmetrical shape of the evolution of α , numerically the mean value of α does not strongly depend on the number of steps per cycle. In the verification process we have compared 100 ~ 1000 time steps per cycle.

For complex cyclic load cases, the idea is to accurately compute the history of plastic dissipation during one cycle (multiscale calculation with time refinement), and to use this precomputed result in the time

integration of the scalar damage evolution law with a time stepping which is adapted to the time variation of α .

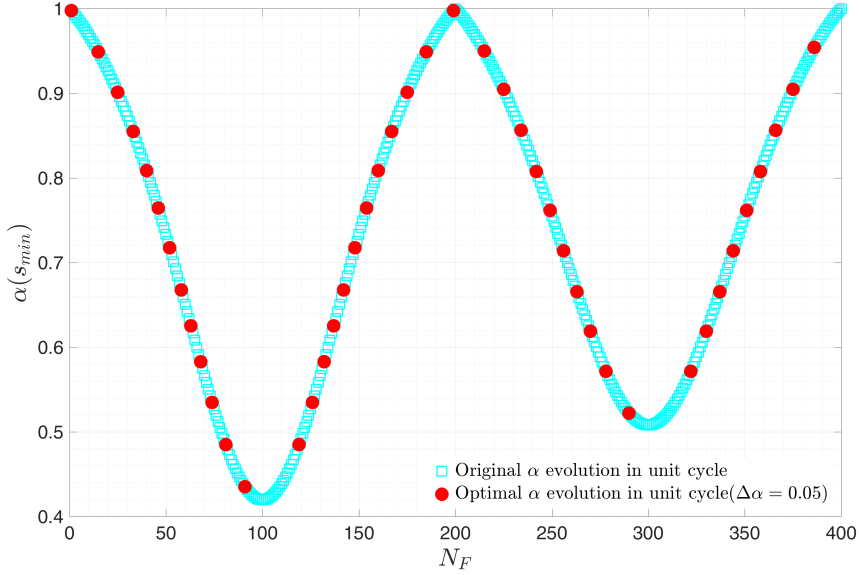


Figure 7: Comparing numerical strategy with optimal time steps in one cycle with the old one, in this way the number of steps in unit cycle is reduced from 400 to 35, meaning reduction factor=0.0875 (with $\Delta\alpha = 0.05$)

If α varies significantly, we use optimal time step numerical method to update D during one time step. In more details, let us suppose that our first few cycles calculation with fine time steps Δt has produced a sequence $\alpha(i)$ and $W_{cyc}(i)$ of exponent and dissipation at time $i\Delta t$.

We then construct an adaptive time stepping strategy with variable time steps $\Delta t_{ref}(j)$, reference exponent $\alpha_{ref}(j)$ and dissipated energy $W_{ref}(j)$ by regrouping together adjacent time steps $\Delta t(i)$ with similar exponents $\alpha(i)$. This sequence is incremented as follows.

For $t_{ref}(j)$ and $\alpha_{ref}(j) = \alpha(t_{ref}(j))$ given, we set

$$\Delta t_{ref}(j) = \sum_{\substack{t(i) \geq t_{ref}(j) \\ \|\alpha(i) - \alpha_{ref}(j)\| \leq \Delta\alpha}} \Delta t, \quad t_{ref}(j+1) = t_{ref}(j) + \Delta t_{ref}(j).$$

The same goes for the dissipated energy:

$$\Delta W_{ref}(j) = \sum_{\substack{t(i) \geq t_{ref}(j) \\ \|\alpha(i) - \alpha_{ref}(j)\| \leq \Delta\alpha}} W_{cyc}(i), \quad W_{ref}(j+1) = W_{ref}(j) + \Delta W_{ref}(j).$$

We finally use these new time steps with corresponding α_{ref} and W_{ref} to update the damage by looping on the new optimal time steps j and cycles N , and updating damage in each cycle by:

$$D = D + D^{\alpha_{ref}(j)} \frac{\Delta W_{ref}(j)}{W_0}.$$

Complexity analysis

The optimal time step method clearly reduces the numerical cost. Typically, we assume the material has fatigue life of 1×10^6 cycles to failure and we implement 1000 time steps in unit cycle. The reduction factor of points in unit cycle for example as in Figure 7 equals $35/400 = 0.0875$. We can then compare the cost between full numerical strategy and the new one.

Full numerical strategy:	$1000 \text{ time steps} \times 64 \text{ scales} \times 1 \times 10^6 \text{ cycles}$
Optimal cyclic strategy:	$1000 \text{ time steps} \times 64 \text{ scales} \times 5 \text{ cycles until stabilization}$ $+ 1 \times 10^6 \text{ cycles} \times (1000 \text{ time steps} \times \text{reduction factor})$
Ratio between optimal and full:	$\approx \frac{\text{reduction factor}}{64 \text{ scales}} = \frac{1}{731}$

The same strategy is applied to random loading situations which are made of repeated sequence of random loads:

- calculation of dissipated energy and exponent on one sequence;
- time coarsening;
- repeated integration of damage through the different sequences.

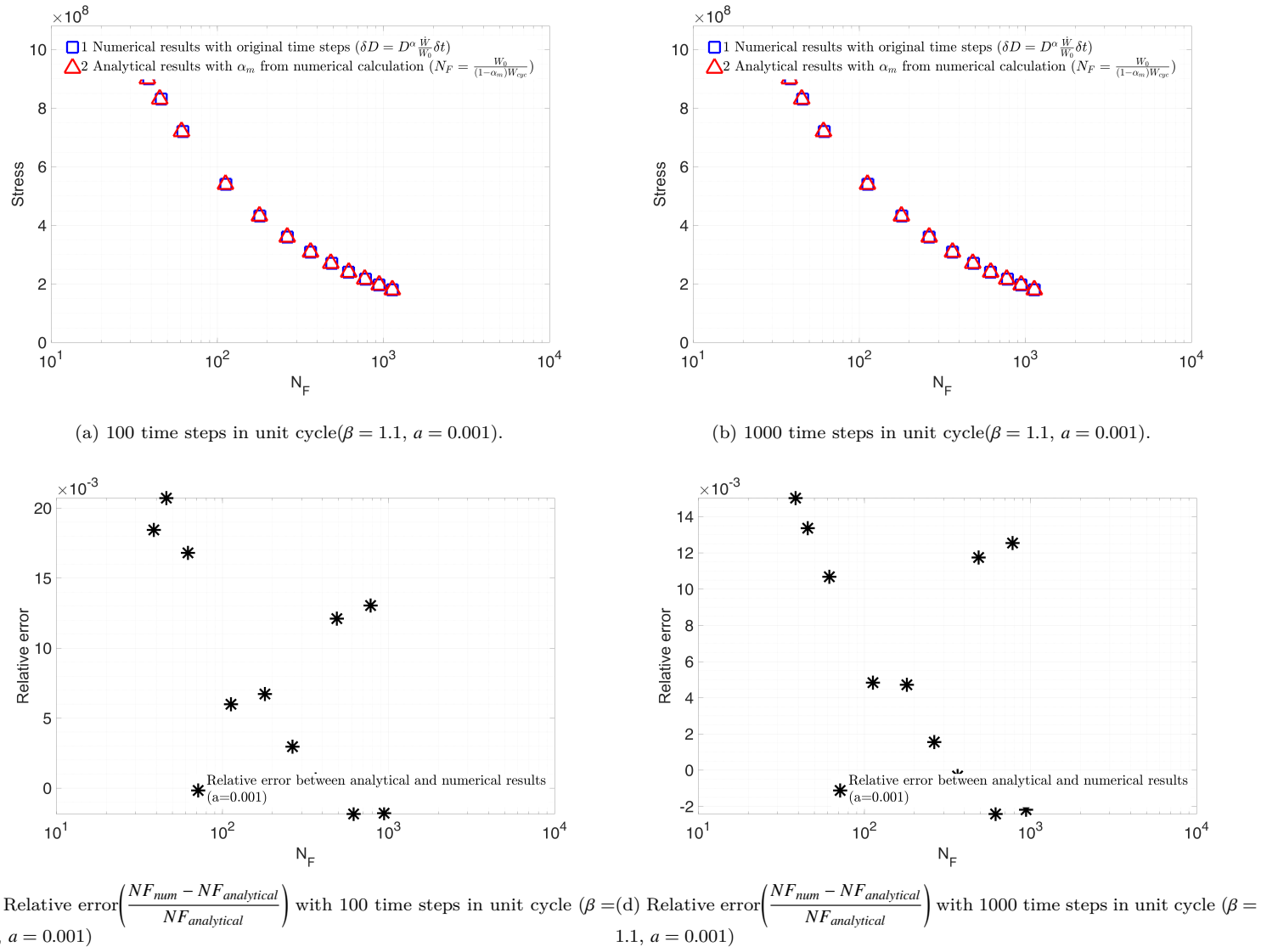


Figure 8: S-N curve of bending test on 30NCD16 steel using numerical and analytical method (Eq.(40)) with different time steps.

In Figure ?? we compare numerical and analytical formula using method 1 and 3 in the following description. After verifying the convergence between these two methods, to reduce numerical cost, we then study the convergence between method 2 and 1(Figure 9 to Figure 12)

1. Numerical results with varying α (equally divide time in unit cycle and do the scale integration all along the fatigue life time, which can be of high numerical cost)

$$\delta D = D^\alpha \frac{\dot{W}}{W_0} \delta t$$

2. Numerical results with optimal time steps(equally divide α , here we have $\Delta\alpha = 0.01$, to reduce time steps needed, after several cycles adaptation we iterate the recorded scalar values of α_{ref} , W_{ref} and t_{ref} to decide fatigue life time.)

$$\delta D = D^{\alpha_{ref}} \frac{W_{ref}}{W_0} \delta t_{ref}.$$

3. Analytical results after integration of D (with mean alpha from numerical strategy)

$$N_F = \frac{W_0}{(1 - \alpha_m)W_{cyc}},$$

which is derived from the differential equation

$$\delta D = D^{\alpha_m} \frac{W_{cyc}}{W_0} \delta N.$$

We can see the more time steps we divide in one cycle, the closer results between method 1 and method 2. This numerical validation results indicates, in constant amplitude loading, we are able to use the optimal numerical method 2 with mean value of α numerically calculated from the first several cycles, given there are sufficient time steps in unit cycle.

Although method 2 is much more numerically efficient than the original numerical method 1. It is still not cheap in the experimental fitting process. We need the analytical formula method 3 to do the fitting process. To validate the feasibility, we now compare only the analytical(method 3) one and optimal time steps(method 2) one. The results are shown in Figure 9 and Figure 10, the relation ship between relative error and $\Delta\alpha$ with 2000 time steps in unit cycle is shown in Figure 11 and Figure 12.

Now we can conclude that with more time steps in unit cycle, we get closer results with the original numerical method(method 2) in HCF regime. With smaller $\Delta\alpha$ value, we get less relative error between numerical(method 3) and analytical(method 1) results. This indicates that in constant amplitude cyclic loading, it is feasible to use the analytical formula, given α_m is calculated using sufficient large time steps and small $\Delta\alpha$ in the first several cycles.

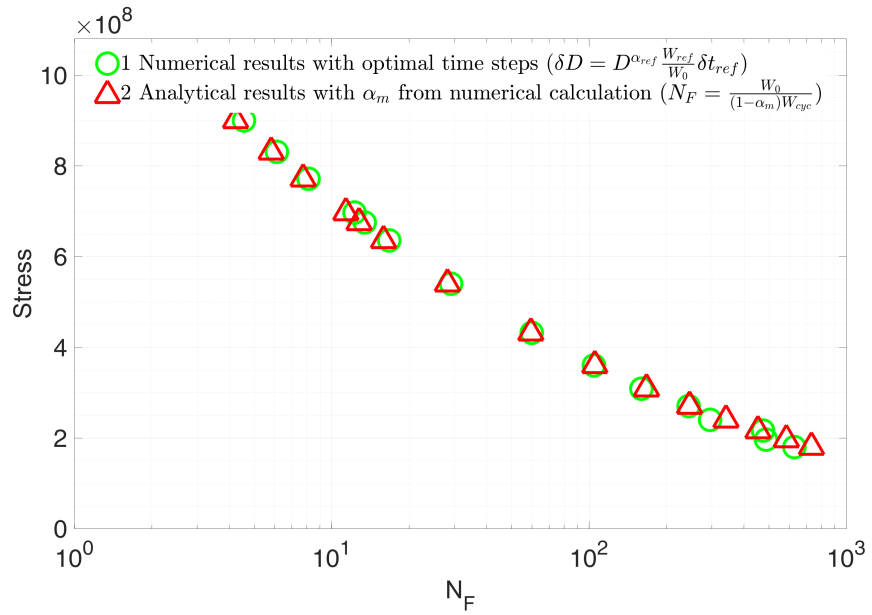


Figure 9: S-N curve using analytical and numerical results with optimal time steps methods ($\Delta\alpha = 0.02$ in unit cycle), yielding 200 full time steps reduced to 17 optimal time steps

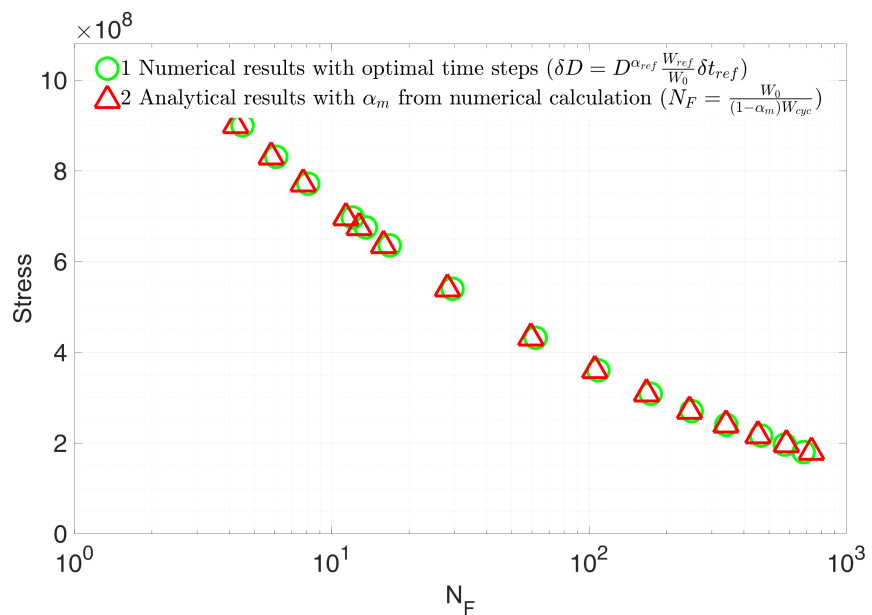


Figure 10: S-N curve using analytical and numerical results with optimal time steps methods ($\Delta\alpha = 0.01$ in unit cycle), yielding 200 full time steps reduced to 26 optimal time steps

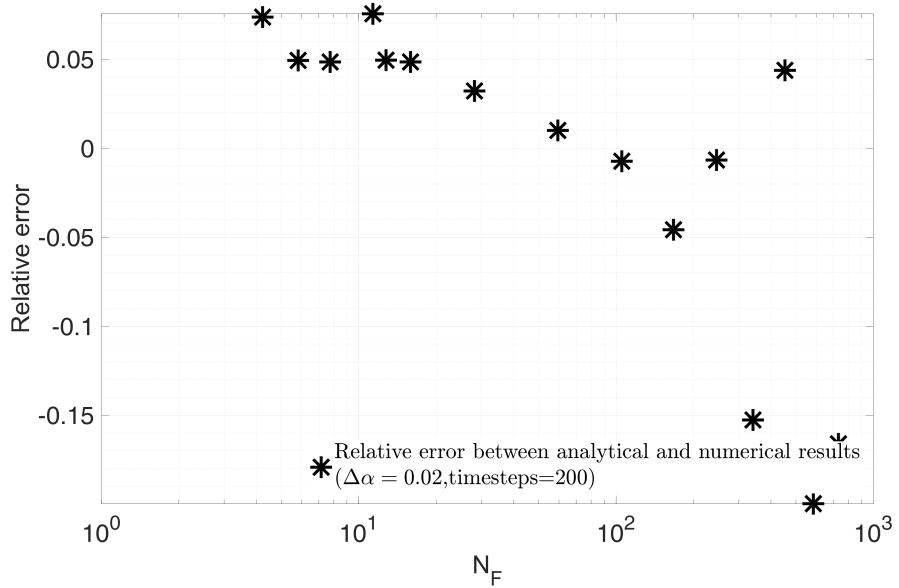


Figure 11: Relative error $\left(\frac{NF_{opt} - NF_{analytical}}{NF_{analytical}} \right)$ between analytical and numerical results with optimal time steps methods ($\Delta\alpha = 0.02$ in unit cycle)

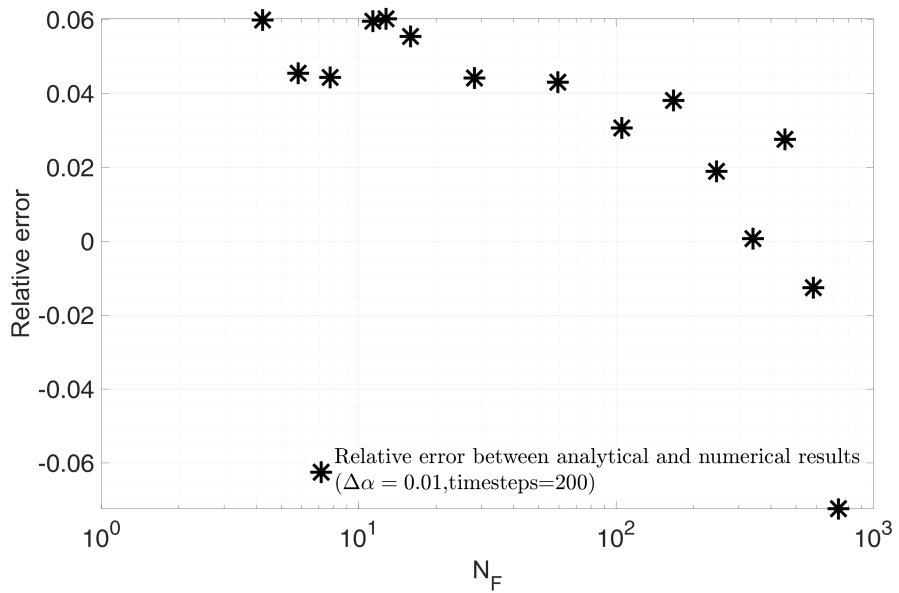


Figure 12: Relative error $\left(\frac{NF_{opt} - NF_{analytical}}{NF_{analytical}} \right)$ between analytical and numerical results with optimal time steps methods ($\Delta\alpha = 0.01$ in unit cycle)

6 Validation on recovery tests

6.1. Recovery of Chaboche law on cyclic loading

The test is first performed on a sinusoidal uniaxial load $\Sigma_{11}(t) = A\sin(t)$, giving a deviatoric amplitude $S_a(t) = \sqrt{J_{2,a}(\text{dev}\Sigma(t))}$ so that $S_a(t) = \left\| \sqrt{\frac{1}{3}}\Sigma_{11}(t) \right\|$. We use parameters in Table 1 to recover the classic Chaboche

law in cyclic loading.

Parameters	Value
Young's modulus	$E = 215$ GPa
Hardening parameter	$k = 1$ GPa
Weakening scales distribution exponent	$\beta = 1.2$
Hydrostatic pressure sensitivity	$\lambda_{+-} = 0$
Macroscopic yield stress	$\sigma_y = 416$ MPa
Sequencing effect sensitivity	$a = 0.5$
Dissipated energy to failure per unit volume	$W_0 = 3$ MJ(MPa)

Table 1: Material parameters in a simple cyclic load

We use matlab to numerically realize our analytical method. We plot $\|\underline{S} - \underline{b}\|_{trial}$ and $\|\underline{S} - \underline{b}\|$ at two different scales ($s_3 = 1.21$ and $s_{10} = 1.13$) as shown in Figure 13 and Figure 14. The local yield limit is reduced in the presence of positive hydrostatic stress whereas negative ones have beneficial effects.

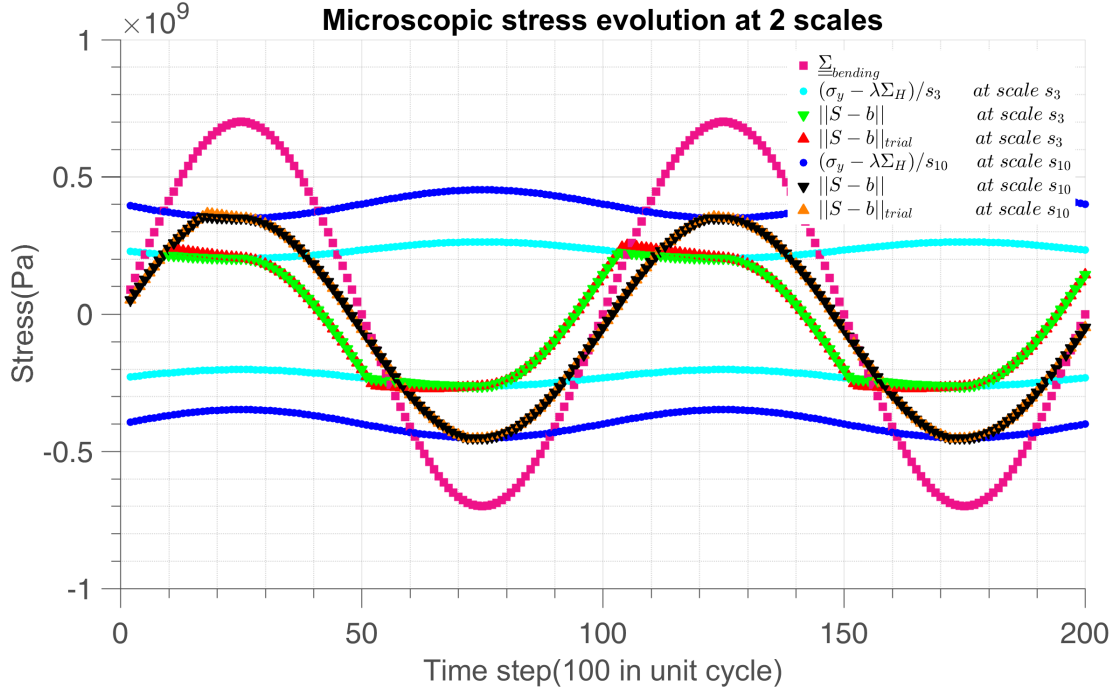


Figure 13: Microscopic $(\underline{S} - \underline{b})_{trial}$ and $(\underline{S} - \underline{b})$ evolution with time under different weakening scales ($s_3 = 1.21$ and $s_{10} = 1.13$) in sinusoidal load with zero mean stress

The dissipated energy per time step is depicted in Figure 15. We scale S_a in the plot to see more clearly the relation between energy dissipation and stress intensity. The choice of α does not affect W ; it only

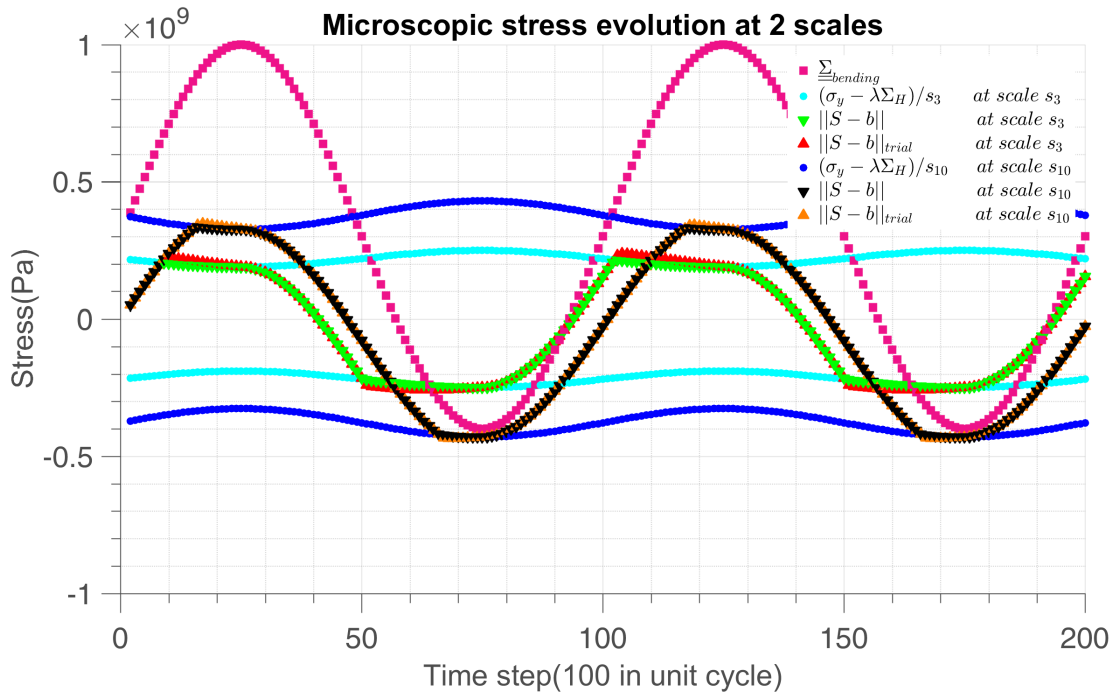


Figure 14: Microscopic $(\underline{\underline{S}} - \underline{\underline{b}})_{trial}$ and $(\underline{\underline{S}} - \underline{\underline{b}})$ evolution with time under different weakening scales ($s_3 = 1.21$ and $s_{10} = 1.13$) in sinusoidal load with non-zero mean stress

concerns damage accumulation rate. Smaller α causes faster accumulation.

The “jump” in energy evolution is due to activation of new scales while in-between two scales the dissipated energy follows the stress increment at each time step. In other words, because in our method the dissipated energy W (Figure 15), sums energy dissipation at all scales, any additional violation of $\|S - b\|_{trial}$ at local yield limit (Figure 13) introduces an additional dissipation.

We take the mean value of α during all the iteration process of numerical method as α_m . The energy and damage accumulation is shown in Figure 17 and Figure 20. Here we give 1000 time steps in one cycle to see the relative difference between changing α and α_m , also \dot{W} and $W_{cyc}/stepnumber$ method. The more time steps we give, the more precision we get. The relative difference between analytical energy loss and numerical one is shown in Figure 19 from which we conclude that the three methods converge in terms of elastic energy dissipation, but due to nonlinear effects the damage evolution does not have the same history per cycle. The frozen α delays damage, the varying α increases damage during the phase of strong loading.

The cyclic load calculation is only valid for very simple such as proportional loading in fatigue. However, the convergence of the two methods is based on the small value of β (close to 1), in case of large values of β (typically around 5), the numerical strategy gives shorter life than the analytical one due to extreme non-linearity. The relative error is around 20% as shown in Figure ?? and Figure ?? . Nevertheless the analytical formula can still be used as a comparison group to verify the numerical results. And in the identification

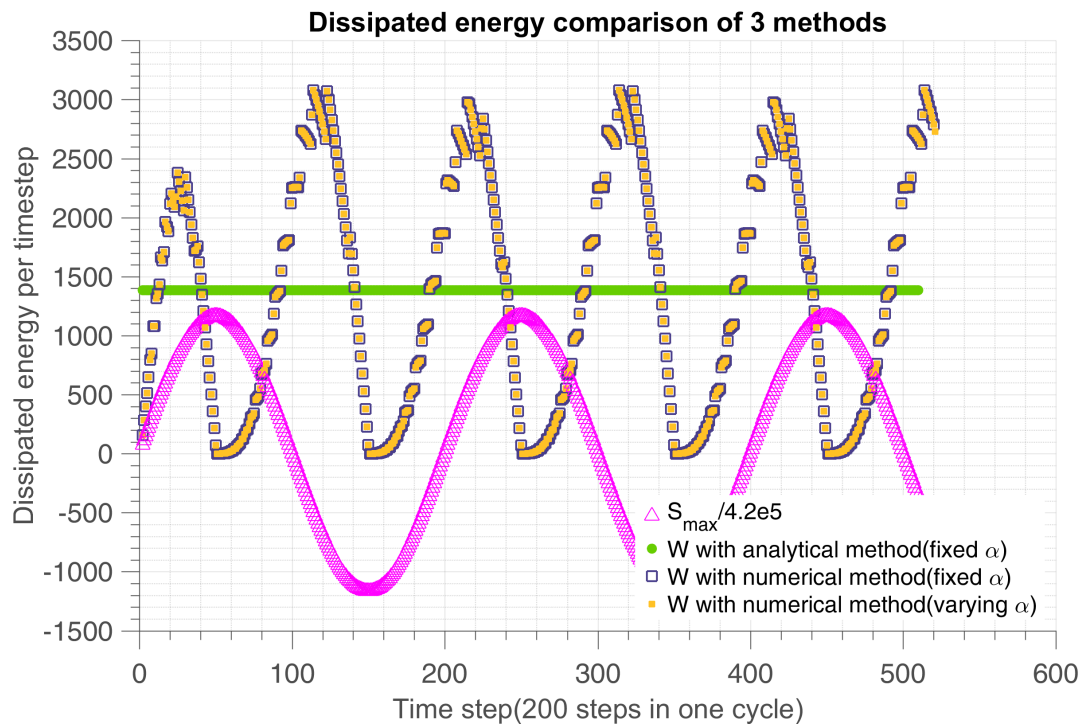


Figure 15: Validation of dissipated energy in all scales with analytical and numerical method

process we need the analytical form to fit the $S - N$ curve of a certain material. The outcome is satisfactory. Hence, to be more general for any loading history, we adopt the numerical method after identification of β .

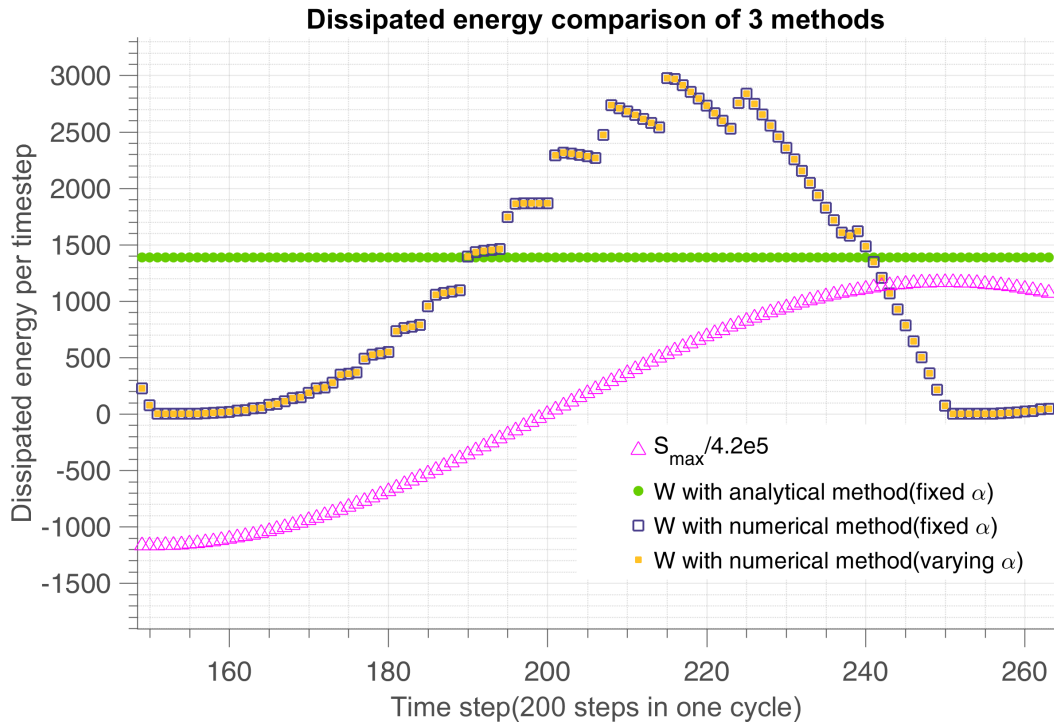


Figure 16: Validation of dissipated energy in all scales with analytical and numerical method(enlargement of Figure 15)

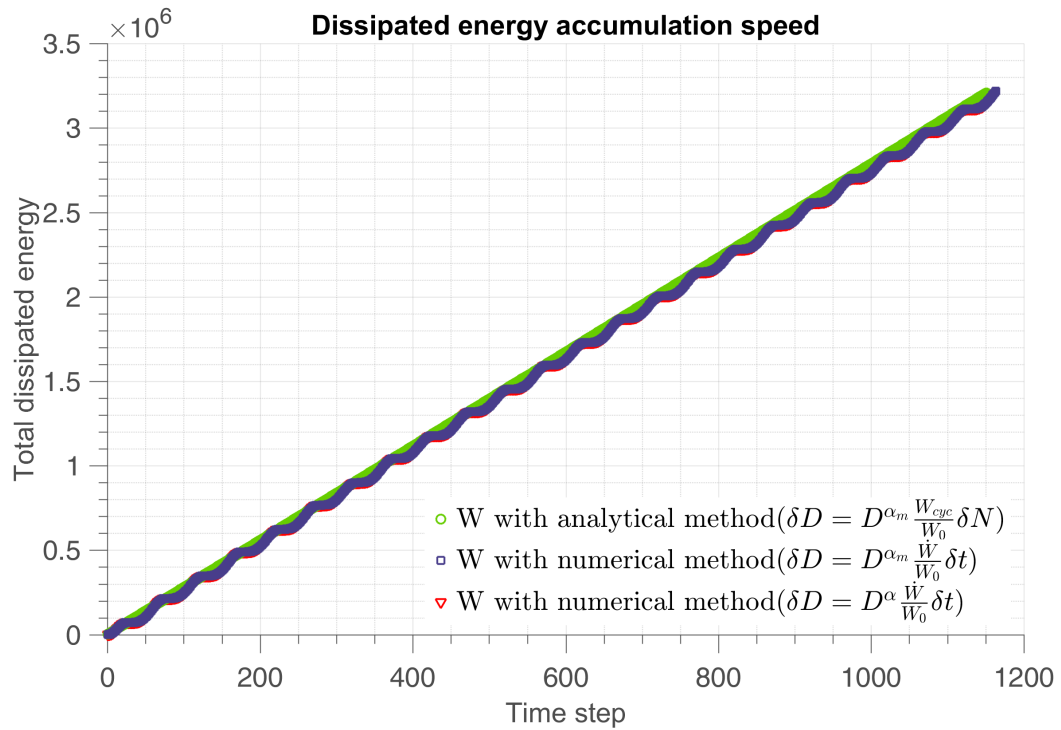


Figure 17: Dissipated energy accumulation through time with different methods, there are 1000 time steps in unit cycle

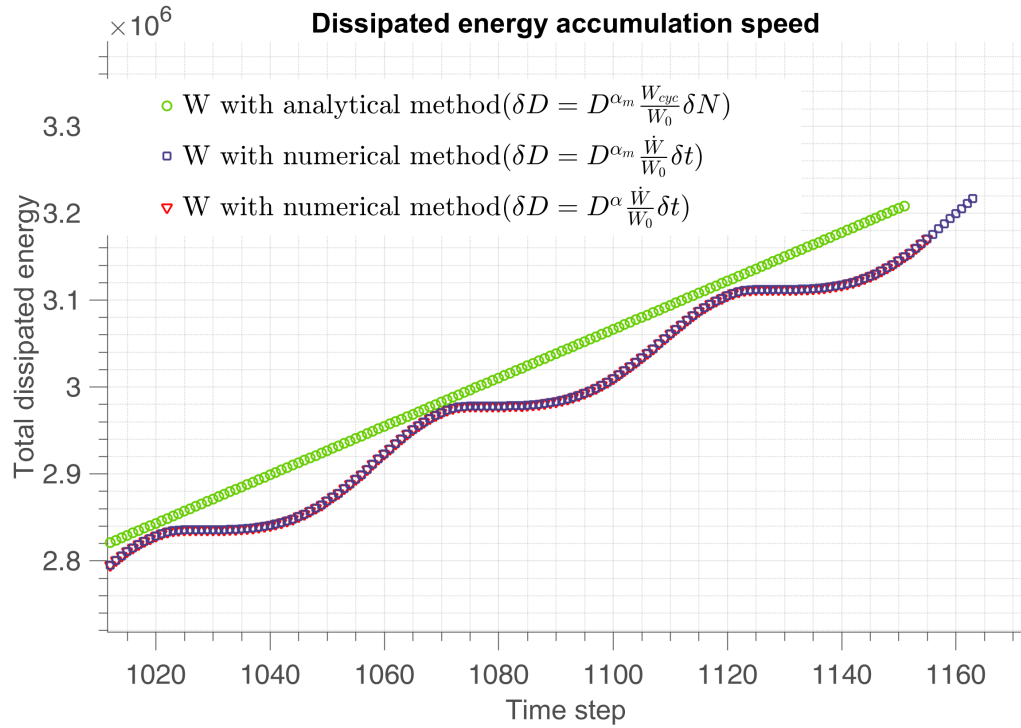
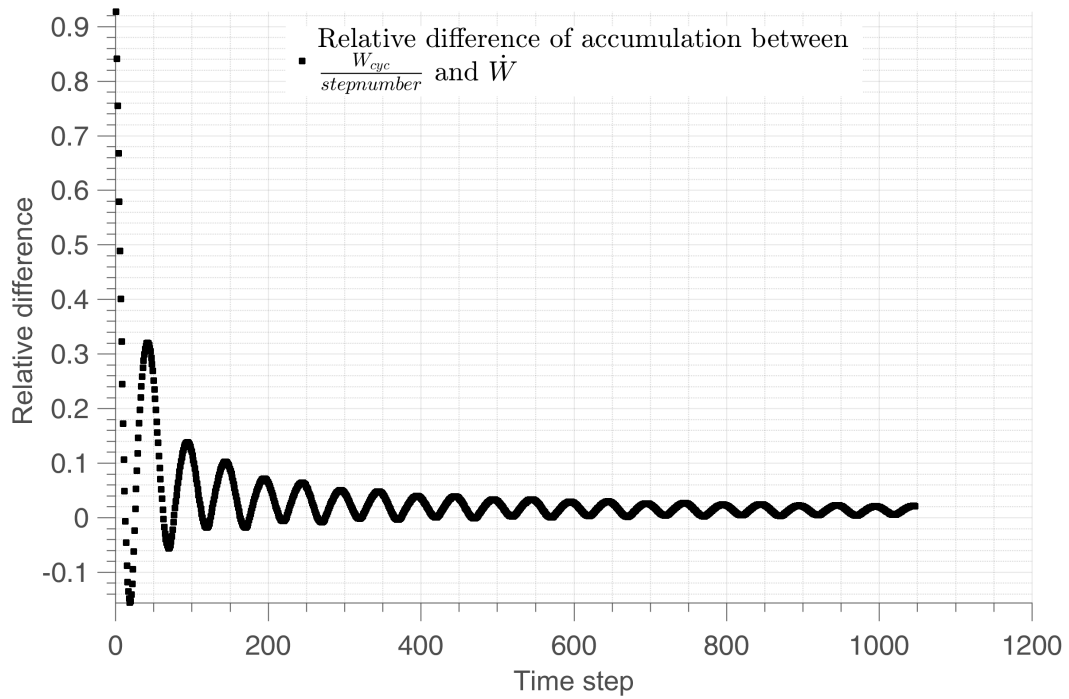


Figure 18: Dissipated energy accumulation through time with of 3 methods enlargement

Figure 19: Relative difference $\frac{W_{analytical} - W_{numerical}}{W_{analytical}}$ between analytical energy loss and numerical one with α varying with time

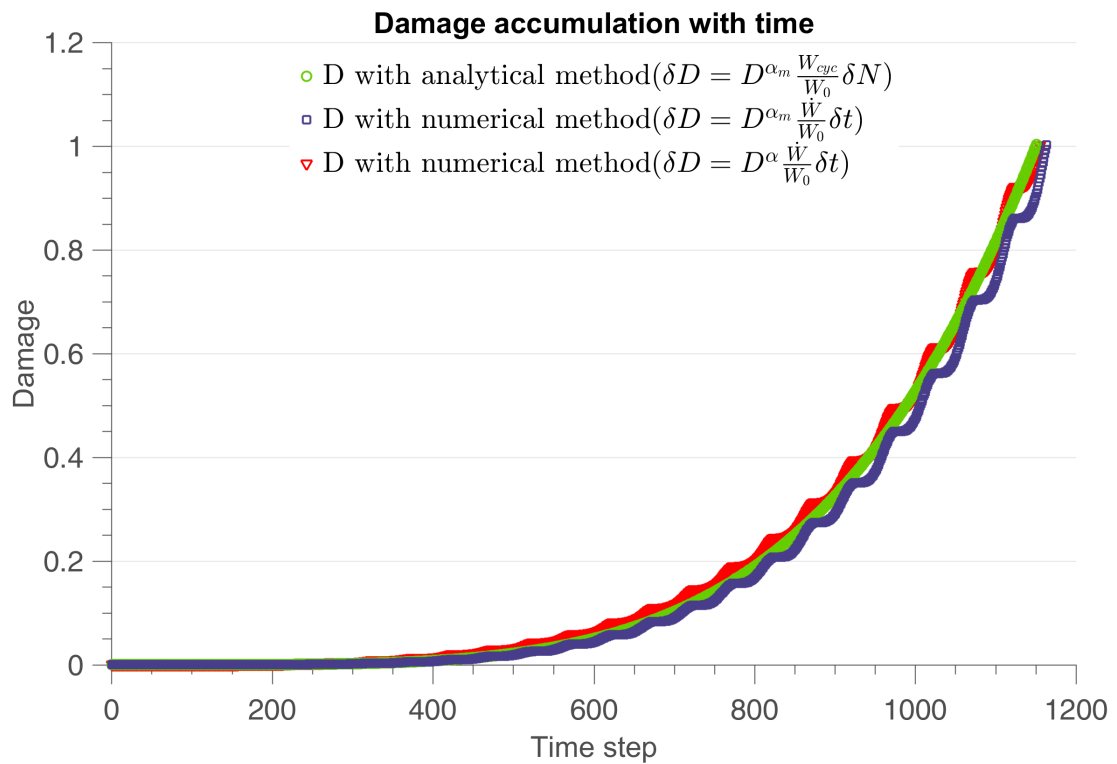


Figure 20: Damage evolution with time under sinusoidal load with different methods, there are 1000 time steps in unit cycle

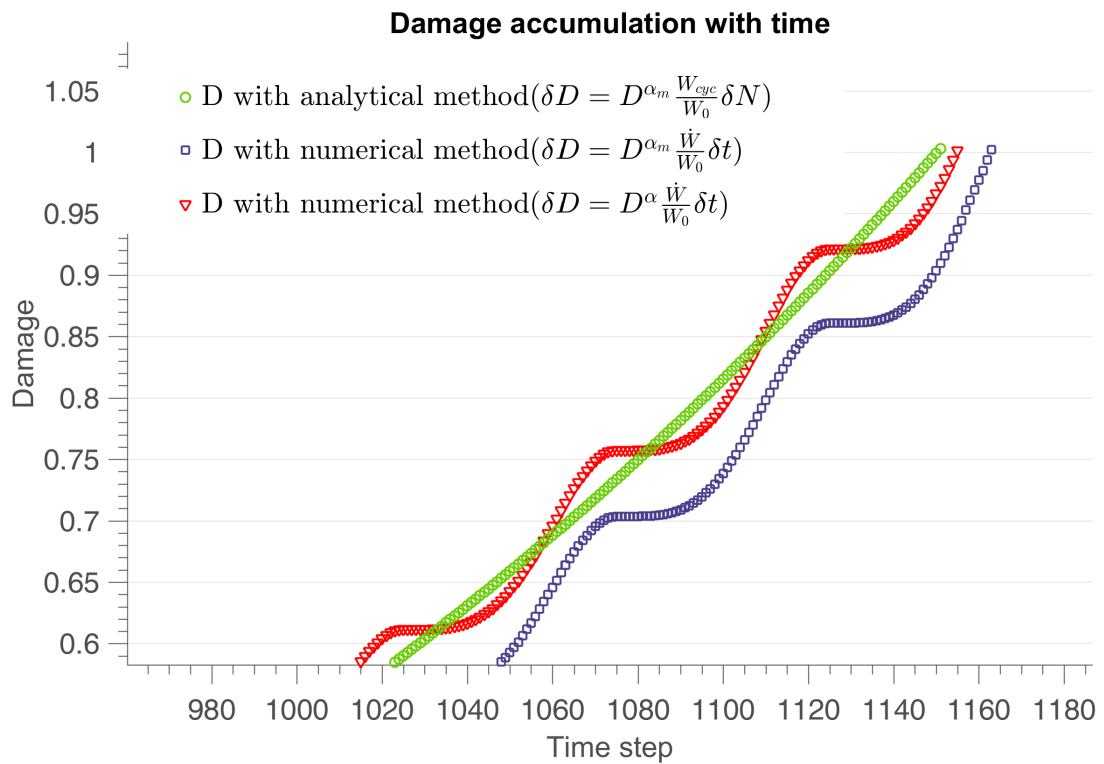


Figure 21: Damage evolution with time under sinusoidal load with two different methods enlargement

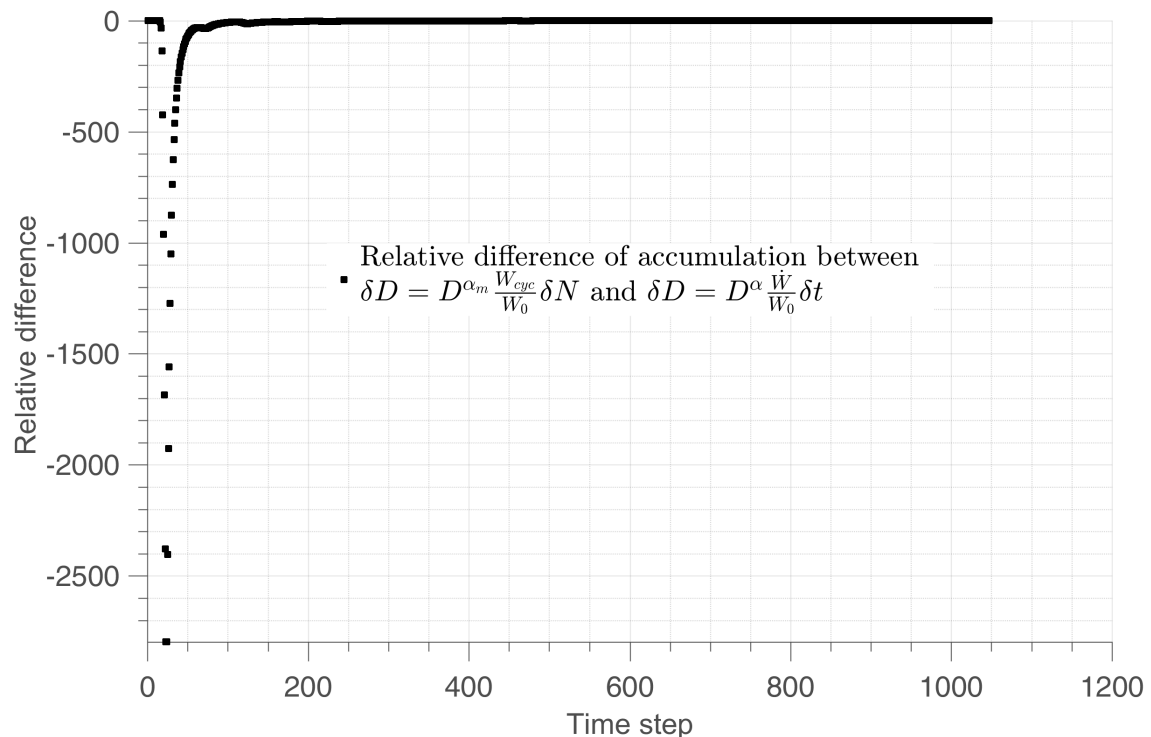


Figure 22: Relative difference $\frac{D_{analytical} - D_{numerical}}{D_{analytical}}$ evolution with time

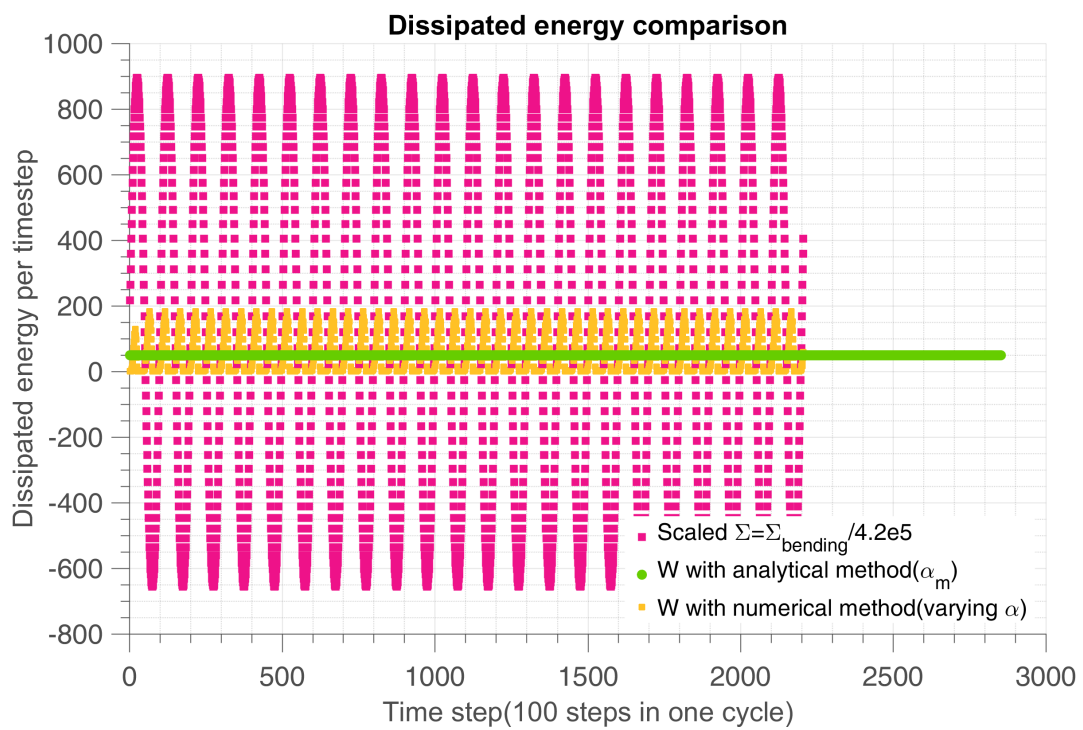


Figure 23: Validation of dissipated energy in all scales with analytical and numerical method with $\beta = 5$

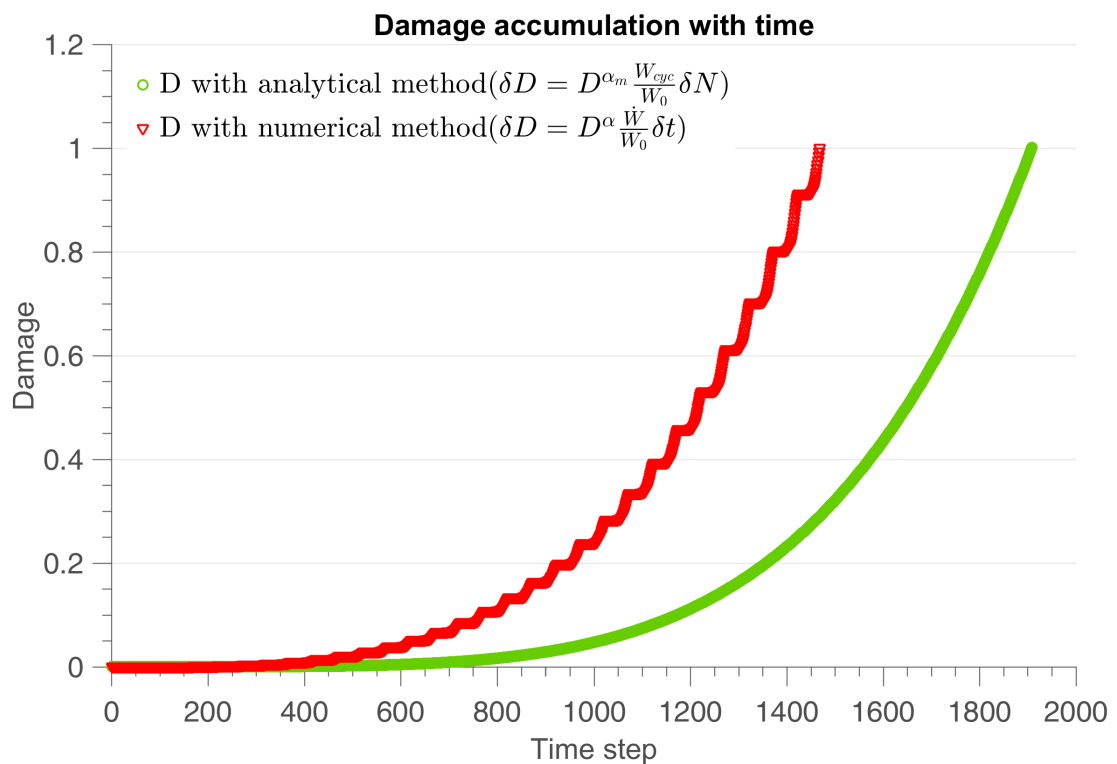


Figure 24: Damage evolution with time under sinusoidal load with $\beta = 5$, there are 100 time steps in unit cycle

6.2. Numerical recovery of sequence effect

We adopt the parameter α to take into account the sequence effect. The high-low loading sequence clearly reduces the fatigue life, as depicted in Figure ???. In order to cover this phenomenon, we let α change with time. Here a is the sequence effect sensitivity. According to Eq.(22), we have:

$$s_{min}(t) = \frac{\Sigma_y - \lambda \Sigma_H(t)}{S_a(t)},$$

which is the minimum weakening scale that activates energy loss. We use a general law for α of the type $\alpha = \alpha(s_{min})$ with the idea that for us s_{min} is a measure of present intensity of macroscopic stress. It is therefore a mechanical based stress norm.

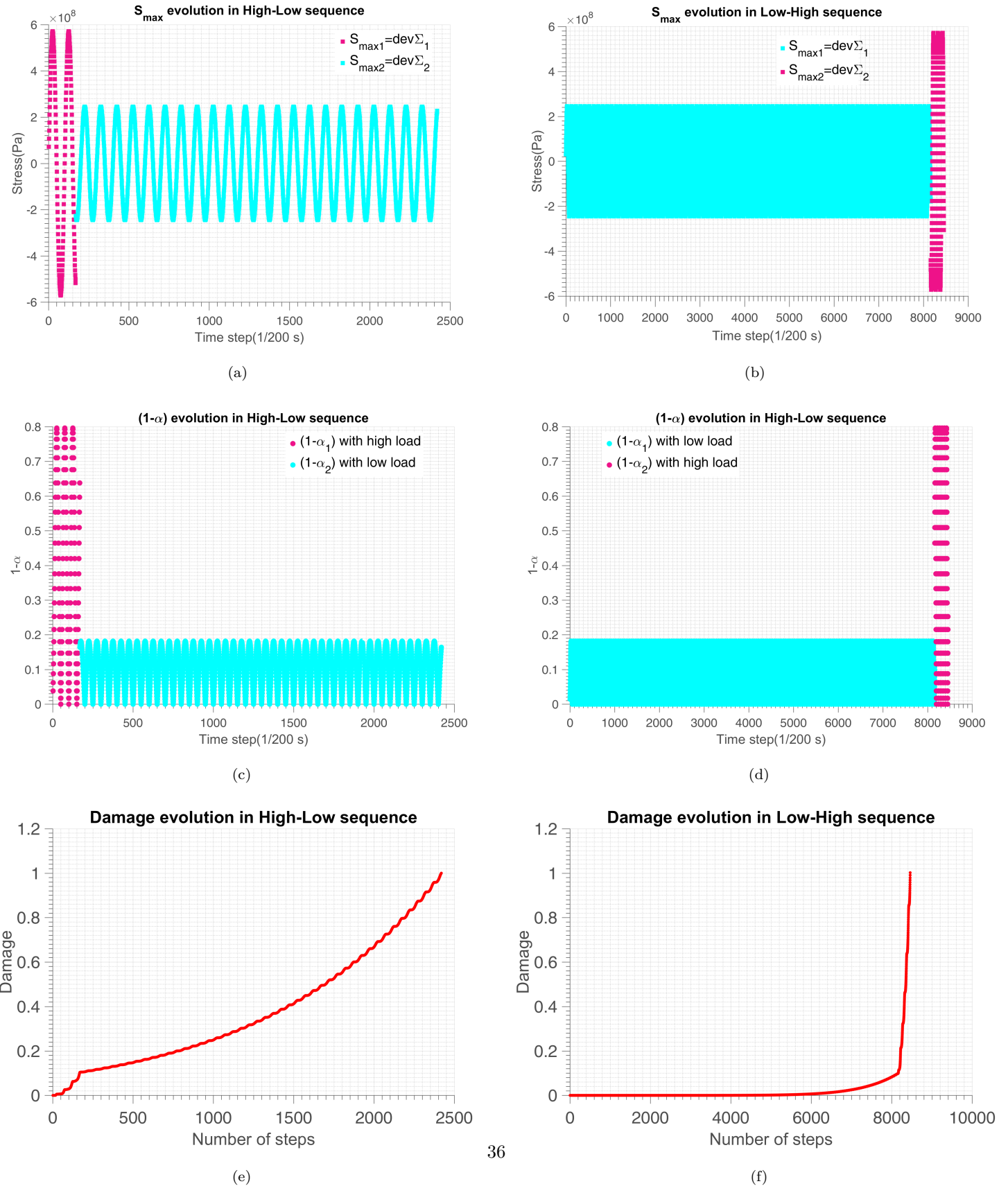


Figure 25: Two level sequence effect. By comparing the vertical figures we can see high stress gives high $(1-\alpha)$ value which causes fast damage accumulation speed. The evolution of $(1-\alpha)$ is highly nonlinear and follows the value of stress at each time step.

6.2.1. Major damage effect

To see the influence of sequence effect factor of α , we first fix α for all tests to see the results. When α is fixed, it becomes denominator in the final expression of N_F (Eq.(16)) and has the same impact as W_0 . We find that the fatigue life of random loading is widely dispersed (Figure 24). In this case we need to use $\alpha = f(s_{min})$ which evolves with time to make large stress intensity deal more damage.

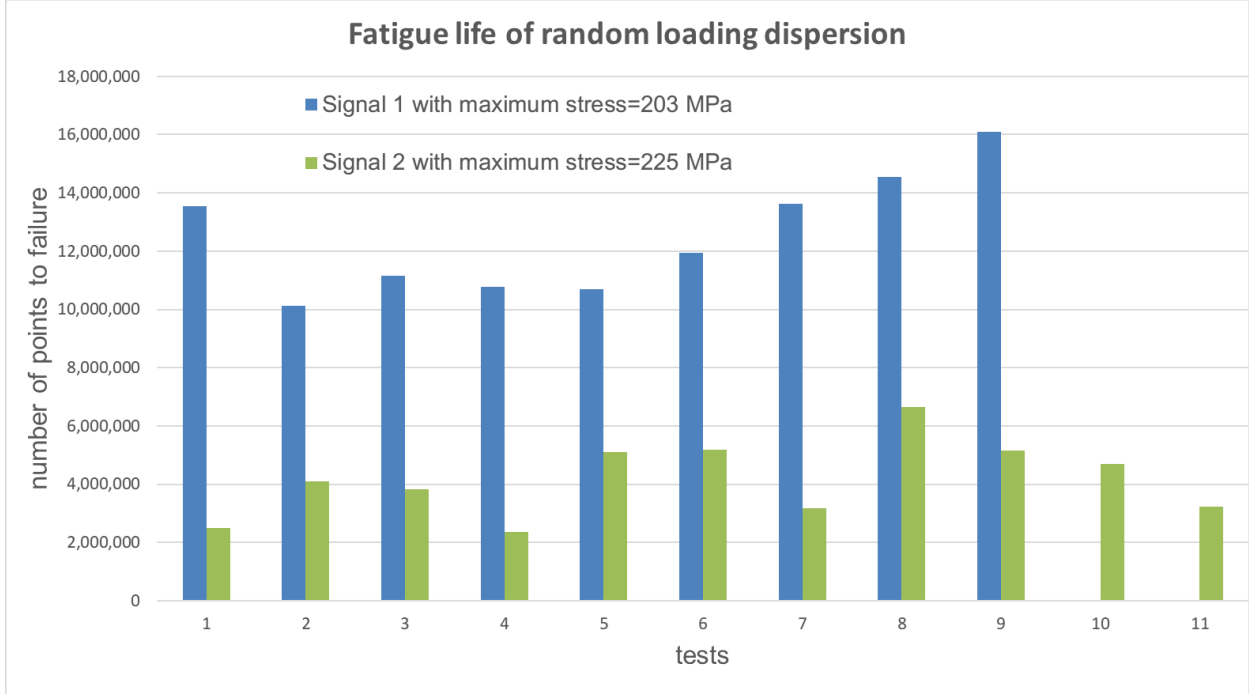


Figure 26: Fatigue life of random loading dispersion

After comparison with the experimental data we find out that large stresses cause much more damage than the smaller ones. It is necessary to include this major stress induced damage to our stress intensity parameter α . With the new α used in Eq.(25) compared to Eq.(23) we are able to calibrate our model better with the experimental results by using

$$\alpha = 1 - a \left(\frac{\frac{1}{s_{min}}}{1 - \frac{1}{s_{min}}} \right)^{1.1}. \quad (41)$$

We use the power to magnify large stress impact and minify lower stress damage. The demonstration of major damage effect using magnification power is depicted in Figure 25. With larger value of power, the sequence effect is more significant(bigger dispersion between high-low and low-high sequence).

The larger value of S_a causes more damage in the presence of the power β , leading to faster increase of

$$(1 - \alpha) = a \left(\frac{\frac{1}{s_{min}}}{1 - \frac{1}{s_{min}}} \right)^1 \cdot 1 = a(s_{min} - 1)^{-1.1}.$$

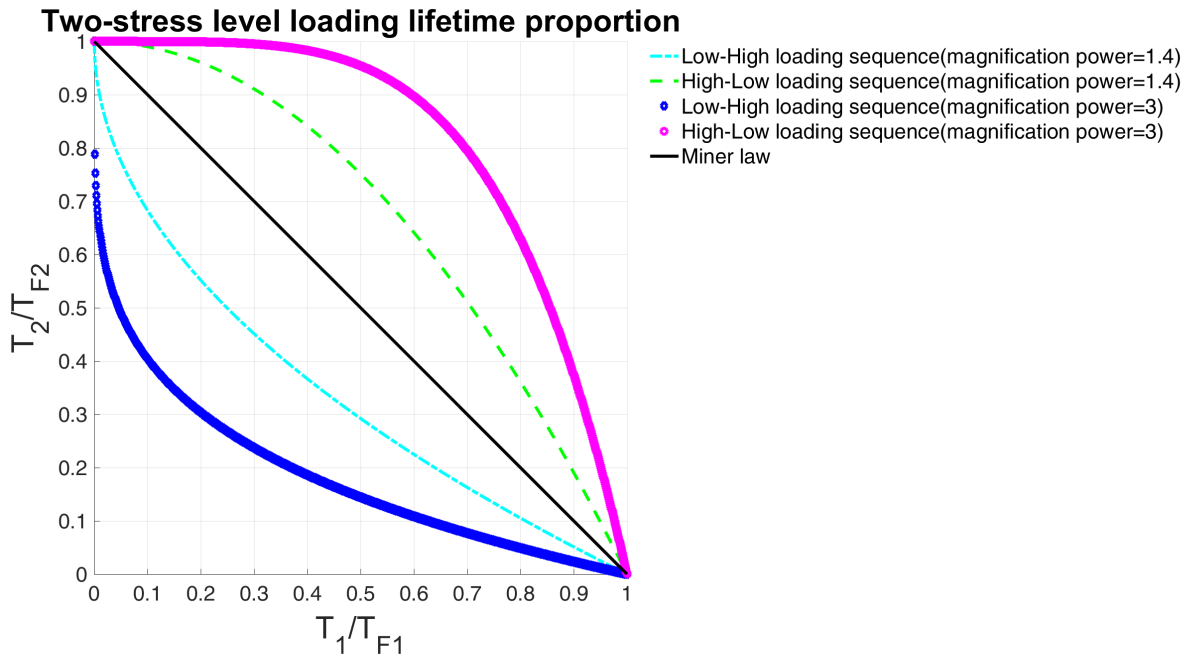


Figure 27: Major damage effect using different magnification power on sequence effect figure. High stress is 1MPa and low stress is 0.8MPa.

which causes faster damage accumulation. We can also see this effect in Figure ???. However, α must be positive.

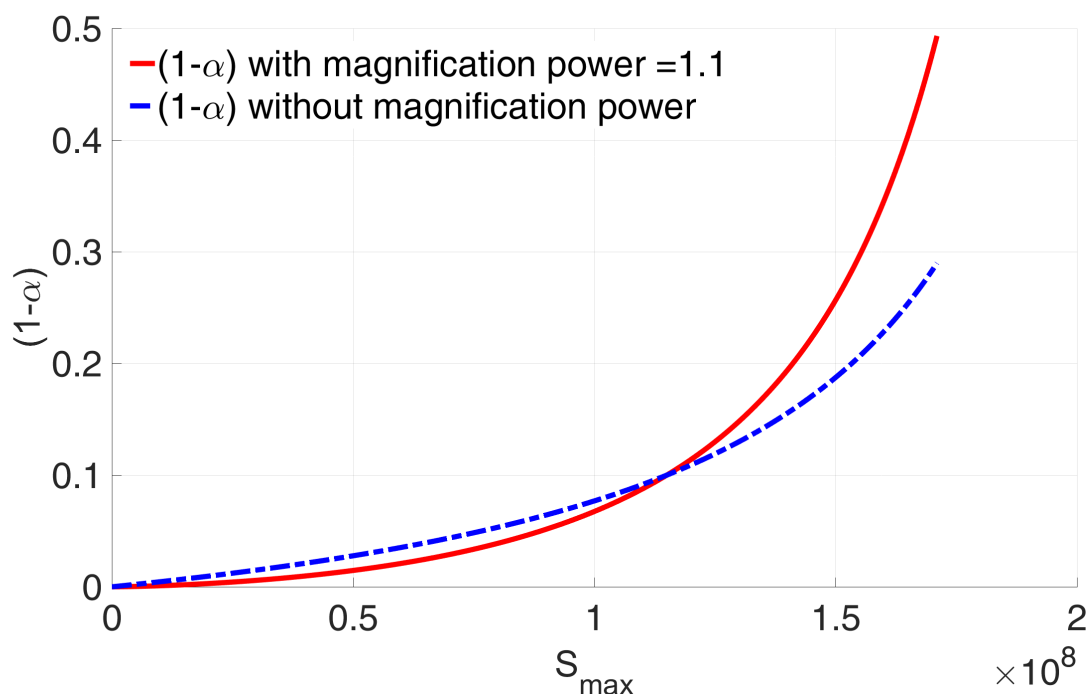
To assess large stress correctly we define the larger stress intensity as the expression in the bracket in the second term of α is greater than $1\left(\frac{1}{s_{min}(t)-1}\right) > 1$, then we use power β to magnify this term, in this way the damage is accelerated for large stresses. The deviatoric stress S_a , above which the damage is magnified, is determined from:

$$\alpha(t) = 1 - a \left(\frac{1}{s_{min}(t) - 1} \right)^{1.1},$$

$$s_{min}(t) = \frac{\Sigma_y - \lambda \Sigma_H(t)}{S_a(t)} < 2,$$

$$S_{large}(t) > \frac{\Sigma_y - \lambda \Sigma_H(t)}{2}.$$

The major damage effect can be seen in Figure 26.

Figure 28: $(1-\alpha)$ term with and without the magnification power $f(\beta)$

7 Identification strategy

The positive hydrostatic stress and negative one have different effect on the yield limit. It is necessary to adopt 2 parameters to describe this behavior. So we divide the hydrostatic sensitivity λ into 2 parts. λ_+ and λ_- . In the analytical formula, the amplitude of the stress intensity is adopted and the average value of tension hydrostatic stress(+) and compressive hydrostatic stress(-).

For a good lifetime prediction, it is necessary to first identify the appropriate parameters of the model. For this purpose, we use the analytical formula Eq.(40) obtained in uniaxial cyclic loading case.

With distinction of the hydrostatic stress in the presence of non-zero mean stress, Eq.(8) now writes:

$$W_{cyc} = \frac{2(E - k)(1 + \nu)(\beta - 1)}{E(E + k\nu)\beta(\beta + 1)} \left[\frac{S_a^{\beta+1}}{(\sigma_y - \lambda_+ \bar{\Sigma}_{H+}(t))^{\beta-1}} + \frac{S_a^{\beta+1}}{(\sigma_y - \lambda_- \bar{\Sigma}_{H-}(t))^{\beta-1}} \right]. \quad (42)$$

$$N_{Fnum} = \frac{W_0}{(1 - \alpha)} \frac{E(E + k\nu)\beta(\beta + 1)}{2(E - k)(1 + \nu)(\beta - 1)} \frac{1}{\frac{S_a^{\beta+1}}{(\sigma_y - \lambda_+ \bar{\Sigma}_{H+}(t))^{\beta-1}} + \frac{S_a^{\beta+1}}{(\sigma_y - \lambda_- \bar{\Sigma}_{H-}(t))^{\beta-1}}}. \quad (43)$$

To use our analytical model Eq.(43) to fit the experiments, we employ matlab Least-Squares (model fitting) algorithm.

The best fitted parameters in uniaxial cyclic loading case are deduced from the minimization of the sum of square of difference between uniaxial numerical and experimental results:

$$\min_{\beta, \lambda, W_0} \left\{ \sum_i (N_{Fnum} - N_{Fexp(i)})_{torsion}^2 \right\} \quad (44)$$

Assume there are i sets of experimental data, to clarify the identification process, we have:

- Experimental data: $\Sigma_{(i)}$, $m_{(i)}$, $N_{Fexp(i)}$, σ_y , E , k , ν .
- Parameter constants: β , λ_{+-} , W_0
- Input data from experimental data: $S_{max(i)}$, $\Sigma_{H(i)}$
- Input data from experimental data and parameter constants: $\alpha_{(i)}$
- Output data: $N_{Fnum(i)}$

In this process, σ_y , E , k and ν are given elastoplastic material constants. For each test (i), the load parameters are $S_{max(i)}$, $\Sigma_{H(i)}$, and the experimental number of cycles to failure is $N_{Fexp(i)}$.

The exponent $\alpha_{(i)}$ is cycle average obtained by

$$\alpha_{(i)} = \text{mean} \left[1 - a \left(\frac{1}{\frac{\Sigma_y - \lambda_{+-} \Sigma_H(t)}{S_a(t)} - 1} \right)^{1.1} \right] (i).$$

The parameters to be calibrated are W_0 , β and λ . Since the exponent $\alpha_{(i)}$ depends on β and λ , we proceed iteratively by:

1. We first identify the S-N curve slope β and the energy scale W_0 using the analytical formula with torsion tests because there is no λ_{+-} impact in this kind of loading. We start from an initial guess β from which we can deduce $\alpha_{(i)}$ and identify β and W_0 by least squares. Because our analytical formula is not derivable in all ranges, when the identified value of β or W_0 get stuck in local minimum value, we regenerate a random β or W_0 in their range so as to get the global least square value.
2. Then, the parameter λ_{+-} are identified from numerical bending tests.

The final parameters correspond to the λ leading to the lowest identification error in β and W_0 . This strategy handles the nonlinearity in β and is well adapted to the low sensitivity in λ .

The analytical formula Eq.(43) with mean stress effect converges with the numerical method very well in the case of small β and λ_{+-} .

Parameter sensitivity analysis

The parameters we introduced during the deduction need to be calibrated. The source of the parameter identification are listed in Table.2. We perform a sensitivity analysis to see the influence of each parameter by comparing the results obtained respectively for the reference value, an upper bound and a lower bound of each parameter.

Parameters	Strategy
Hydrostatic pressure sensitivity λ	hydrostatic stress sensitivity (identified)
Non-linearity of damage accumulation α	amplification factor of load intensity (guessed)
Weakening scales distribution exponent β	to be calibrated (identified)
Dissipated energy to failure per defect W_0	energy scaling (identified)

Table 2: Parameters concerned

We analyze the sensitivity of parameters separately as in Table.3(uniaxial) and Table.7(random loading). The parameter β has more influence on the random loading case because it acts not only as the S-N curve slope but also the power magnification factor of large stress intensity. The λ has little influence because both tests are conducted on very small or zero mean stress load history.

In Miner's law the parameter α is zero, the maximum value is below 1. For $\alpha = 1$ the damage accumulation line becomes flat and there will be unlimited lifetime. To keep α in the range of $[0, 1]$ where in random amplitude tests there is $S_a = 163.3\text{MPa}$; we set the sensitivity of load intensity α to a maximum value of 0.29 to keep α positive.

The weakening scale distribution exponent(also the slope of S-N curve of the material) β ranges from 1 to 5. The hydrostatic pressure sensitivity λ is from positive mean stress test, which has the range of $0 \sim 0.8$.

In constant amplitude cyclic loading, the dissipated energy to failure per defect W_0 (in MPa) is related to fatigue lifetime of the material.

Constant,amplitude sensitivity test with $f(\beta) = \beta$							
	Ref	Min	Max	Ref_n	Min_n	Max_n	Sensitivity
β	1.1	1.05	1.50	414233	783723	243300	-3.19
λ	0.1	0.05	0.50	414233	449598	443376	0.00
W_0	3.27e8	1.00e8	5.00e8	414233	137498	687209	1.08
a	0.1	0.05	0.15	414233	672869	324754	-0.84

Table 3: Parameters sensitivity at cyclic loading of ep02 on AW-6106 T6 aluminum

8 Experimental verification

8.1. Introduction

The aim of this chapter is to validate the predictive model proposed. This consists in simulating tests available in the literature to determine the lifetime at initiation of crack by the application of the model and to compare these with the experimental lifetimes. The validation of the model involves a wide variety of metallic materials. The loads tested are of two types: cyclic loading of multiaxial stress of constant amplitude and repeated sequences of uniaxial stresses of variable amplitudes. The fatigue data of the materials used and the loads tested are taken from laboratory experiments or the literature.

8.2. Random amplitude 1D tests from Cetim on AW-6106 T6 aluminum

What makes automobile fatigue so difficult to predict is that, unlike standard tests done in a laboratory, an automobile's structure has to endure a complex, mostly random, set of static as well as cyclical stresses when in service, such as in Figure 27 which could represent load data from testing or measurement, extracting the cyclic information can be challenging.

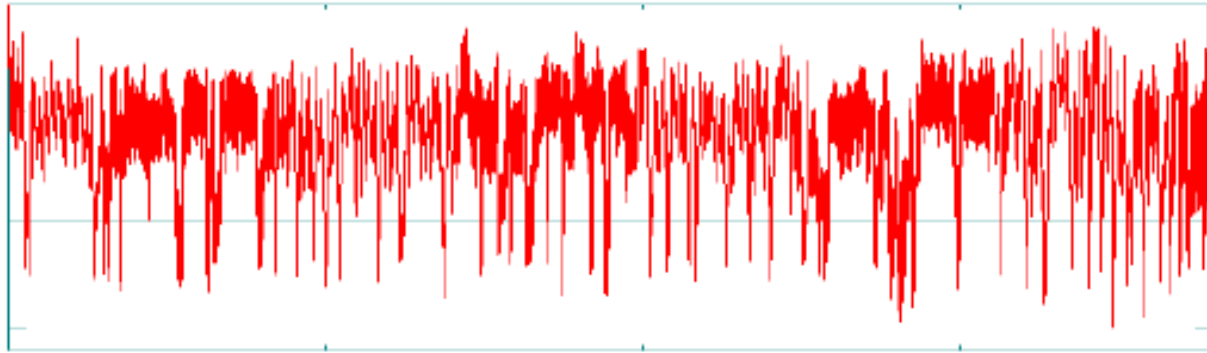


Figure 29: Complex Cyclic Loading

As we mentioned before, the mean value of α depends on the loading pattern(sinusoidal, linear division points between max and min stresses in unit cycle,...), but the our optimal time step numerical strategy is not loading pattern dependent because it equally divides the range of α during the load history, which means it only concerns the variation amplitude of stress intensity. So in random loading case with only recorded maximum and minimum load history, we divide linearly between every 2 recorded points into 100 time steps, and issue numerical results with optimal time step method.

The tests are performed on aluminum batches, the characteristics of the sample are shown in table 4.

Specimen geometry for fatigue and corrosion fatigue tests ($t < 3,5$ mm):

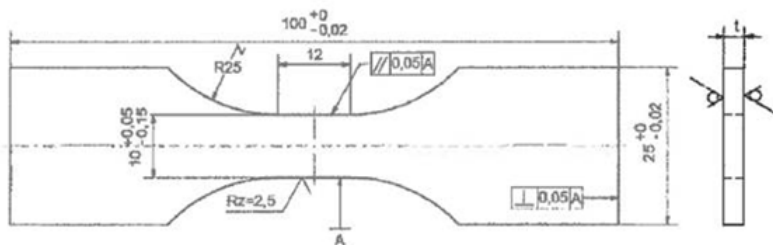


Figure 30: Specimen geometry for fatigue tests of AW-6106 T6 aluminum

There are 12 validated uniaxial fatigue tests on the AW-6106 T6 aluminum sample, in which 2 are constant amplitude load case and 10 random load case. The cyclic stress of test number 1(ep01) and test

Parameters	Value
Young's modulus	$E = 72 \text{ GPa}$
Hardening parameter	$k = 8.5 \text{ MPa}$
Macroscopic yield stress	$\sigma_y = 230 \text{ MPa}$
Thickness	$e = 2.9 \text{ mm}$
Width	$l = 9.95 \text{ mm}$

Table 4: Material parameters

number 2(ep02) are respectively 131.9 MPa and 97.0 MPa . We first identify the same parameters feasible to both loading cases.

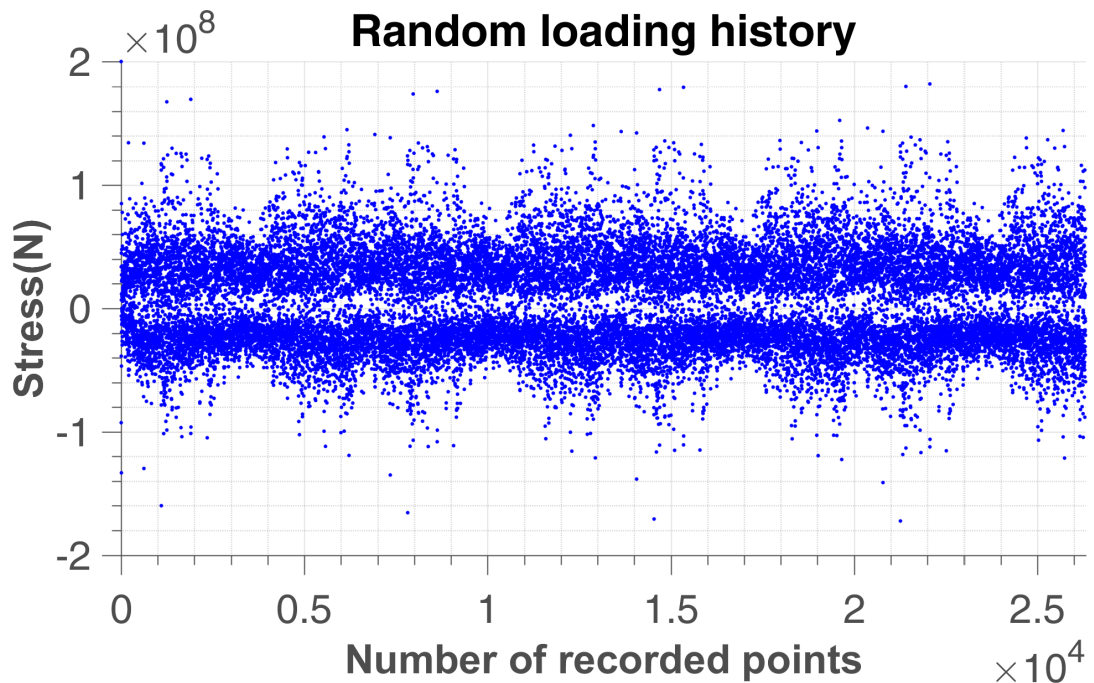


Figure 31: Random loading history on batch 06 of AW-6106 T6 aluminum

The detailed tests information are shown in table 5. There are $27000(\pm 2.4\%)$ recorded points per repetition.

We assume the material parameters like Young's modulus, hardening parameter, hydrostatic pressure sensitivity, macroscopic yield stress, Wohler curve exponent and sequence effect parameters are known. We first identify the weakening scales distribution, and dissipated energy to failure from cyclic tests ep01 and ep02. Then change the parameter n_0 to see if our assumption is correct or need to be changed.

The numerical fitting process show that the damage is caused mainly by large stresses. The definition

Specimen	Fmax (kN)	Σ_{max} in the block	Number of repetition	Number of points
BATCH_A_01	3.375			99892
BATCH_A_02	2.475			414298
BATCH_A_04	nom	225.88	95	2500000
BATCH_A_05	nom	225.88	156	4105263
BATCH_A_06	nom	225.88	145	3815789
BATCH_A_07	nom	225.88	90	2368421
BATCH_A_08	nom	225.88	194	5105263
BATCH_A_09	nom	225.88	197	5184211
BATCH_A_10	nom x 0,9	203.292	515	13552632
BATCH_A_11	nom x 0,9	203.292	385	10131579
BATCH_A_12	nom x 0,9	203.292	424	11157895
BATCH_A_13	nom x 0,9	203.292	409	10763158
BATCH_B_01	nom	225.88	121	3184211
BATCH_B_02	nom x 0,8	180.704	380	10000000
BATCH_B_03	nom x 0,8	180.704	380	10000000
BATCH_B_04	nom x 0,9	203.292	406	10684211
BATCH_B_05	nom x 0,9	203.292	454	11947368
BATCH_B_06	nom x 0,9	203.292	518	13631579
BATCH_B_07	nom x 0,9	203.292	553	14552632
BATCH_B_08	nom x 0,9	203.292	612	16105263
BATCH_B_09	nom	225.88	253	6657895
BATCH_B_10	nom	225.88	196	5157895
BATCH_B_11	nom	225.88	178	4684211
BATCH_B_12	nom	225.88	123	3236842

Table 5: Cetim fatigue tests result on AW-6106 T6 aluminum

of major stress now need to be specified according to the material. To take into account this effect we first find out the proportion stress above a certain value in the repetition signal of random loading, as shown in Table 6. Here ep_a and ep_b are the same material. Since the samples were extracted from aluminum profiles of industrial products, the two batches correspond to two different times of sampling in the production. The variation is supposed to be representative of the regular tolerances you might have in the production. ep_a_01 and ep_a_02 are constant amplitude loading which helps identify the power of weakening scale distribution β . ep_a_03 is low cycle fatigue data. ep_b_02 and ep_b_03 have infinite life

time. The data in the table are grabbed from random signal high cycle fatigue loading history.

Stress(MPa)>	70	90	110	130	150	170	190
S_a (MPa)>	57.15	73.48	89.81	106.14	122.47	138.80	155.13
ep_a_04		1.962%	0.904%	0.077%	0.037%	0.018%	0.007%
ep_a_05		1.604%	0.784%	0.044%	0.030%	0.007%	0.007%
ep_a_06		1.645%	0.784%	0.045%	0.030%	0.007%	0.007%
ep_a_07		1.632%	0.788%	0.048%	0.029%	0.007%	0.007%
ep_a_08		1.644%	0.787%	0.048%	0.037%	0.007%	0.007%
ep_a_09		1.655%	0.800%	0.048%	0.037%	0.007%	0.007%
ep_a_10		0.768%	0.134%	0.007%	0.000%	0.000%	0.000%
ep_a_11		0.772%	0.145%	0.007%	0.000%	0.000%	0.000%
ep_a_12		0.779%	0.133%	0.011%	0.000%	0.000%	0.000%
ep_a_13		0.775%	0.141%	0.007%	0.000%	0.000%	0.000%
ep_b_01	4.739%	1.737%	0.840%	0.224%	0.049%	0.034%	0.004%
ep_b_04	1.999%	0.745%	0.156%	0.034%	0.004%	0.000%	0.000%
ep_b_05	2.010%	0.749%	0.148%	0.034%	0.008%	0.000%	0.000%
ep_b_06	1.999%	0.790%	0.118%	0.034%	0.008%	0.000%	0.000%
ep_b_07	2.029%	0.756%	0.152%	0.034%	0.008%	0.000%	0.000%
ep_b_08	1.999%	0.737%	0.137%	0.034%	0.008%	0.000%	0.000%
ep_b_09	4.663%	1.687%	0.798%	0.205%	0.049%	0.034%	0.004%
ep_b_10	4.712%	1.744%	0.809%	0.224%	0.046%	0.034%	0.004%
ep_b_11	4.636%	1.664%	0.790%	0.209%	0.049%	0.034%	0.004%
ep_b_12	0.775%	0.141%	0.007%	0.000%	0.000%	0.000%	0.000%

Table 6: Proportion of stress(MPa) above which there is major damage with $\Sigma_y=230$ MPa, test data provided by CETIM on AW-6106 T6 aluminum.

Random amplitude sensitivity test with $f(\beta) = \beta$							
	Ref	Min	Max	Ref_n	Min_n	Max_n	Sensitivity
β	1.1	1.05	1.50	4220452	7469257	1799585	-3.28
λ	0.1	0.05	0.50	4220452	4566335	2175991	-0.13
W_0	3.27e8	1.00e8	5.00e8	4220452	1321761	6420810	0.99
a	0.1	0.05	0.15	4220452	7156622	2827894	-1.03

Table 7: Parameters sensitivity at random loading of ep05 on AW-6106 T6 aluminum

From Table.8 and Table.9 we can see $f(\beta)$ has positive correlation with β in high cycle fatigue which is the regime we focus on. So we give $f(\beta) = \beta$ in high cycle random loading case to minimize the parameters to collaborate. The sensitivity of parameters is calculated by dividing the percentage of variation of number

Constant amplitude sensitivity test with $f(\beta) \neq \beta$							
	Ref	Min	Max	Ref_n	Min_n	Max_n	Sensitivity
β	1.1	1.05	1.50	414233	797377	213682	-3.44
λ	0.1	0.05	0.50	414233	449598	443376	0.00
W_0	3.27e8	1.00e8	5.00e8	414233	137498	687209	1.08
a	0.1	0.05	0.15	414233	672869	324754	-0.84
$f(\beta)$	1.1	1.05	1.5	414233	441661	511644	0.41

Table 8: Parameters sensitivity at cyclic loading of ep02 on AW-6106 T6 aluminum

Random amplitude sensitivity test with $f(\beta) \neq \beta$							
	Ref	Min	Max	Ref_n	Min_n	Max_n	Sensitivity
β	1.1	1.05	1.50	4220452	7254554	2472791	-2.77
λ	0.1	0.05	0.50	4220452	4566335	2175991	-0.13
W_0	3.27e8	1.00e8	5.00e8	4220452	1321761	6420810	0.99
a	0.1	0.05	0.15	4220452	7156622	2827894	-1.03
$f(\beta)$	1.1	1.05	1.5	4220452	4341560	3052299	-0.75

Table 9: Parameters sensitivity at random loading of ep05 on AW-6106 T6 aluminum

of points to failure with respect to the reference number of points to failure, by the percentage of variation of parameter with respect to the reference parameter. As is shown in Eq.(45).

$$sensitivity = \frac{(Max_n - Min_n) / Ref_n}{(Max - Min) / Ref}. \quad (45)$$

The reference parameters value we use are in Tab.10.

Constant α	W_0 (MPa)	λ	β	α
	326.9	0.1	1.1	0.7
Changing α	W_0 (MPa)	λ	β	a
	326.9	0.1	1.1	0.1

Table 10: The parameters in 1D cyclic and random loading on AW-6106 T6 aluminum fatigue tests by Cetim

The best fitted results with constant α are shown in Figure 30. The dispersion is relatively large. In

conclusion, we are not able to predict the random stress amplitude fatigue life with fixed α , because random stresses not only cause different energy dissipations, but also have influence on damage accumulation speed, so we have to update the value of α at each time step.

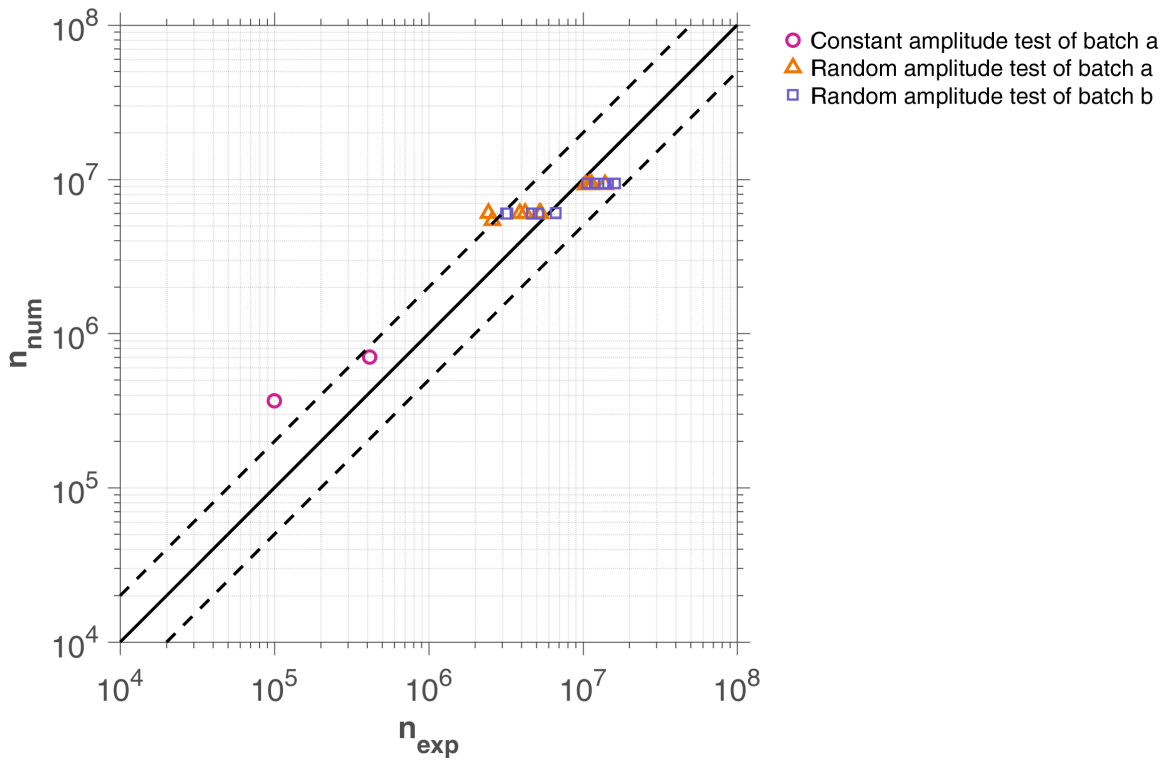


Figure 32: Comparison between experimental and numerical results of 1D cyclic and random loading on aluminum fatigue tests by CETIM with constant α

We can find that the numerical results are satisfactory with major damage effect. The dispersion figure with distinction of major damage is depicted in Figure 31. Here it is necessary to control the parameter α to make sure $\alpha > 0$ in the most severe situation.

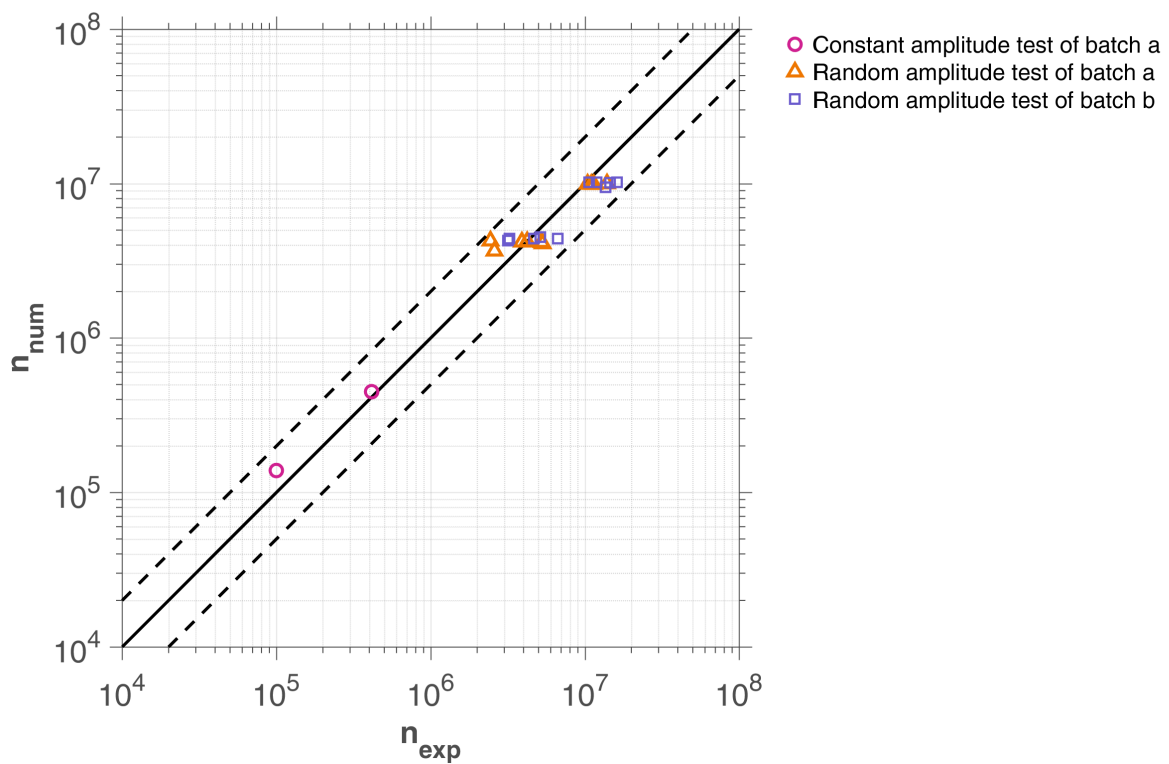


Figure 33: Comparison between experimental and numerical results of 1D cyclic and random loading on aluminum fatigue tests by Cetim

8.3. Experimental validation of the model on aluminum 6082 T6

8.3.1. Presentation of aluminum 6082 T6

The material tested is aluminum 6082 T6, used by [24] to validate their method of lifetime prediction. The mechanical properties of this material are summarized in Table 11.

E [GPa]	σ_y [MPa]	σ_u [MPa]	ν
69.4	298	343	0.33

Table 11: Mechanical and dynamic characteristics of aluminum 6082 T6 ([24])

8.3.2. Specimens of aluminum 6082 T6

The specimens were made from the drawn bars (diameter 30 mm) and the geometrical shape of which is given in Figure 32. They are successively polished with 6- m diamond compounds until a good mirror-like finish is obtained.

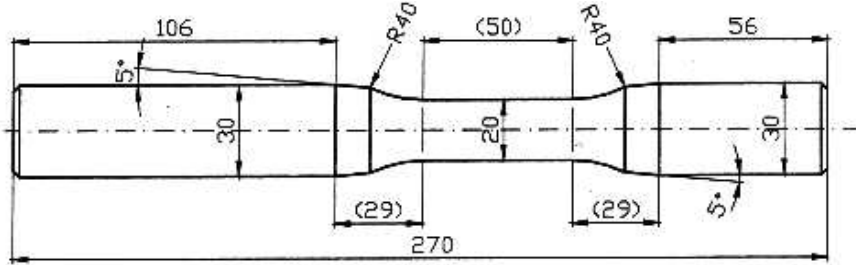


Figure 34: Specimen geometry for fatigue tests of aluminum 6082 T6

8.3.3. Fatigue tests on aluminum 6082 T6

The simulated tests are purely alternate and summarized in Tables 12 and 13. They consist of simple tests in bending, torsion and bending-torsion in phase and out-phase for two cases of biaxial stress ratio, $\lambda = \tau_{xy,a}/\sigma_{x,a}$ ($\lambda > 1$ and $\lambda < 1$). The expected lifetimes range from 10^4 to 1.5×10^6 cycles.

In the Tables 12 and 13, $\sigma_{x,a}$ is the normal stress amplitude, $\tau_{xy,a}$ is the torsion amplitude, λ is the biaxial stress ratio, δ is the phase shift between the components of applied stresses and $N_{f,5\%}$ represents the number of cycles at break, defined by a 5% decrease in flexural or torsional stiffness.

It is interesting to note that a reduced amount of plasticity was measured by strain gauges in the PC10T2, PC14T2 and P36BT11 tests[24]. They are therefore located in the field of oligocyclic fatigue. Therefore, they are not simulated as we only deal with the field of polycyclic fatigue3.

Batch N°	$\sigma_{x,a}$ [MPa]	$\tau_{xy,a}$ [MPa]	λ	δ [°]	$N_{f,5\%}$ [Cycles]
P1B1	190	0	0	0	160000
P2B2	180	0	0	0	248518
P3B3	164	0	0	0	444411
P4B4	144	0	0	0	1069220
P5B5	224	0	0	0	56285
P6B4	145	0	0	0	1238325
P7B1	187	0	0	0	200480
P8B3	161	0	0	0	423590
PC9T1	0	117	∞	0	534032
PC10T2	0	155	∞	0	26987
PC11T3	0	127	∞	0	76665
PC12T3	0	127	∞	0	132295
PC13T1	0	117	∞	0	203535
PC14T2	0	155	∞	0	16195
PC15T4	0	106	∞	0	>1.1E6
PC16T4	0	104	∞	0	565150

Table 12: Simple bending and torsion tests (R = -1)[24]

8.3.4. Application of the model

Identification of model parameters

Once α_m is fixed in constant amplitude cyclic loading, it has the same influence as W_0 . The parameters remain to calibrate are λ on the mean stress sensitivity which makes a distinction between bending and torsion, and the exponent β on the slope of $S - N$ curve.

In Figure 33a and Figure 33b the diagonal represents a good correlation between the experimental and predicted lifetimes. The line segments on either side of the diagonal correspond to a fatigue lifetime error of a factor of two. The parameters of the 6082 T6 aluminum model are given in Table 14.

The model predictive results for the periodic loads of constant amplitude with a radial path are in good agreement with the durations of experimental life. For the latter condition, 90 deg out-of-phase loading was also investigated (Figure 33c). These tests indicated a dramatic decrease in the number of cycles to failure, N_F , as a result of out-of-phase loading. The influence of the plastic strain path on life is thus clearly demonstrated. It is shown that the total strain energy density, $W_t = W_e + W_p$ ([11]), correlates with both the in-phase and out-of-phase cyclic tests, and therefore is a proper damage parameter to be used for life

Batch N°	$\sigma_{x,a}$ [MPa]	$\tau_{xy,a}$ [MPa]	λ	δ [°]	$N_{f,5\%}$ [Cycles]
P17BT1	57	100	1.75	0	266435
P18BT2	51	84	1.65	0	1119254
P19BT2	51	84	1.65	0	1416225
P20BT3	71	118	1.66	0	83000
P21BT3	70	118	1.69	0	75695
P22BT1	59	99	1.68	0	630325
P23BT4	132	97	0.73	0	157210
P24BT4	132	99	0.75	0	126470
P25BT5	144	107	0.74	0	35450
P26BT5	149	105	0.7	0	68465
P27BT6	122	90	0.74	0	252658
P28BT7	116	83	0.72	0	316149
P30BT8	148	66	0.45	90	278836
P31BT9	152	47	0.31	90	465010
P32BT8	149	68	0.46	90	118965
P33BT9	155	72	0.46	90	447525
P34BT10	190	105	0.55	90	47940
P35BT10	189	106	0.56	90	30995
P36BT11	79	129	1.63	90	23080
P37BT12	69	110	1.59	90	202807
P38BT13	68	99	1.46	90	262980
P39BT13	68	99	1.46	90	398615
P41BT15	79	116	1.47	90	46045

Table 13: In-phase and out-of-phase bending-torsion tests ($R = -1$)^[24]

β	λ_+	λ_-	W_0	a
5.126	0.9	0	1E8 Pa	0.4

Table 14: Parameter identification of AL6082T6 steel

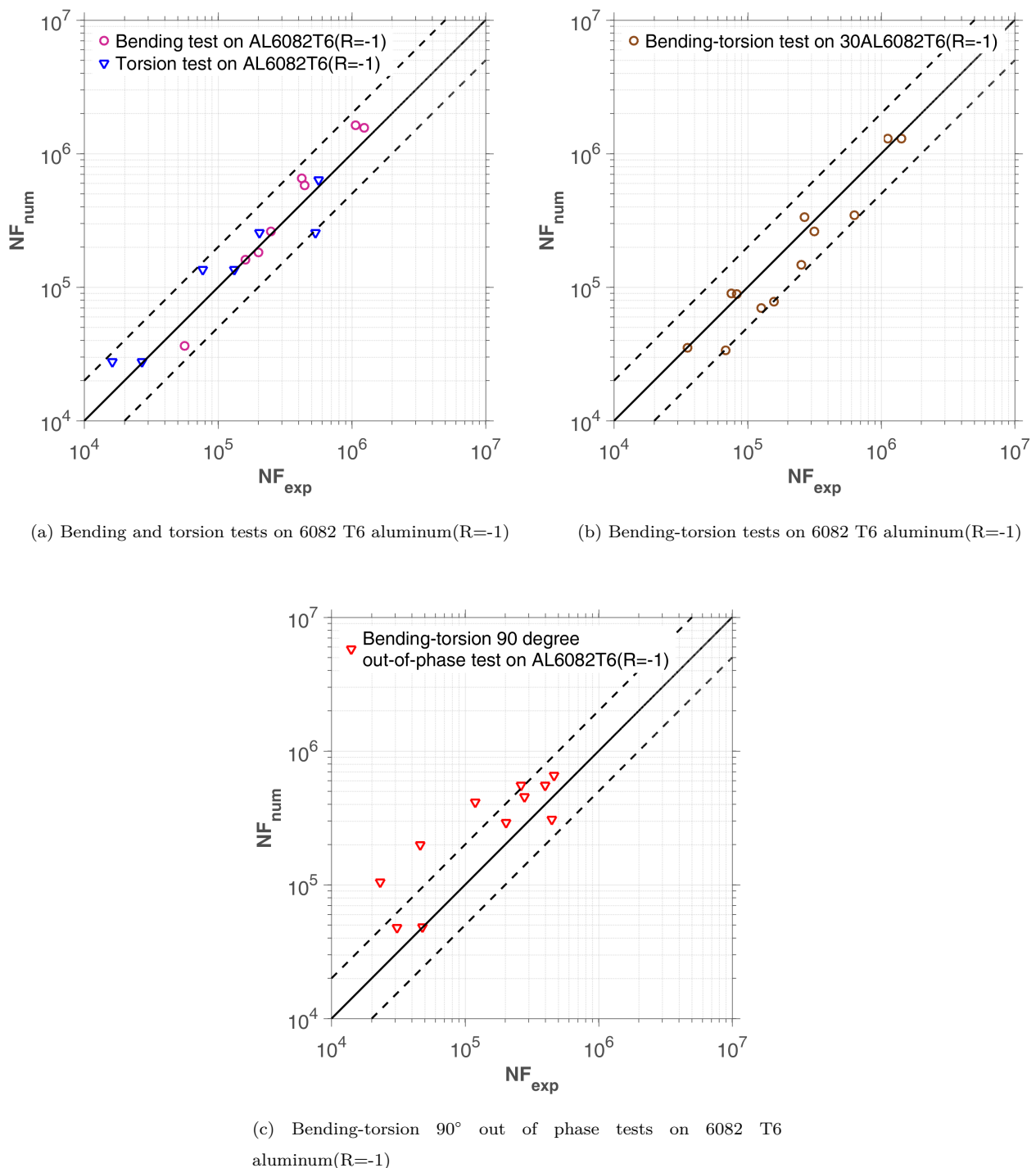


Figure 35: Calibration on on 6082 T6 aluminum ([24])

predictions. A brief description of how ΔW_t can be calculated is given for the case of proportional loading. The predicted results are compared with the experimental data, and the agreement is found to be very good indeed.

8.4. Experimental validation of the model on 30NCD16 steel

8.4.1. Presentation of steel 30NCD16

Tests with blocks of loading from database are compared to our model predictions. The material for testing is steel 30NCD16. The mechanical characteristics relating to each lot were determined by Dubar [25] by effecting monotonic tensile test batch. He eventually define “average material” one who has characteristics listed in Table. 15:

$\sigma_{y0.02\%}$ [MPa]	$\sigma_{y0.2\%}$ [MPa]	σ_u [MPa]	σ_{-1} [MPa]	τ_{-1} [MPa]	E [GPa]
895	1080	1200	690	428	191

Table 15: Mechanical and dynamic characteristics of 30NCD16 steel [25]

8.4.2. Fatigue tests performed by Dubar on steel 30 NCD 16

Tests carried out under simple bending and torsional stresses are grouped together in Table. 16 and 17.

Bending Tests (R=-1)	N [Cycles]	$\sigma_{x,m}$ [MPa]	$\sigma_{x,a}$ [MPa]
1	51000	0	820
2	80000	0	795
3	90000	0	790
4	95000	0	785
5	100000	0	780
6	120000	0	765
7	140000	0	752
8	200000	0	725
9	210000	0	720
10	230000	0	715
11	250000	0	708
12	51000	450	640
13	140000	450	620
14	120000	290	695
15	250000	290	660

Table 16: 30NCD16 steel fully reversed bending tests [25]

Torsion Tests (R=-1)	N [Cycles]	$\tau_{xy,a}$ [MPa]
16	51000	527
17	80000	505
18	90000	500
19	95000	497
20	100000	495
21	120000	482
22	140000	470
23	200000	450
24	210000	446
25	230000	445
26	250000	440

Table 17: 30NCD16 steel fully reversed torsion tests [25]

The results of combined bending-torsion tests in phase with or without mean stress $\sigma_{x,m}$ are given in the following table:

Bending Tests (R=-1)	N [Cycles]	$\sigma_{x,m}$ [MPa]	$\sigma_{x,a}$ [MPa]	$\tau_{xy,a}$ [MPa]
27	80000	0	600	335
28	200000	0	548	306
29	120000	290	0	460
30	120000	450	0	460
31	250000	450	0	430
32	95000	450	490	285
33	120000	290	500	290

Table 18: 30NCD16 steel bending-torsion tests [25]

8.4.3. Identification of model parameters for steel 30 NCD 16

Indeed, the identification of the parameters consists in minimizing the relative difference between the experimental lifetimes and calculated for purely alternating bending tests (R = -1). This is clearly indicated in figure (3.13) by obtaining a good correlation between these different lifetimes

β	λ_+	λ_-	W_0	a
5.3	0.55	0	4.97E8 Pa	0.4

Table 19: Parameter identification of 30NCD16 steel

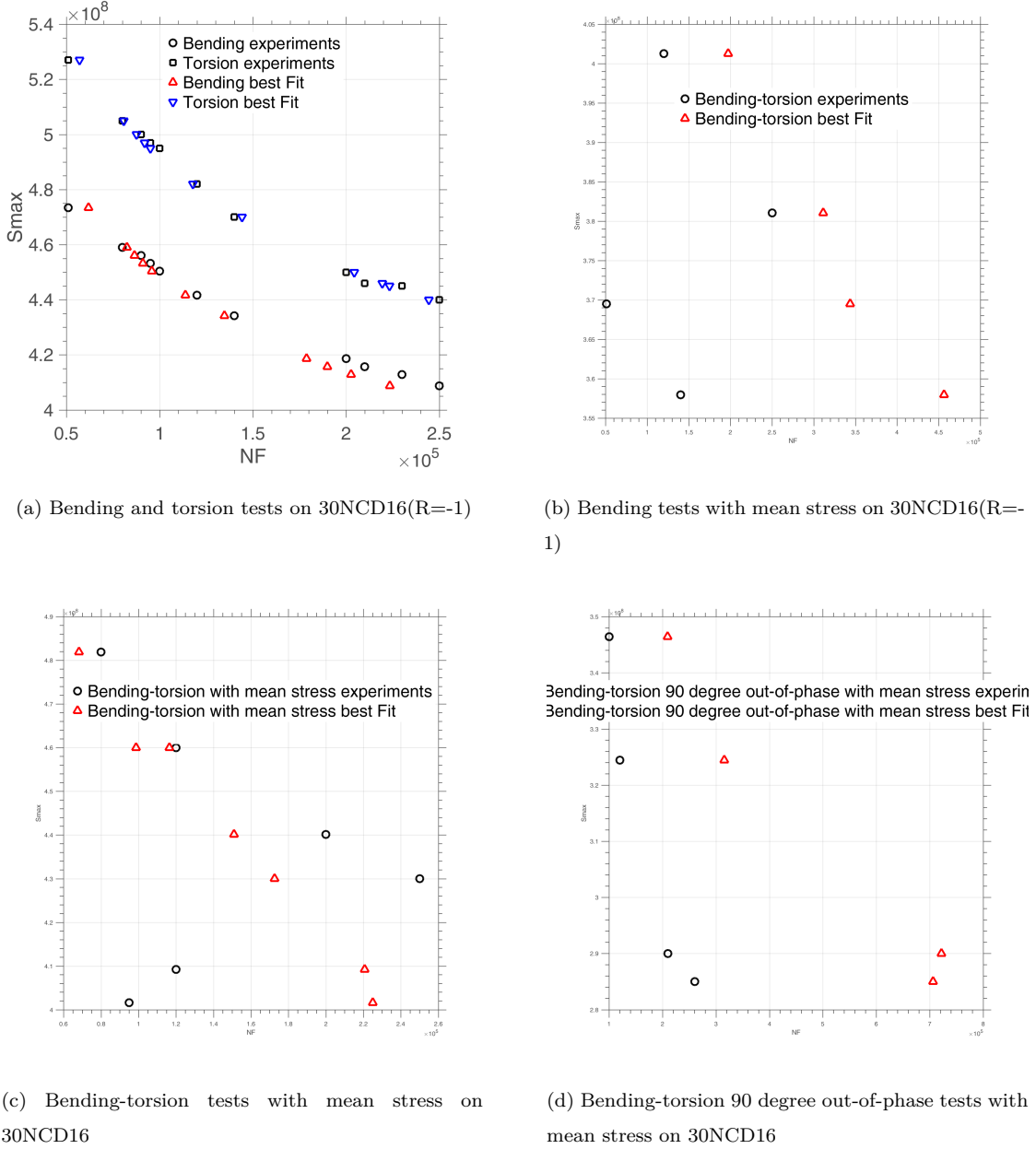


Figure 36: Calibration on 30NCD16 ([25])

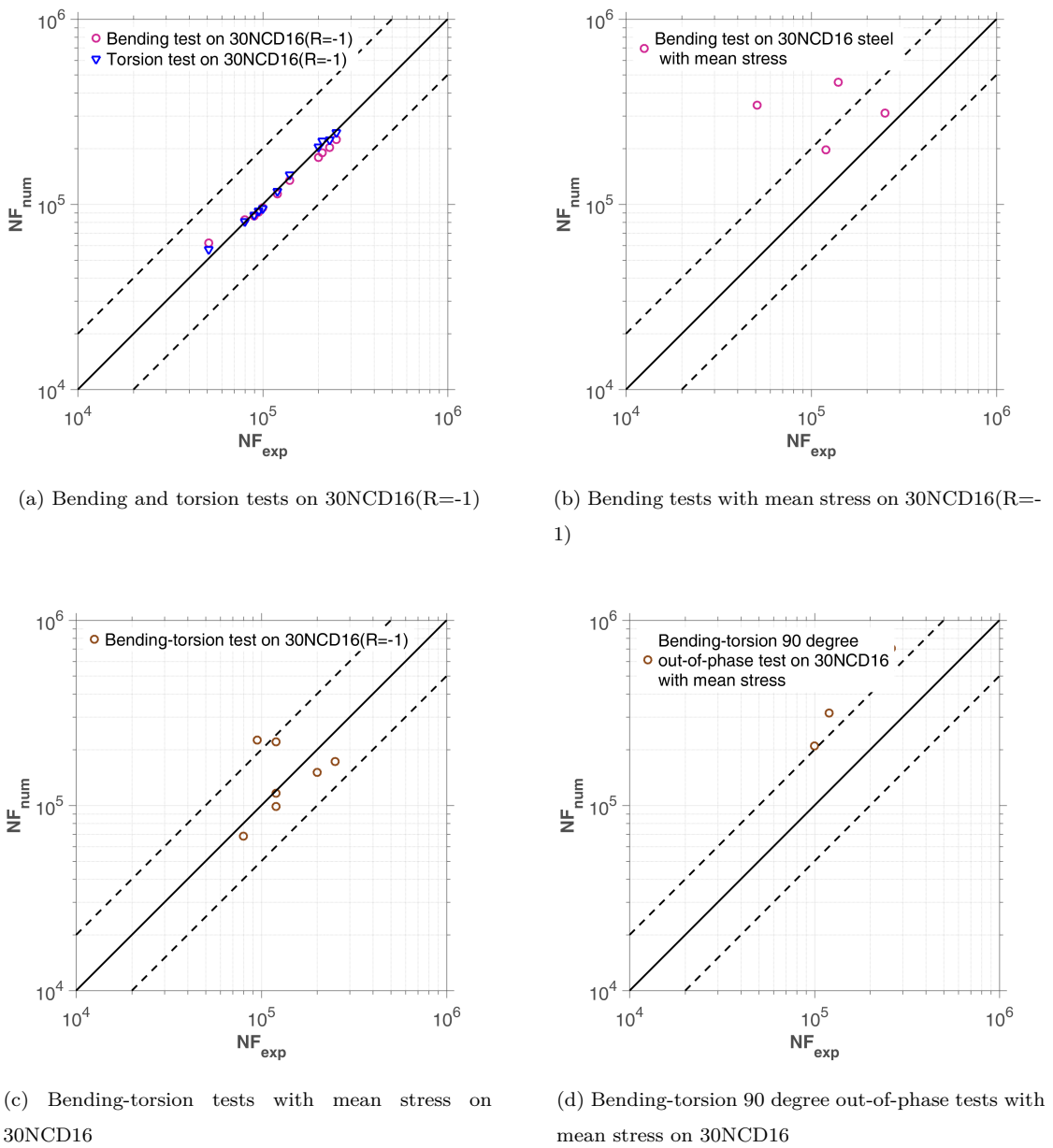


Figure 37: Calibration on 30NCD16 ([25])

8.5. Experimental validation of the model on SM45C steel

8.5.1. Presentation of steel SM45C

This is a structural steel widespread use for the crankshafts and the structural components. The chemical composition and mechanical properties of this material is given in Table. 20 and Table. 21.

C	Mn	P	S	Si	Ni	Cr	Cu
0.42	0.73	0.02	0.012	0.28	0.14	0.18	0.13

Table 20: Chemical composition of SM45C steel

σ_y [MPa]	σ_u [MPa]	E [GPa]	G [GPa]	ν	A
638	824	213	82.5	0.29	22

Table 21: Mechanical and dynamic characteristics of SM45C steel

E: Young's modulus,

G: Shear modulus,

ν : Poisson ratio,

A: Elongation at break.

8.5.2. Fatigue tests performed by Dubar on steel SM45C

Preliminary fatigue tests in purely alternating torsion and purely alternating flexion were performed by Lee [26]. These two types of tests were carried out with test pieces of the same geometric shape. In addition, the author had performed moderate stress bending fatigue tests to study its effect on the lifetime of SM45C steel. All uniaxial fatigue tests performed by Lee [26] are illustrated in Figure 36. This figure shows a reduction in bending life of SM45C steel in the presence of a positive mean stress. Crack initiation was detected when the stiffness of the specimen or specimen used was reduced by 10%.

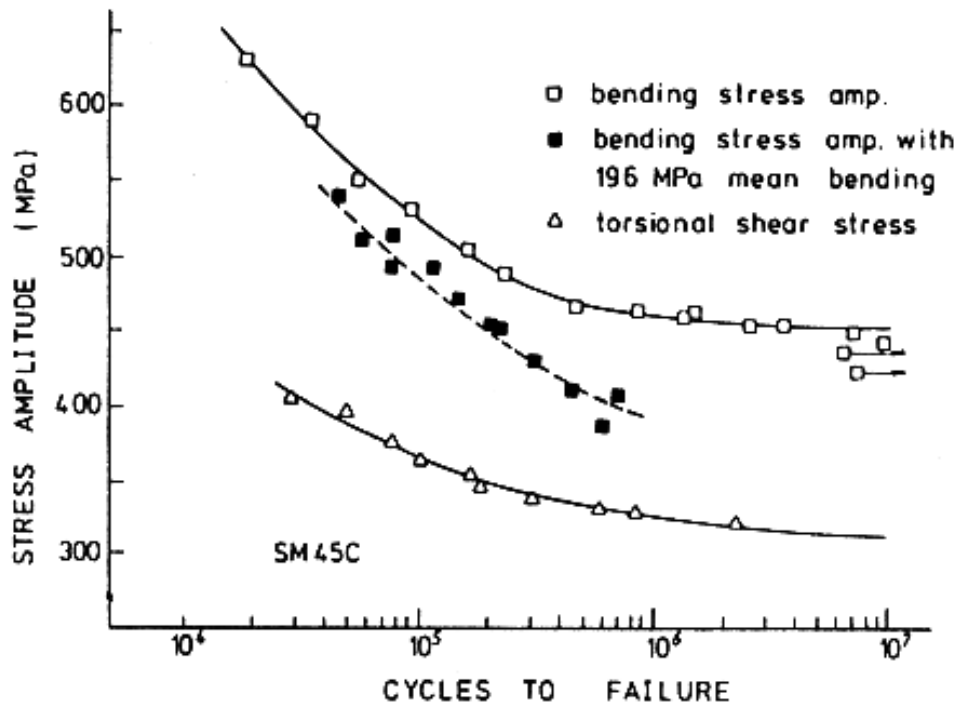


Figure 38: Fatigue curves made on SM45C steel by Lee [26]

Preliminary fatigue tests were carried out under fully reversed bending and torsion separately.

In the case of multiaxial bending-torsion block tests (Table. 24), we could alternatively adopt Von Mises stress as the value of S_a :

$$S_a = \sigma_{von} = \sqrt{\frac{1}{2} [(\sigma_{xx} - \sigma_{yy})^2 + (\sigma_{yy} - \sigma_{zz})^2 + (\sigma_{zz} - \sigma_{xx})^2] + 3(\tau_{xy}^2 + \tau_{yz}^2 + \tau_{zx}^2)} \quad (46)$$

Bending Tests R=-1	N [Cycles]	$\sigma_{x,a}$ [MPa]	$\sigma_{x,m}$ [MPa]
1	1.9E4	620	0
2	3.6E4	590	0
3	5.8E4	552	0
4	9E4	535	0
5	1.7E5	505	0
6	2.2E5	490	0
7	4.4E5	470	0
8	8E5	465	0
9	1.4E6	462	0
10	1.5E6	465	0
11	2.4E6	460	0
12	3.3E6	460	0
13	6E6	440	0
14	6.6E6	458	0
15	7E6	430	0
16	9E6	448	0
17	4.5E4	540	196
18	5.4E4	515	196
19	7E4	520	196
20	7.1E4	485	196
21	1.1E5	485	196
22	1.5E5	475	196
23	2E5	460	196
24	2.1E5	455	196
25	3E5	435	196
26	4.3E5	415	196
27	6.9E5	410	196
28	5.8E5	390	196

Table 22: SM45C steel fully reversed bending tests(extracted from [26])

Torsion Tests R=-1	N [Cycles]	$\tau_{xy,a}$ [MPa]
1	2.9E4	405
2	5E4	399
3	7.8E4	380
4	1E5	365
5	1.8E5	355
6	1.9E5	349
7	3E5	340
8	5.8E5	335
9	8.2E5	333
10	2.25E6	325

Table 23: SM45 steel fully reversed torsion tests(extracted from [26])

8.5.3. Identification of model parameters for steel SM45C

We use the Von Mises yield strength combining the bending and torsion yield limits as σ_y . The fitted curve using experimental data in Table. 24 and data with mean stress effect is shown in Figure 38b. The tests on SM45C steel have illustrated that the mean bending stress has an influence on both uniaxial and multiaxial fatigue life.

Although the uniaxial experimental data we extracted from Lee's curve [26] of SM45C steel are slightly dispersed, we can find our model quite satisfactory in the case of SM45C steel. As for multiaxial 90 degree out of phase, fully reversed bending-torsion fatigue tests, our model is able to evaluate the cycles to failure.

Group	N	τ_a	σ_a	σ_m
	[Cycles]	[MPa]	[MPa]	[MPa]
A	29.9E3	282	449	0
	35.7E3	334	354	0
	50E3	223	485	0
	73.8E3	309	357	0
	106E3	217	449	0
	106E3	285	370	0
	112E3	199	449	0
	131E3	194	457	0
	333E3	252	354	0
B	431E3	154	437	0
	53E3	215	441	196
	59.2E3	309	286	196
	70.1E3	155	464	196
	86.3E3	136	473	196
	89.9E3	334	173	196
	92.1E3	209	403	196
	102E3	177	437	196
	135E3	321	167	196
	351E3	179	357	196
	394E3	274	182	196

Table 24: With and without mean bending stress on out-of-phase(90°) fatigue of SM45C steel [26]

β	λ_+	λ_-	W_0	a
8	1	0	4.17E8 Pa	0.4

Table 25: Parameter identification of SM45C steel

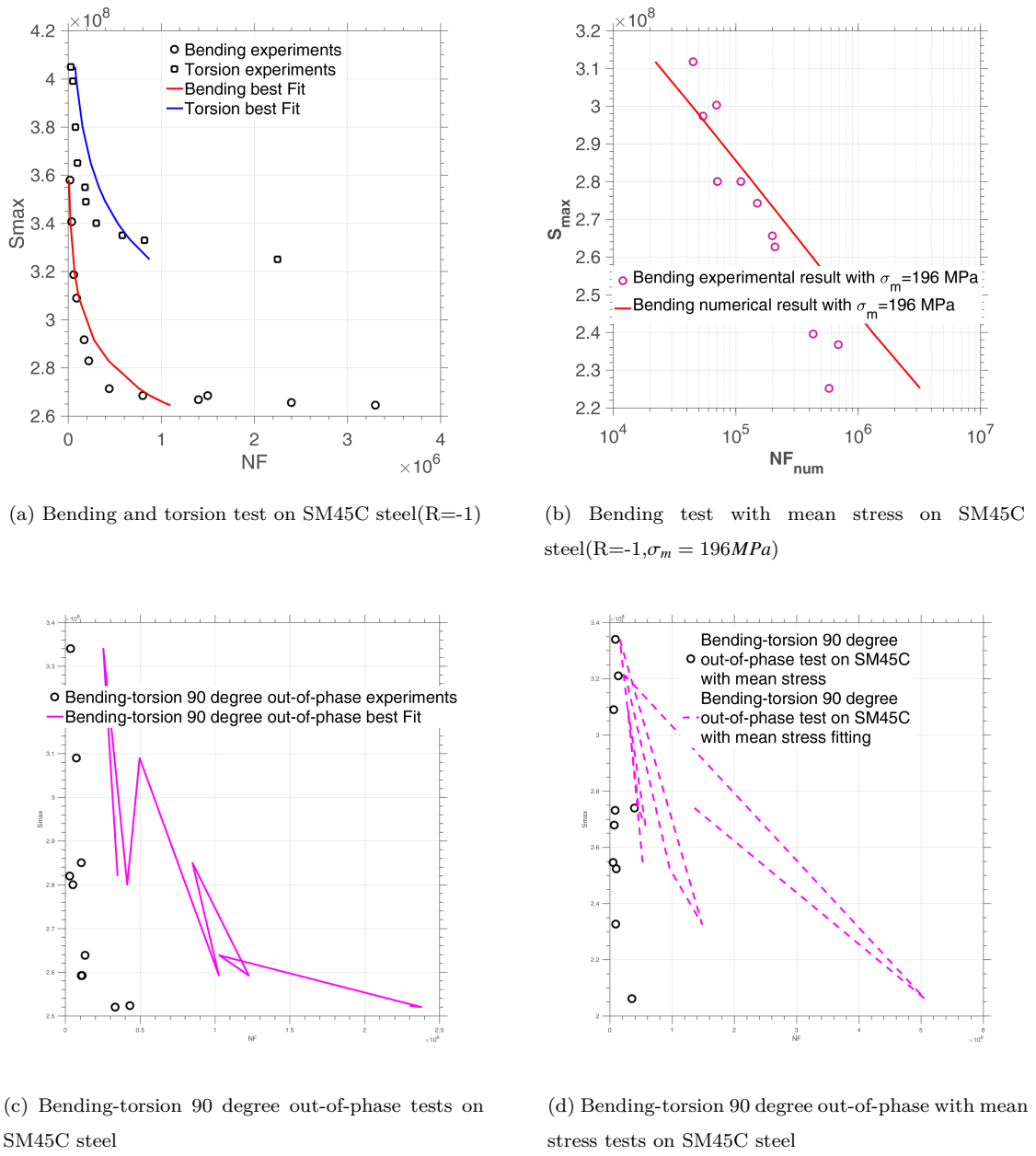


Figure 39: Calibration on SM45C ([26])

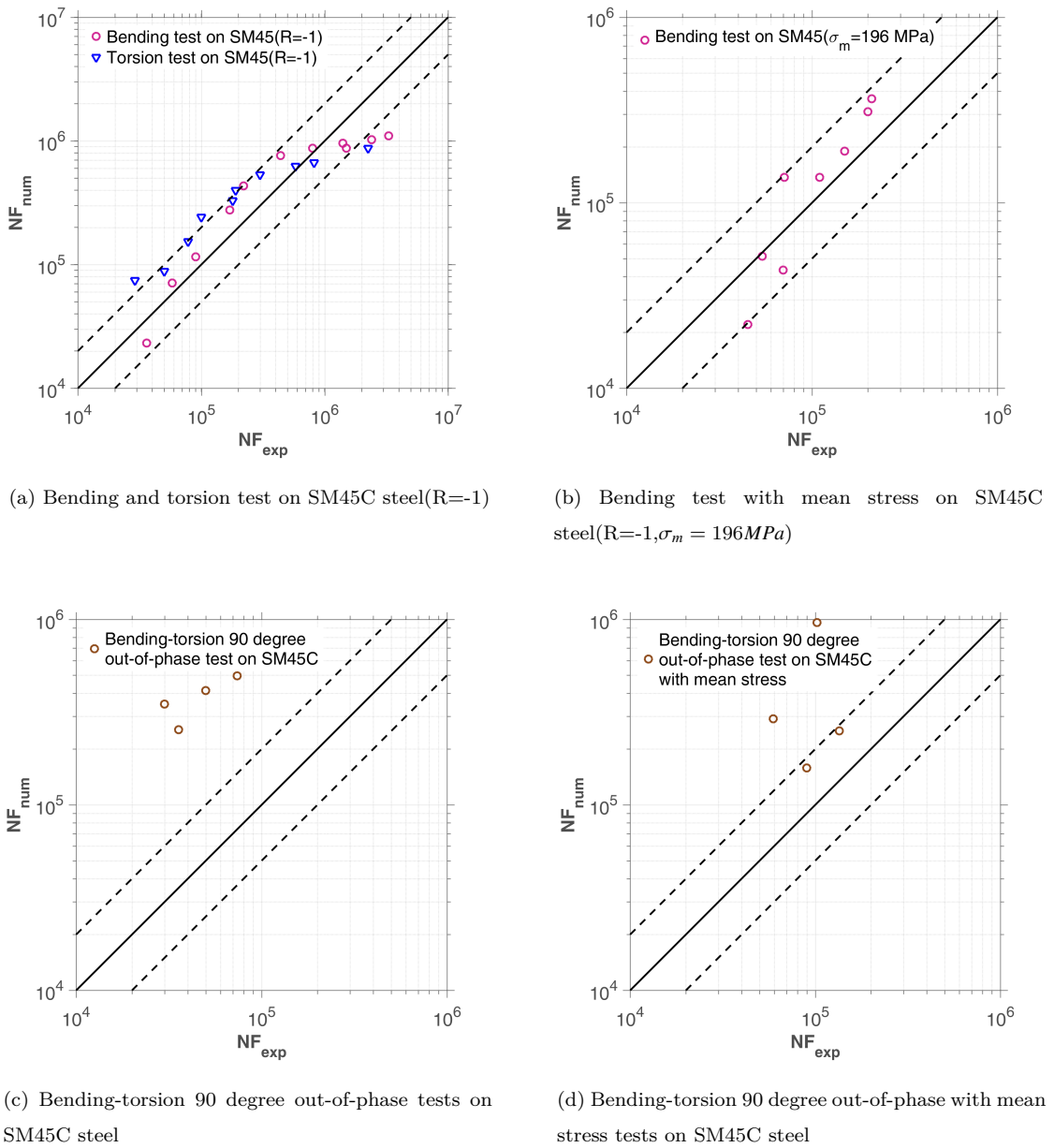


Figure 40: Calibration on SM45C ([26])

8.6. Experimental validation of the model on 10 HNAP steel

8.6.1. Presentation of the material

Fatigue tests were performed on the HNAP steel. It is a very low carbon steel which resembles the 10 CN 6. In Table 26, its chemical composition is given: The mechanical properties of this steel are given in

C	Mn	Si	P	S	Cr	Cu	Ni	Fe
0.12%	0.71%	0.41%	0.08%	0.03%	0.81%	0.30%	0.50%	the rest

Table 26: Chemical composition of 10 HNAP steel[27]

Table 27:

$Re_{0.2\%}$	R_m	A	ν	E
418 MPa	566 Mpa	32%	0.29	215000 Mpa

Table 27: Mechanical characteristics of steel 10 HNAP[?]

where

- $Re_{0.2\%}$: elastic limit at 0.2% of plastic deformation,
- R_m : maximum tensile strength,
- A : elongation at break,
- ν : Poisson's coefficient,
- E : Young's modulus.

8.6.2. Description of fatigue tests on 10 HNAP steel

The Macha team performed a large number of fatigue tests on the HNAP steel. Thus, it performed not only simple tensile compression and torsion tests ($R = -1$) in order to establish the corresponding Wöhler curves but also tests under variable loading on cylindrical specimens of the same material[28]. VIDAL[29] carried out tensile tests on this material for various mean stress values. It has established the Wöhler curve in repeated traction in order to validate on this steel the method of Robert whose use requires three Wöhler curves in symmetrical alternating traction, symmetrical alternating torsion and repetitive traction.

Wöhler curve in tension-compression

The model chosen by Macha and recovered by Jabbado[30] for the tensile-compression Wöhler curve is that of Basquin:

$$\ln N = 68.361 - 9.82 \ln (\sigma_{-1}) \quad (47)$$

67

Wöhler curve in symmetrical alternating torsion

The symmetric alternating torsion Wöhler curve was recovered by Jabbado[30] using following equation:

$$\ln N = 21.55 - 0.0385\tau_{-1} \quad (48)$$

Tensile fatigue tests for various mean stress values

VIDAL[29] carried out tensile tests on HNAP steel for various values of mean stress. The results are summarized in Table.28. They allowed us to plot the Wöhler curves for different values of the mean stress σ_m . These curves are modeled by the Wöhler equation:

$$\ln N = A - B\sigma_{max} \quad (49)$$

In the Table.??, the values of the constants A and B of Eq.(49).

σ_a (MPa)	σ_m (MPa)	N_{exp} (cycles)
250	75	439300;402500
270	75	358200;854700;318700
290	75	252300;376300;379700
310	75	54800;123400;45000
250	150	157400;1333000
270	150	172100;121500;233100
290	150	124300;41900;60500
230	225	413900;204500;545200
250	225	122400;229600;104000
270	225	110000;29900;66000
190	300	497100;234300;524800
210	300	463500;367300;259500
230	300	219000;179400;222400
250	300	95300;118200;59100

Table 28: Experimental results of tensile tests for various values of σ_m

Fatigue testing under variable loading

Random multiaxial loading fatigue tests were performed on cylindrical HNAP steel specimens[28]. The load considered is proportional and results from a combination of bending and torsion. The random signal is stationary and has a normal distribution as a probability distribution. Tests of this type have been analyzed and simulated by Carpinteri et al.[31]. They were provided to us in the form of tests carried out on the HNAP steel for two values of the angle α' : $\alpha' = \pi/8$ and $\alpha' = \pi/4$. α' is the angle made by the resultant moment M with the bending moment M_B (see Figure 39).

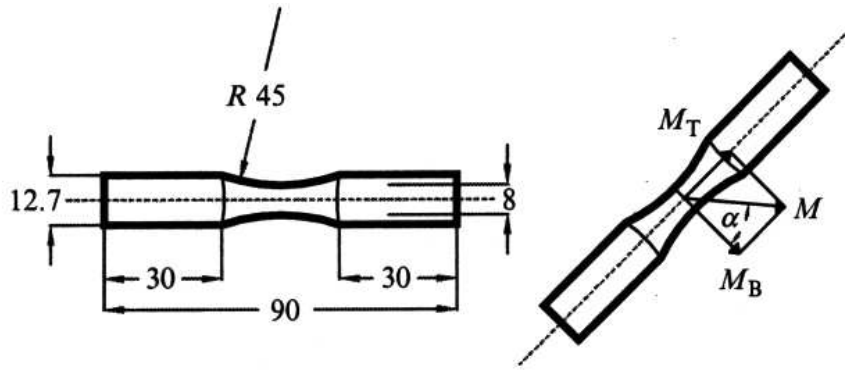


Figure 41: Bending-torsion fatigue tests on cylindrical specimens[31]

The stationary random loading sequence contains 49152 values recorded by a time interval of 0.00375 seconds (frequency = 266.67 Hz). It is shown in Figure 40. Its total duration is 184.32 seconds. This sequence is multiplied by load coefficients corresponding to bending $f(\sigma_{xx})$ and torsion $f(\tau_{xy})$ in order to obtain random multiaxial loading sequences. As the signal is stationary, the breaking life is determined in terms of number of sequences with break N_{Sg} . Knowing N_{Sg} and the total time in seconds of the sequence studied, it is easy to express the lifetime of the piece in seconds. The results of fatigue tests under variable loads are summarized in Table.29 and Table.30 as a function of angle α' and ratio r ; $r = f(\tau_{xy})/f(\sigma_{xx})$.

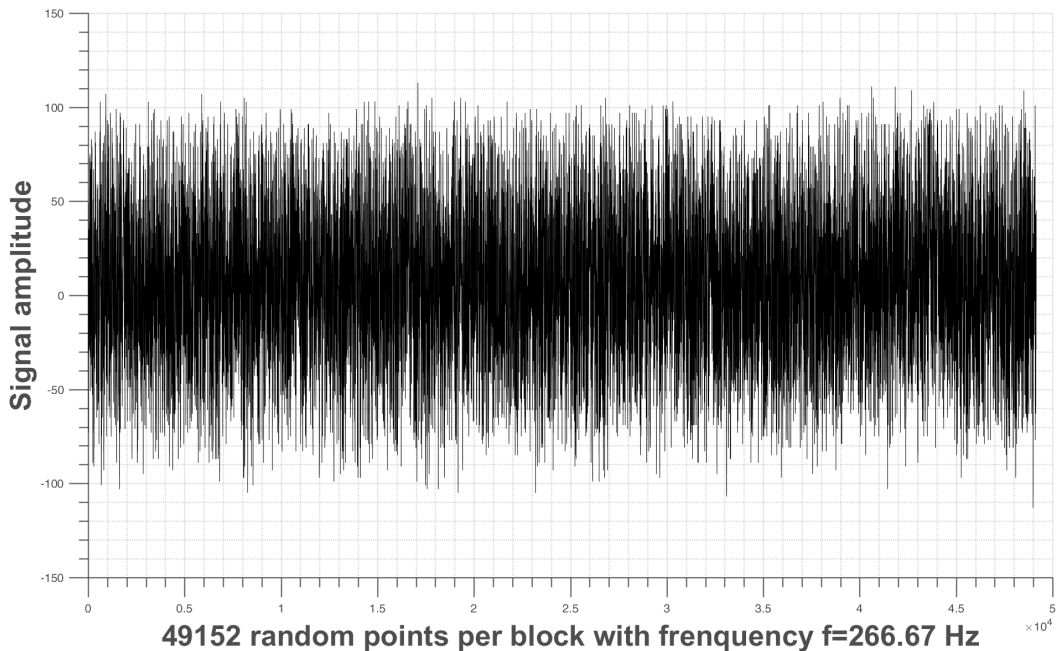


Figure 42: Bending-torsion fatigue tests on cylindrical specimens[31]

1st type of tests: $\alpha' = \pi/8$ and $r = f(\tau_{xy})/f(\sigma_{xx}) = 0.2$.

N^o	$f(\sigma_{xx})$	$f(\tau_{xy})$	r	$T_{exp}(s)$
1	5.7084	1.1822	0.2	16843.2
2	5.2917	1.0959	0.2	17780.1
3	4.8337	1.0010	0.2	24416.5
4	5.2674	1.0909	0.2	24858.2
5	5.4534	1.1294	0.2	26518.3
6	5.2002	1.0769	0.2	36162.3
7	4.7944	0.9929	0.2	47600.4
8	4.3862	0.9084	0.2	57993.9
9	4.6241	0.9576	0.2	60428
10	4.0194	0.8324	0.2	73373.3
11	4.0127	0.8310	0.2	87609.1
12	4.2292	0.8758	0.2	89185.2
13	3.9213	0.8121	0.2	106900
14	3.7731	0.7814	0.2	117358
15	4.1148	0.8521	0.2	118902
16	3.6150	0.7486	0.2	132448
17	3.3135	0.6862	0.2	170571
18	4.1298	0.8553	0.2	178215
19	3.4761	0.7199	0.2	225288
20	3.3430	0.6923	0.2	352635
21	3.0135	0.6241	0.2	355720

Table 29: Fatigue results under variable loads for $\alpha' = \pi/8$ and $r = f(\tau_{xy})/f(\sigma_{xx}) = 0.2$

2nd type of tests: $\alpha' = \pi/4$ and $r = f(\tau_{xy})/f(\sigma_{xx}) = 0.5$.

In Figure 41, an example of a random multiaxial loading sequence is given.

8.6.3. Identification of model parameters of 10HNAP steel

As mentioned earlier, the identification of the model parameters requires a Wöhler curve. This initiates the value of β , in the mean stress tests we have got the value of λ . And the value of W_0 and α comes from random loading. The parameters of the HNAP steel model can be identified by referring to Table 31. They are grouped in the following table:

N^o	$f(\sigma_{xx})$	$f(\tau_{xy})$	r	$T_{exp}(s)$
1	4.2519	2.126	0.5	15379.4
2	4.0567	2.0284	0.5	21465.7
3	3.8982	1.9491	0.5	25350.4
4	3.7823	1.8912	0.5	45949
5	3.5963	1.7982	0.5	62434.8
6	3.4497	1.7249	0.5	75225.7
7	2.9423	1.4712	0.5	115009
8	2.8814	1.4407	0.5	136794
9	2.3299	1.165	0.5	203365
10	2.8399	1.42	0.5	221370
11	2.8493	1.4247	0.5	244757
12	2.2542	1.1271	0.5	251723
13	2.3651	1.1826	0.5	288080
14	2.4215	1.2108	0.5	405444

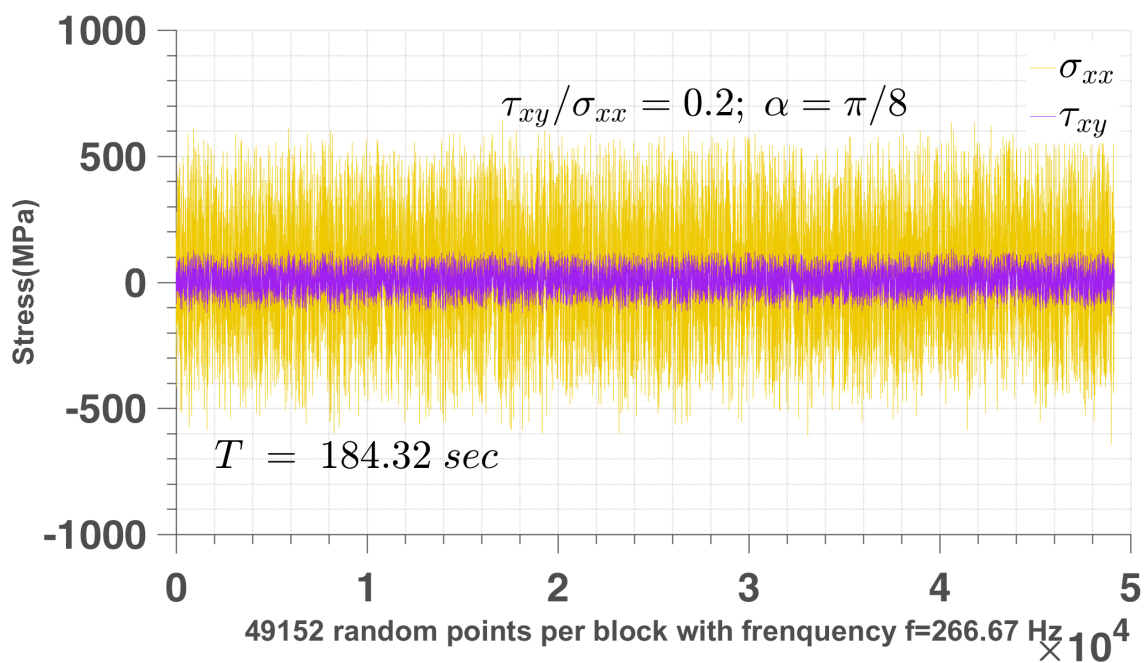
Table 30: Fatigue results under variable loads for $\alpha' = \pi/4$ and $r = f(\tau_{xy})/f(\sigma_{xx}) = 0.5$ 

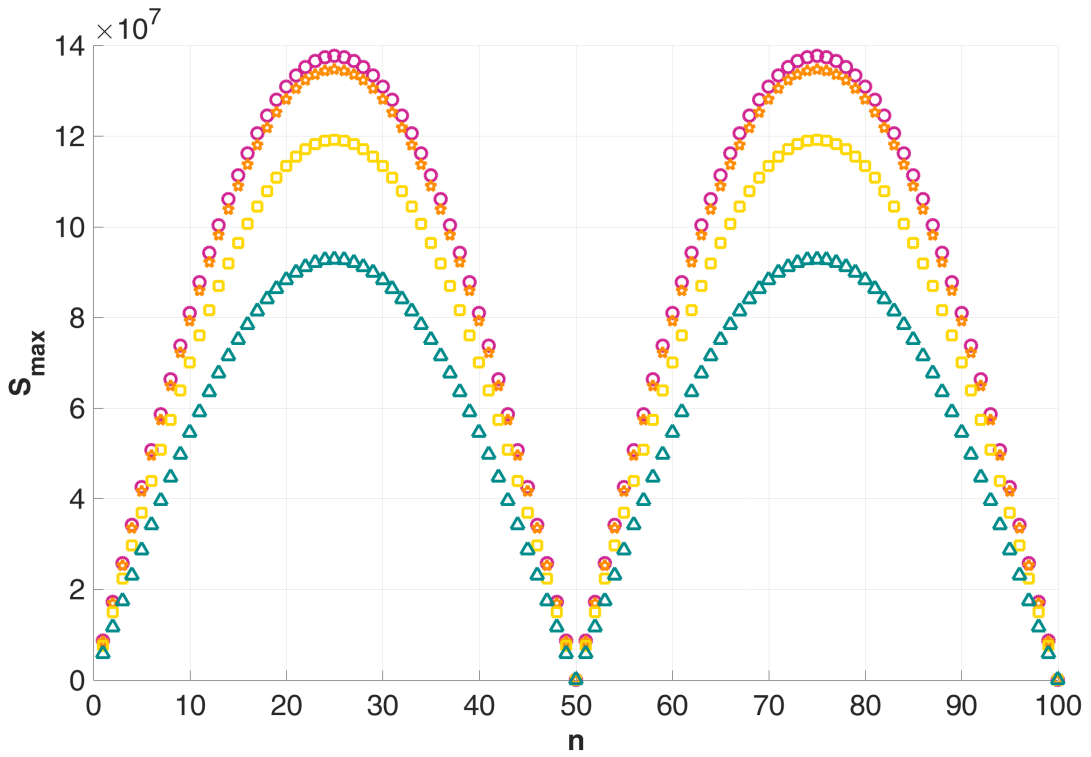
Figure 43: Multiaxial random loading sequence

β	λ_+	λ_-	W_0	a
5.34	1.7	0	6.48E8 Pa	0.4

Table 31: Model parameters for 10HNAP steel

8.6.4. Simulation of fatigue tests performed on 10HNAP steel

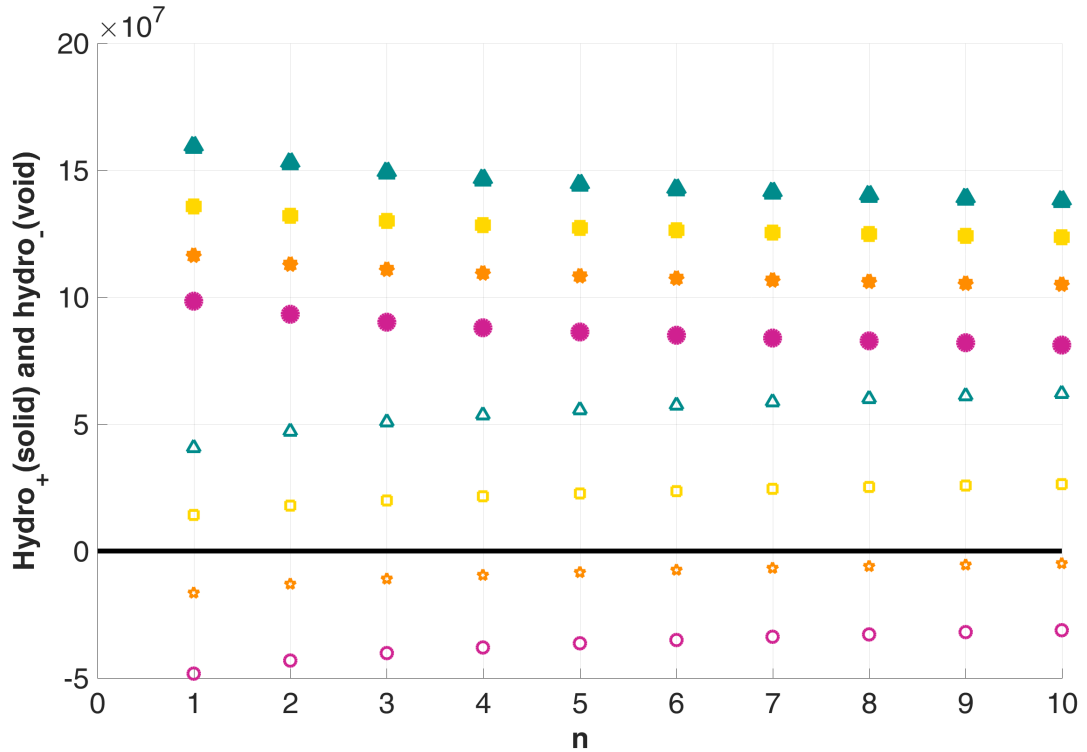
After determining the parameters of the HNAP steel model and calculated pcs for each of the tests tested, the number of priming cycles can be obtained by directly applying equation (40) for the proportional periodic loads of constant amplitude and for multiaxial loadings of variable amplitude.

Figure 44: S_a of bending tests with mean stress on 10HNAP

In Figure 46 and Figure 47, we give the prediction results of the torsion tests used to identify β and W_0 of the model, then we use the bending with various mean stress to get the parameter λ . These are to be taken with caution because of the effect of the gradient because the specimens stressed in tension and in torsion are not of the same nature.

The prediction results of the tensile tests for various values of the mean stress m are summarized in Figure 47. These results correlate well with the experimental lifetimes.

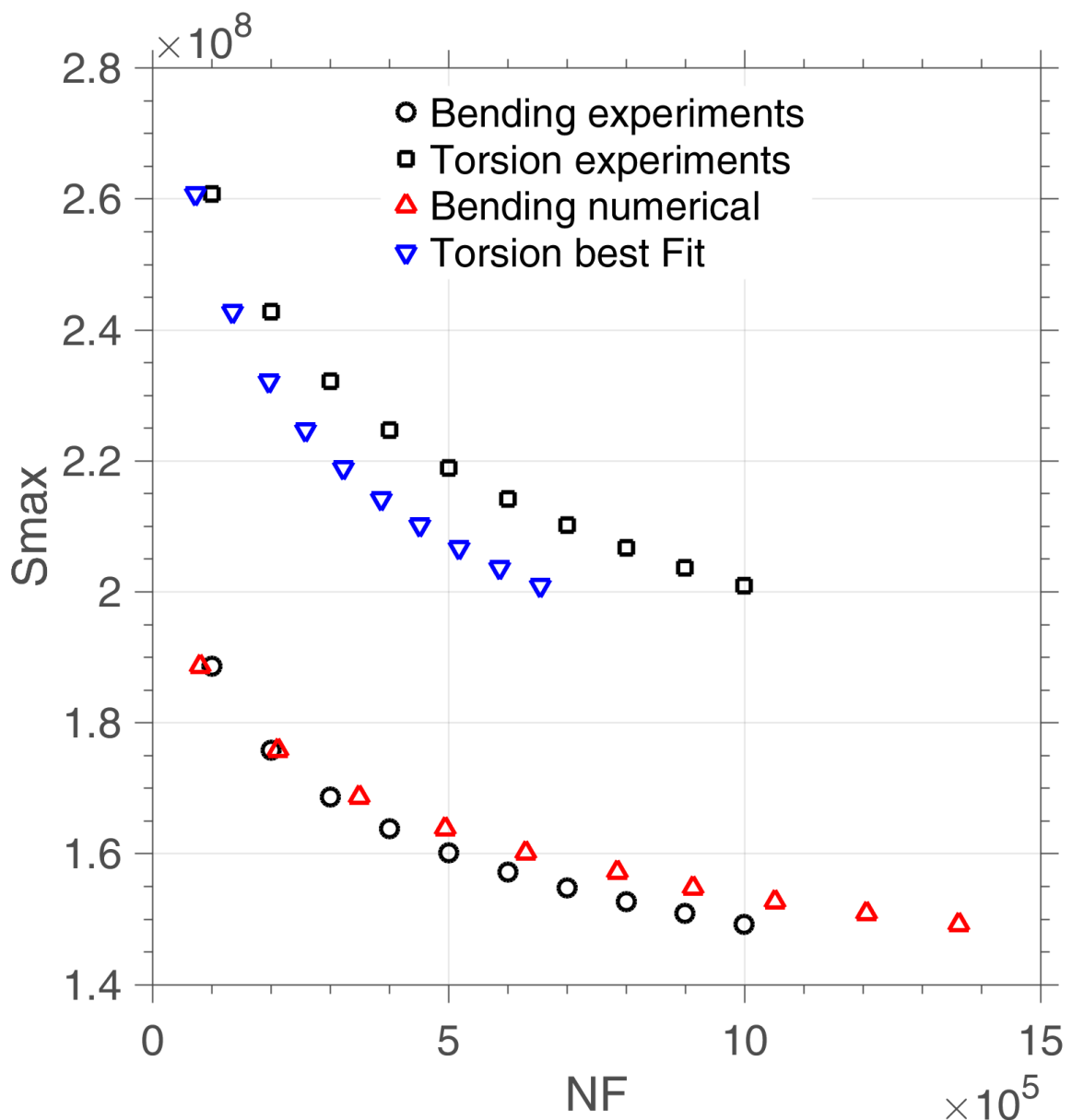
The tests of multiaxial loadings of variable amplitude are plotted in Figures (3.27) and (3.28) as a

Figure 45: $Hydro_{+-}$ of bending tests with mean stress on 10HNAP

function of the angle α_M and the ratio r . In these figures, the prediction results of the proposed model and that presented by Carpinteri et al. [17]. For the first type of tests ($\alpha_M = \pi/8$ and $r = 0.2$), the best predictions are given by the proposed model. However, for the second type of tests ($\alpha_M = \pi/4$ and $r = 0.5$), the predictions of Carpinteri et al. [17] are relatively better.

FIG. 3.27(random load results($\alpha_M = \pi/8$ and $r = 0.2$), fail too early due to big λ_+)

FIG. 3.28(random load results($\alpha_M = \pi/4$ and $r = 0.4$), fail too early due to big λ_+)

Figure 46: Bending and torsion test on 10HNAP steel($R=-1$)

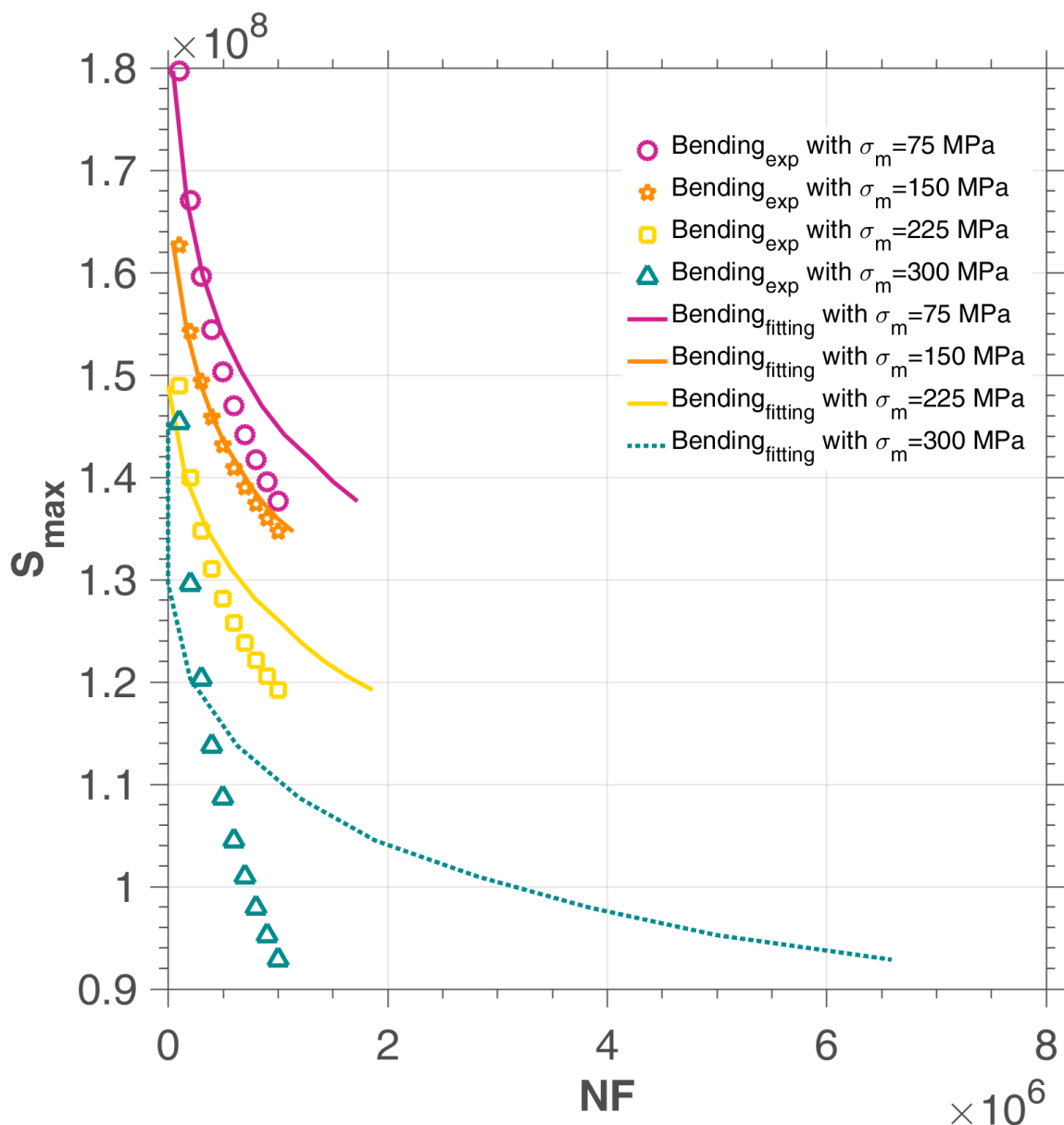


Figure 47: Wöhler tensile curves for various mean stress values

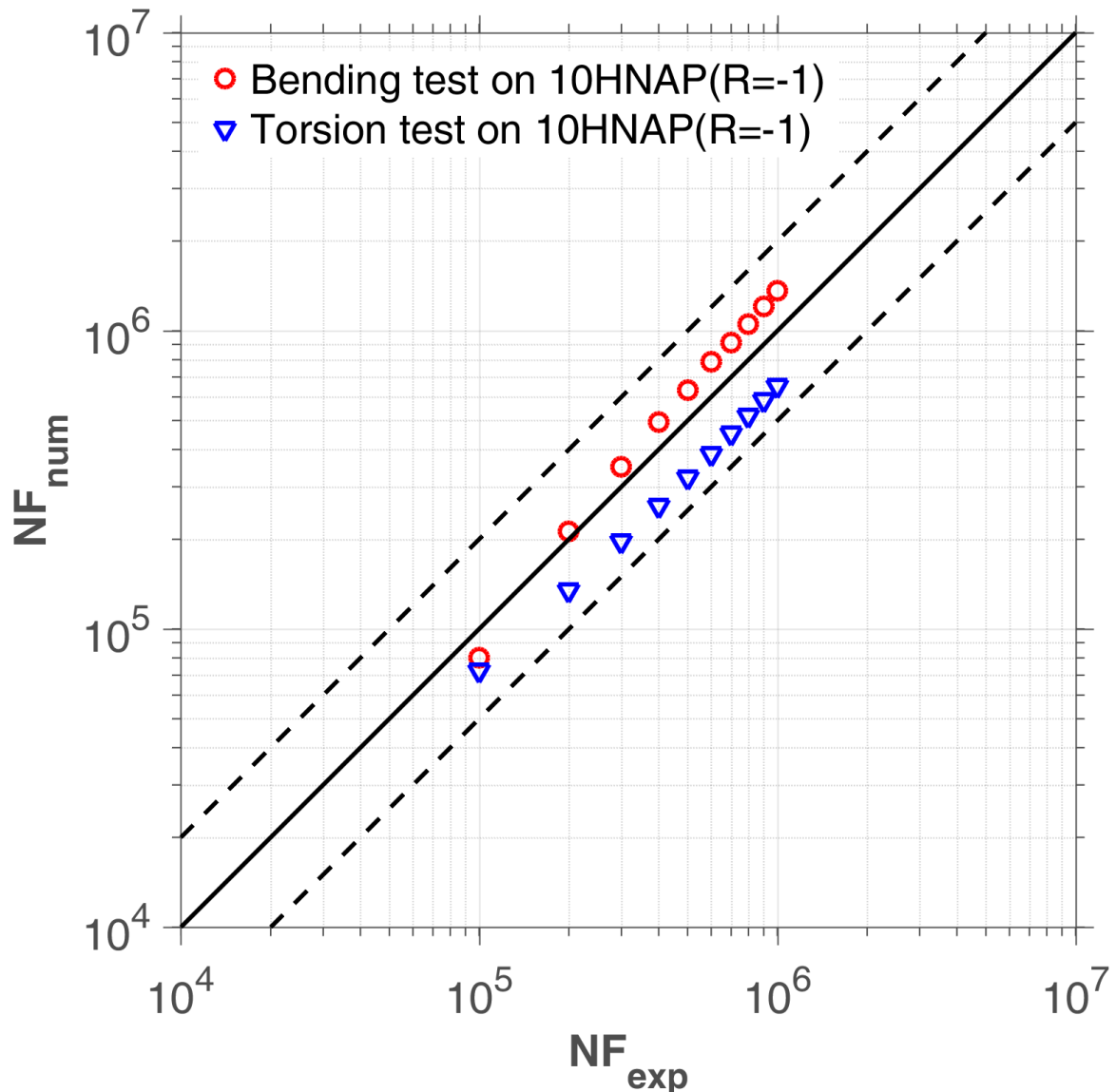


Figure 48: Calibration on 10HNAP steel([30]),bending and torsion tests on 10HNAP(R=-1)

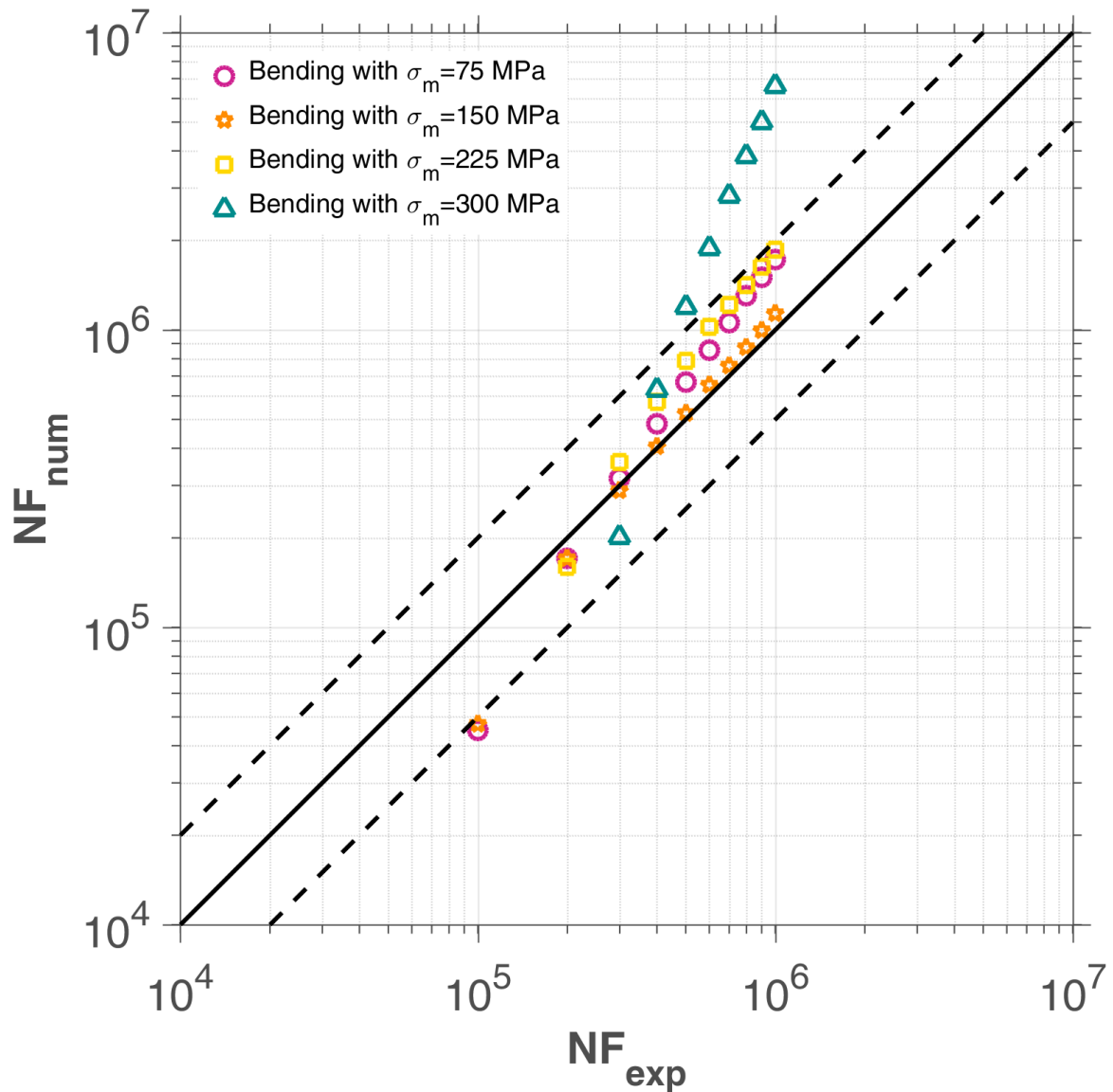


Figure 49: Calibration on 10HNAP steel([30]),bending tests with various mean stress on 10HNAP

9 Conclusions

We work on the stress tensor directly in 3D analysis in stead of using the multidimensional equivalent stress. The strategy can be made more complex by introducing a local space averaging process in the calculation of the local damage, and by taking more general plastic flows. The energy based fatigue approach takes into account impurities and hardness in the material and is applicable to any type of micro plasticity law and multiaxial load geometry. The time implicit strategy gets rid of cycle counting which is hardly applicable to complex loading, big fluctuation is magnified which reflects the real situation.

There are several advantages and drawbacks of our proposed model. The time implicit method does not take the unit of cycle so as to avoid cycle counting and relevant methods such as rain-flow filter. The possibility to handle different S-N curves corresponding to various materials and load conditions via changing the parameters. We also have the random loading suitability with nonlinear damage accumulation. The drawback is this strategy requires a scale by scale analysis which can be complicated for very high cycle fatigue. However, as introduced above, we can use the optimal time step method to calculate precisely the representative loading history sequence and use scalar integration for the rest of fatigue life. In this way the numerical cost can be dramatically reduced without losing the precision.

Since our method is based on the Dang Van paradigm, to deal with mean stress effect and multiaxial loads we only have the parameter γ , which is insufficient to fit the experiments.

Also, we need more experimental data and comparison with other peoples' methods.

10 General conclusions

This study was devoted to the development of a phenomenological and deterministic model of lifetime prediction of structures working in limited endurance under multiaxial stresses of variable amplitude without resorting to the counting of cycles. Special attention is paid to the model so that it can be applied to a wide variety of metallic materials and easy to use for use in design offices.

Our work consisted firstly of describing the methods of calculation of life in limited endurance (finite lifetime regime). We have classified these methods according to the type of stress (uniaxial or multiaxial), the nature of the signal (with constant amplitude or variable amplitude) and whether or not to adopt a cycle count. It was found that the mesoscopic approach, initiated by Dang Van [32] and developed later by Papadopoulos [2], gives a physical interpretation of polycyclic fatigue damage. Papadopoulos [2], Morel [5] and Zarka-Karaouni [33] used it and chose cumulated mesoscopic plastic deformation as a variable of damage. The authors assumed that the break occurs when this variable reaches a critical value.

To construct the predictive model of lifetime, we adopted the mesoscopic approach (or macro-meso approach) and used in part the ideas proposed by Papadopoulos and Morel. Indeed, we considered the

mesoscopic plasticity induced energy accumulated on the stabilized cycle as variable of the damage. However, unlike the authors, the rupture is not linked to a critical value of the cumulated mesoscopic plastic deformation ϵ_s^{pc} , it is defined by a stochastic distribution of weak points which will undergo strong plastic yielding, which contribute to energy dissipation and cause damage, without affecting the overall macroscopic stress. Moreover, the criterion of plasticity at the mesoscopic scale is different. Indeed, the nucleation of microcracks and cracks is a complex phenomenon involving not only plasticity, but also the creation and growth of voids. Although the metallic plasticity is generally independent of the hydrostatic pressure, the growth of the voids depends on the hydrostatic pressure. For this purpose, we have chosen an elastoplastic model with linear kinematic hardening with a mesoscopic elastic limit dependent on the hydrostatic pressure to account for this influence.

A first approach using mesoscopic plastic deformation with a non-zero mean stress and a method of direct calculation of the mesoscopic stabilized cycle is formulated. The difficulty of obtaining an explicit formula for the simple mesoscopic plastic deformation of the stabilized cycle makes the procedure for identifying the parameters of the model complicated.

In limited endurance, the mesoscopic lifetime criterion was defined for the affine cyclic loads of constant amplitude as a power relation between the stress intensity on the stabilized cycle and the number of cycles at the crack initiation. This criterion was used to identify model parameters using simple loads. An extension of this law to consider the repeated multiaxial loading sequences of variable amplitude is done via a damage factor D depending on energy dissipation and certain parameters characteristic of the material and the loading. Failure is assumed when $D = 1$.

The dissipated energy to failure per defect W_0 is directly related to the fatigue life scaling. Weakening scales distribution exponent β controls the distribution of weakening scales leading to defining the slope of S-N curve. β also takes into account the major damage effect mentioned above. λ is the hydrostatic pressure sensitivity of the elastoplastic material on the mesoscopic scale. a controls the speed of non-linear damage accumulation. The identification of these parameters involves two steps:

1. Application of the method to the uniaxial case to get 1D best fit (in bending and in torsion): this mainly leads to the identification of β , which will be used later in an optimization problem.
2. Identification of all parameters of the model by solving a least-square optimization problem (previously obtained relationships): this is to minimize the error between the simulated curve and the experimental Wöhler curve of a test.

The procedure for identifying model parameters requires knowledge of a Wöhler curve (ideally in symmetrical alternate bending) and mean stress effect on fatigue life.

To validate the model, we simulated fatigue tests from the literature and carried out on smooth specimens of four materials (aluminum Al 6082 T6, steel 30NCD16, steel SM45C and steel 10 HNAP) under multiaxial loadings of constant and variable amplitudes.

A good correlation of the model prediction results with the experimental results was obtained for the proportional loads used, either at constant amplitude or at variable amplitude. The results of prediction are worse for tests carried out on aluminum Al 6082 T6 under non-proportional loads of constant amplitude.

In addition, the model has been applied to study the fatigue strength of AW-6106 T6 aluminum carried out by CETIM(Centre Technique des Industries Mécaniques) under two constant and random signals. The results showed that, in the absence of major damage effect, the life time prediction of the material under random loading is worse.

The most immediate prospects are validation of the model for different out-of-phase or non-proportional paths. Its application to other industrial structures with a comparison with experimental results is essential for its use in design offices.

Acknowledgments

We are grateful for the financial and technical support of Chaire PSA.

References

- [1] D. N. Van, The khmu in viet nam, Vietnamese studies 36 (2) (1973) 62–140.
- [2] I. V. Papadopoulos, Long life fatigue under multiaxial loading, International Journal of Fatigue 23 (10) (2001) 839–849.
- [3] B. Crossland, Effect of large hydrostatic pressures on the torsional fatigue strength of an alloy steel, in: Proc. Int. Conf. on Fatigue of Metals, Vol. 138, Institution of Mechanical Engineers London, 1956.
- [4] G. Sines, Behavior of metals under complex static and alternating stresses, Metal fatigue 1 (1959) 145–169.
- [5] F. Morel, [A fatigue life prediction method based on a mesoscopic approach in constant amplitude multiaxial loading](#), Fatigue and Fracture of Engineering Materials and Structures 21 (3) (1998) 241–256. doi:[10.1046/j.1460-2695.1998.00452.x](https://doi.org/10.1046/j.1460-2695.1998.00452.x).
URL <http://dx.doi.org/10.1046/j.1460-2695.1998.00452.x>
- [6] H. N. T. Thu, Effet des hétérogénéités microstructurales sur le comportement en fatigue multiaxiale à grand nombre de cycles: application à l’usinage assisté laser, Ph.D. thesis, Arts et Métiers ParisTech (2008).
- [7] W. Findley, Engng. Industry 81(4) (1959) 301.
- [8] J. Liu, H. Zenner, Berechnung der dauerSchwingfestigkeit bei mehrachsiger beanspruchung—teil 1, Materialwissenschaft und Werkstofftechnik 24 (7) (1993) 240–249.
- [9] F. Ellyin, A criterion for fatigue under multiaxial states of stress, Mechanics Research Communications 1 (4) (1974) 219–224.
- [10] M. F. Lefebvre, Cognitive distortion and cognitive errors in depressed psychiatric and low back pain patients., Journal of consulting and clinical psychology 49 (4) (1981) 517.
- [11] F. Ellyin, K. Golos, Z. Xia, In-phase and out-of-phase multiaxial fatigue, ASME J. Eng. Mater. Technol 113 (1991) 112.
- [12] D. L. Froustey C., Laserre S., Validité des critères de fatigue multiaxiale à l’endurance en flexion-torsion. (1992) Mat–Tech ‘92, IITT–International, France, 79–85.
- [13] T. Palin-Luc, Fatigue multiaxiale d’une fonte gs sous sollicitations combinées d’amplitude variable, Ph.D. thesis (1996).
- [14] A. Banvillet, Prévision de durée de vie en fatigue multiaxiale sous chargements réels: vers des essais accélérés, These de Doctorat.

- [15] J. Lemaitre, J. Sermage, R. Desmorat, A two scale damage concept applied to fatigue, International Journal of fracture 97 (1) (1999) 67–81.
- [16] J. Lemaître, J. L. Chaboche, Mécanique des matériaux solides.
- [17] L. Flacelière, Contribution a la modélisation du dommage en fatigue multiaxiale d'un acier c36: confrontation à l'expérience, Ph.D. thesis, Poitiers (2004).
- [18] V. Monchiet, Contributions à la modélisation micromécanique de l'endommagement et de la fatigue des métaux ductiles, Ph.D. thesis, Lille 1 (2006).
- [19] M. Maitournam, C. Krebs, A. Galtier, [A multiscale fatigue life model for complex cyclic multiaxial loading](#), International Journal of Fatigue 33 (2) (2011) 232 – 240. [doi:
http://dx.doi.org/10.1016/j.ijfatigue.2010.08.017](http://dx.doi.org/10.1016/j.ijfatigue.2010.08.017).
URL <http://www.sciencedirect.com/science/article/pii/S0142112310001933>
- [20] S. Bosia, A. Constantinescu, [Fast time-scale average for a mesoscopic high cycle fatigue criterion](#), International Journal of Fatigue 45 (2012) 39 – 47. [doi:
http://dx.doi.org/10.1016/j.ijfatigue.2012.06.015](http://dx.doi.org/10.1016/j.ijfatigue.2012.06.015).
URL <http://www.sciencedirect.com/science/article/pii/S0142112312002162>
- [21] M. Zepeng, Structures under multiaxial fatigue taking consideration of gradients of the constraints with time and space variation.
- [22] J. Lemaitre, J.-L. Chaboche, Mechanics of solid materials, Cambridge university press, 1990.
- [23] Legendre Gauss Quadrature weights and nodes, <https://www.mathworks.com/matlabcentral/fileexchange/4540-legendre-gauss-quadrature-weights-and-nodes>, accessed: 2004-05-11.
- [24] L. Susmel, N. Petrone, Multiaxial fatigue life estimations for 6082-t6 cylindrical specimens under in-phase and out-of-phase biaxial loadings, European Structural Integrity Society 31 (2003) 83–104.
- [25] L. DUBAR, Fatigue multiaxiale des aciers - passage de l'endurance à l'endurance limitée -prise en compte des accidents géométriques., Thèse de Doctorat, Ecole Nationale Supérieure d'Arts et Métiers, Toulouse, France.
- [26] S.-B. Lee, Out-of-phase combined bending and torsion fatigue of steels, ICBMFF2.
- [27] W. Bedkowski, Determination of the critical plane and effort criterion in fatigue life evaluation for materials under multiaxial random loading. experimental verification based on fatigue tests of cruciform specimens (1994) s.435–447.
- [28] B. W. G. J. M. E. ACHTELIC, H., Fatigue life of 10hnap steel under synchronous random bending and torsion. (1994) 421–434.
- [29] E. VIDAL, Prévision de la durée de vie en fatigue multiaxiale sous sollicitations d'amplitude variable à l'aide d'un critère global.
- [30] M. Jabbado, [High-Cycle Fatigue of Metallic Structures : Lifetime Duration under Variable Loadings.](#), Theses, Ecole Polytechnique X (Mar. 2006).
URL <https://pastel.archives-ouvertes.fr/pastel-00002116>
- [31] A. Carpinteri, A. Spagnoli, S. Vantadori, A multiaxial fatigue criterion for random loading, Fatigue & Fracture of Engineering Materials & Structures 26 (6) (2003) 515–522.
- [32] K. D. Van, G. Cailletaud, J. Flavenot, A. Le Douaron, H. Lieurade, Criterion for high-cycle fatigue failure under multiaxial loading, in: ICBMFF2, 1986.
- [33] D. S. De Vasconcellos, Comportement en fatigue avant et après impact de composites tissés chanvre/époxy, Ph.D. thesis, ISAE-ENSMA Ecole Nationale Supérieure de Mécanique et d'Aérotechnique-Poitiers (2013).